Universidad de Valladolid

PhD Program in Biomedical Research

DOCTORAL THESIS

Insulin-Degrading Enzyme is a modulator of pancreatic beta-cell function via primary cilium and cytoskeletal dynamics

Submitted by Alba Sanz González

To apply for PhD degree at the

University of Valladolid

Thesis advisors:

Irene Cózar Castellano, PhD

Beatriz Merino Antolín, PhD

Valladolid

2025

Universidad de Valladolid

Programa de Doctorado en Investigación Biomédica

TESIS DOCTORAL

La Enzima Degradadora de Insulina es un modulador de la función de la célula beta pancreática vía cilio primario y dinámica del citoesqueleto

Presentada por Alba Sanz González para optar al grado de doctora por la Universidad de Valladolid

Dirigida por:

Dra. Irene Cózar Castellano

Dra. Beatriz Merino Antolín

Valladolid

2025

This research was conducted at the Institute of Biomedicine and Molecular Genetic (IBGM) in Valladolid, Spain, in cooperation with the University of Valladolid (UVa), and the Spanish National Research Council (CSIC). It has been possible thanks to the following funding:

- Proyectos del Ministerio de Ciencia, Innovación y Universidades:
    - PID2019-110496RB-C21
    - PID2022-136605OB-C21;
- Junta de Castilla y León and the European Social Fund: Predoctoral Contract granted by EDU/875/2021
- Universidad de Valladolid:
    - Becas de movilidad ERASMUS+ Prácticas de la Universidad de Valladolid (Convocatoria 2023/2024).
    - Ayudas de Movilidad de la Universidad de Valladolid para estancias breves en el desarrollo de tesis doctorales (Convocatoria 2024).

AGRADECIMIENTOS:

INDEX

INDEX

ABBREVIATIONS

1. ABBREVIATIONS

%	Percent
A.U.	Arbitrary units
5-HT	Serotonin (5-hydroxytryptamine)
+TIPs	Plus-end tracking proteins
A-IDE-KO	Alpha IDE Knockout mouse
ADP	Adenosine Diphosphate
ALMS	Alström syndrome
APC	Adenomatous Polyposis Coli
ATP	Adenosine Triphosphate
B-IDE-HT	Beta cell specific IDE Heterozygous knockout mouse
B-IDE-KO	Beta cell specific IDE Knockout mouse
B-IDE-WT	Wild Type mouse
BBS	Bardet-Biedl syndrome
β-cell	Pancreatic Beta-cells
α-cell	Pancreatic Alpha-cells
δ-cell	Pancreatic Delta-cells
ε-cell	Pancreatic Epsilon-cells
cAMP	Cyclic adenosine monophosphate
CAMSAPs	Calmodulin-regulated spectrin-associated proteins
CBP	CREB-binding protein
CREB	cAMP response element-binding protein
CRP	C-reactive protein
Cx36	Connexin 36
DAG	Diacylglycerol
DM	Diabetes mellitus
EMAPs	Endothelial-Monocyte Activating Polypeptide
EPAC	Exchange proteins directly activated by cAMP
ER	Endoplasmic reticulum
ERK	Extracellular signal-regulated kinase
GαS	G alpha subunit of the stimulatory G protein
FGF	Fibroblast growth factor
GA	Glutaraldehyde
GABA	Gamma-aminobutyric acid
GDMTs	Golgi-derived microtubules
GDP	Guanosine Diphosphate
GcgR	Glucagon receptor
GEF	Guanine nucleotide exchange factor

GIP	Glucose dependent insulinotropic peptide
GK	Glucokinase
GLP-1	Glucagon-like peptide-1
GLP-1R	Glucagon-like peptide-1 receptor
GlcNAc	N-acetylglucosamine
GLUT	Glucose transporters
GPCR	G Protein-Coupled Receptor
GSIS	Glucose-stimulated insulin secretion
GTP	Guanosine Triphosphate
Hh	Hedgehog
His	Histidines
h	Hour
IDE	Insulin-degrading enzyme
IDE-C	C-terminal portion of IDE
IDE-KO	Whole body IDE Knockout
IDE-N	N-terminal portion of IDE
IDF	International Diabetes Federation
IFT	Intraflagellar transport
IL-6	Interleukin 6
IGT	Impaired glucose tolerance
IP_3	Inositol 1,4,5-trisphosphate
IR	Insulin receptor
KO	Knockout
MAPs	Microtubule-associated proteins
min	Minutes
MOI	Multiplicity of infection
MTOC	Microtubule organizing center
mTOR	mechanistic target of rapamycin
MTBPs	Microtubule-binding proteins
NGS	Normal goat serum
NOD	Non-Obese diabetic
OGA	O-GlcNAcase
OGT	O-GlcNAc transferase
O/N	Overnight
PBS	Phosphate-buffered saline
pCREB	Phosphorylated CREB
PDGF	Platelet-derived growth factor
PIF	Pre-Implantation Factor
PKC	Protein kinase C

PKA	Protein kinase A
PLC	Phospolipase C
PMCA	Plasma membrane Ca^{2+} ATPase
PP	Pancreatic polypeptide
PTMs	Post-translational modifications
RPE-1	Retinal pigment epithelial cells
RP	Reserve pool
RNA	Ribonucleic acid
RRP	Readily releasable pool
RT	Room temperature
SERCA	Sarco-endoplasmic reticulum Ca^{2+} ATPase
shRNA	Short Hairpin Ribonucleic Acid
siRNA	Silencing Ribonucleic Acid
SIRT4	Sirtuin 4
SNARE proteins	Soluble N-ethylmaleimide-sensitive factor Attachment Protein Receptors
SNX5	Sorting Nexin 5
STORM	Stochastic Optical Reconstruction Microscopy
T1D	Type 1 diabetes
T2D	Type 2 diabetes
TCA	Tricarboxylic acid
TTL	Tubulin tyrosine ligase
TNF-α	Tumor Necrosis Factor alpha
UCN3	Urocortin-3
VDCC	Voltage-dependent Ca^{2+} channels
WHO	World Health Organization
WT	Wild Type
w/v	weight/volume
Zn^{2+}	Zinc ions
γ-TuRC	γ-tubulin ring complex

SUMMARY

2. SUMMARY

Primary cilia are microtubule-based organelles essential for cellular signaling and the integration of extracellular cues. These structures are present in pancreatic β-cells, where they play a key role in regulating cell function, particularly in the integration of paracrine signals from neighboring cells. Recent studies have implicated primary cilia dysfunction in the pathogenesis of diabetes. The microtubule cytoskeleton is also central to orchestrating the dynamic changes required for efficient insulin vesicle trafficking and secretion. These microtubules extend from the Golgi apparatus to the plasma membrane and are highly dynamic, responding to metabolic changes such as glucose levels. Insulin-degrading enzyme (IDE) is expressed in pancreatic β-cells, where it plays a major role in the regulation of insulin secretion. While our group has previously reported that IDE is decreased in β-cells of type 2 diabetes (T2D) patients, the therapeutic potential of targeting IDE remains unclear.

The aim of this study was to elucidate the physiological role of IDE in pancreatic β-cell function, particularly through its regulation of the tubulin cytoskeleton and primary cilium. We also investigated how IDE influences β-cell behavior under both stimulatory and inhibitory glucose conditions. To this end, we partially inhibited IDE expression both *in vitro* using shRNA silencing in two β-cell models (Min6-shIDE, Ins1E-shIDE), and *in vivo* by generating a mouse line with β-cell-specific *Ide* partial ablation (B-IDE-HT). In these models, we evaluated β-cell function and metabolic responses to glucose. Additionally, we analyzed the primary cilium and the microtubule network under these conditions. To better understand the role of the primary cilium in paracrine signaling, we used a Min6-IFT88-KD model, which lacks primary cilia.

Our results demonstrated that physiological levels of IDE are essential for proper β-cell function. IDE knockdown impaired glucose-stimulated insulin secretion and calcium dynamics, altered the tubulin cytoskeleton, and reduced the number and size of primary cilia. Moreover, insulin and glucagon receptors were dysregulated in IDE-deficient cells.

Interestingly, IDE is not located in the primary cilium but partially colocalizes with the Golgi apparatus (~45%). In cells lacking primary cilia (IFT88-KD), we observed reduced levels of insulin and glucagon receptors, while IDE expression and glucagon signaling remained unchanged. These findings indicate that IDE regulates β-cell function by modulating cytoskeletal dynamics and ciliogenesis, which in turn affect paracrine insulin and glucagon receptor expression.

We propose that IDE plays a critical role regulating insulin secretion and integrating paracrine signals in pancreatic β-cells through the control of tubulin cytoskeleton dynamics and primary cilium structure. Dysregulation of these processes in the absence of IDE leads to β-cell dysfunction. These findings highlight **IDE as a potential therapeutic target for preserving β-cell function and preventing the development of diabetes.**

INTRODUCTION

3. INTRODUCTION

3.1 Glucose homeostasis

Glucose homeostasis refers to the regulation of blood glucose levels. As the primary energy source for all organisms, glucose must be tightly regulated to ensure normal body functions and to maintain a continuous energy supply to tissues. This process involves numerous organs and hormones, among them, the pancreas plays a key role in maintaining blood glucose within a narrow range of 4–6 mM, through the release of two antagonistic hormones: insulin and glucagon (1). **Figure 1** illustrates the regulation of glucose levels and the opposing actions of these two hormones.

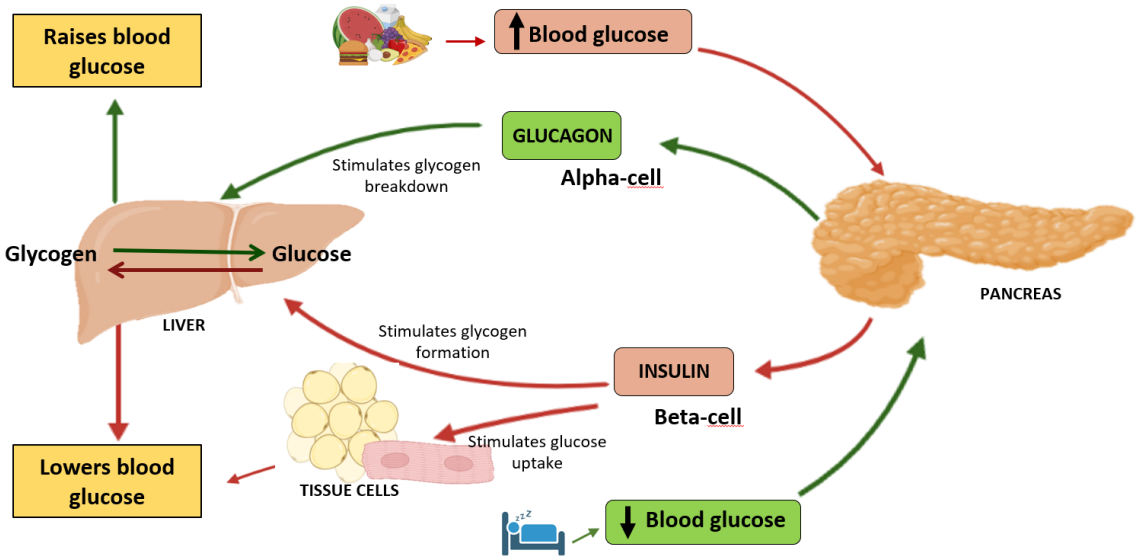

Figure 1: Maintenance of blood glucose levels by glucagon and insulin. After a meal, when blood glucose levels are high, insulin from pancreatic β-cells is released to trigger glucose uptake into insulin-dependent muscle and adipose tissues, as well as to promote glycogenesis in the liver. When blood glucose levels are low, in fasting, the pancreas secretes glucagon from pancreatic α-cells, which increases endogenous glucose production by glycogenolysis and gluconeogenesis. This figure was created using *Biorender*.

After a meal, rising blood glucose levels trigger insulin secretion from pancreatic β-cells. Once insulin binds to its receptor in muscle or adipose tissue, it facilitates glucose uptake into these cells, promoting its storage as intracellular triglycerides and glycogen in fat and muscle (2). This process helps to lower blood glucose levels by removing the glucose from the bloodstream. Additionally, insulin stimulates glycogenesis (3,4) lipogenesis (5) and protein synthesis (6).

Conversely, during fasting periods, such as between meals or during sleep, when blood glucose levels are low, glucagon is released from pancreatic α-cells. As a hyperglycemic hormone, glucagon stimulates hepatic glycogenolysis and promotes gluconeogenesis in

the liver and kidneys, increasing endogenous glucose production to maintain adequate blood glucose levels (1).

3.2 Diabetes mellitus

3.2.1 A worldwide health problem

The World Health Organization (WHO) defines diabetes as *"a chronic metabolic disease characterized by elevated blood glucose levels, which over time leads to serious damage to the heart, blood vessels, eyes, kidneys, and nerves."* The most common form is type 2 diabetes (T2D), which etiology is insulin resistance, a condition that includes reduced insulin receptors or their downstream signaling. Over the past three decades, the prevalence of T2D has risen dramatically across the whole world. Type 1 diabetes (T1D), also known as insulin-dependent diabetes, is a chronic condition in which the pancreas produces little or no insulin (7).

Diabetes mellitus (DM) is a growing global health challenge with profound social and economic consequences. In 2021, it was responsible for 6.7 million deaths, equivalent to one every five seconds. According to the International Diabetes Federation (IDF), an estimated 537 million adults (aged 20–79) were living with diabetes in 2021, a figure projected to rise to 783 million by 2045, affecting one in eight adults. More than 90% of cases correspond to T2D, largely driven by urbanization, sedentary lifestyles, aging populations, and the global rise in obesity (2).

Beyond its health impact, diabetes also imposes a substantial economic burden. In 2021, global health expenditures attributable to diabetes reached $966 billion USD, a 316% increase over the past 15 years. Furthermore, 541 million adults currently exhibit impaired glucose tolerance (IGT), placing them at high risk of developing T2D. Despite international efforts, including the global target to halt the rise in diabetes and obesity by 2025, over half of individuals with diabetes remain undiagnosed or untreated. These alarming trends underscore the urgency of more effective prevention and treatment strategies (2) **(Figure 2).**

Current therapeutic approaches for T2D focus primarily on increasing insulin secretion, reducing intestinal glucose absorption, or improving insulin sensitivity in target tissues. However, no definitive cure exists, and long-term glycemic control remains challenging for many patients. The persistence of unmet clinical needs and knowledge gaps in the disease's pathophysiology highlights the critical need for continued research into the mechanisms underlying diabetes onset and progression.

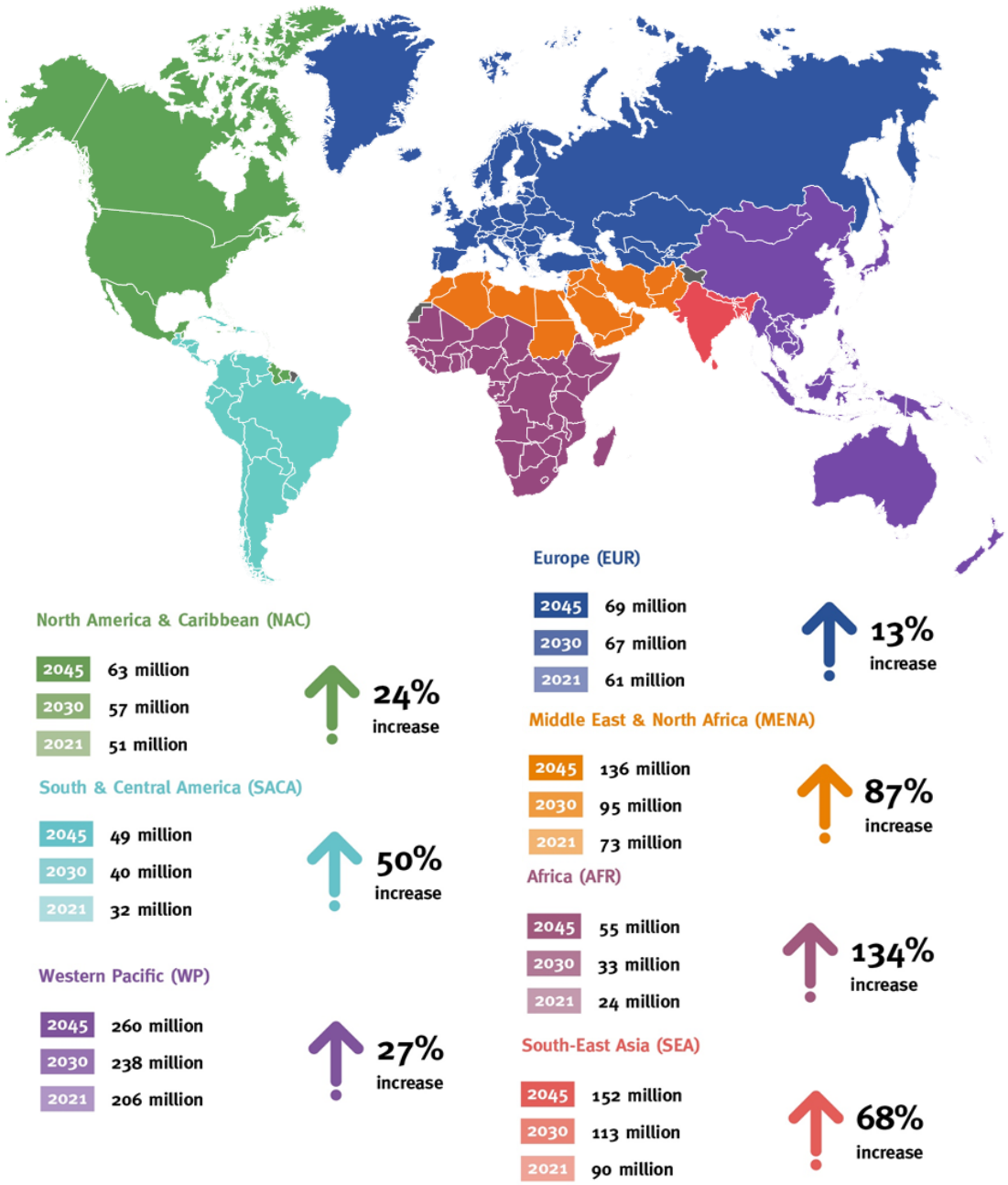

Figure 2: Diabetes prevalence and worldwide distribution in 2021 by IDF Regions and projections for 2030 and 2045. Taken from reference (2).

3.2.2 Types of diabetes

The disruption of glucose homeostasis, caused by insufficient insulin secretion, resistance to insulin action, impaired downstream signaling, and also dysregulation of glucagon secretion, leads to sustained elevations in blood glucose levels. Over time, this imbalance can contribute to metabolic diseases such as DM, leading to persistent hyperglycemia and its associated complications (1,8). There are two main types of diabetes:

Type 1 diabetes:

T1D is a subtype of diabetes (5-10%) and is usually diagnosed at a young age. The main feature in the disease is insulin deficiency and resultant hyperglycemia (9). Due to this deficiency, patients require lifelong exogenous insulin administration, which is why the disease is also referred to as insulin-dependent DM (10).

T1D results from the autoimmune disorder characterized by the selective destruction of insulin-producing pancreatic β-cells by infiltrating immune cells (11). The condition results from a complex interaction of genetic predisposition and environmental triggers. Diagnosis is based on hyperglycemia, autoantibody presence, and low C-peptide levels. The management of diabetes involves exogenous insulin therapy, continuous glucose monitoring, and innovative technologies such as artificial pancreas systems. Despite advances, T1D remains a lifelong condition with risks of complications (9).

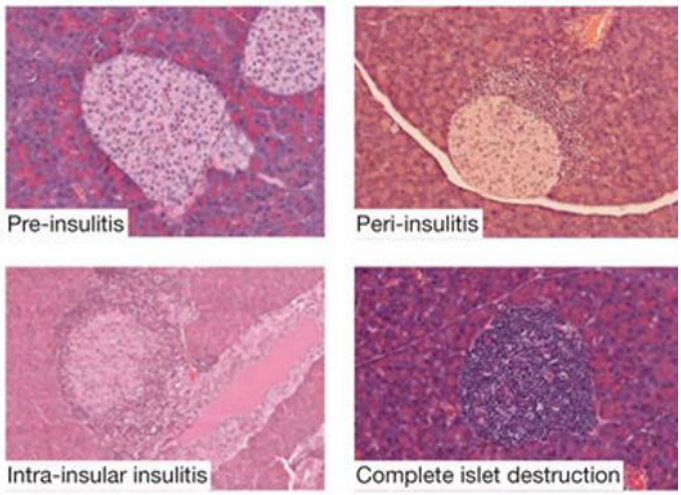

Figure 3: Islet invasion by lymphocytes of Non-Obese Diabetic (NOD) mice is asynchronous during progression to diabetes, often with a mixture of normal islets, peri-insulitis, intra-islet insulitis, and complete β-cell destruction. Taken from (12).

Type 2 diabetes:

T2D is the most common form of disease, accounting for more than 90% of diabetes cases worldwide. It is strongly linked to obesity, genetic predisposition and lifestyle factors. This condition is characterized by insulin resistance and dysfunction of pancreatic β-cells and α-cells, leading to hyperglycemia, an imbalance in blood glucose regulation (13).

Insulin facilitates glucose uptake by muscle and fat cells, promoting its storage as intracellular glycogen and triglycerides. Additionally, insulin suppresses glucose production and release from the liver by inhibiting gluconeogenesis and glycogenolysis. In a healthy individual, this mechanism prevents excessive increases in blood sugar levels (13). In the early stages of T2D, blood glucose levels remain elevated despite

normal or even high insulin concentrations in the bloodstream, this occurs due to the reduced ability of muscle and fat cells to transport glucose and the liver's failure to regulate glucose output in response to insulin, a condition known as insulin resistance. In later stages of T2D, insulin production declines as pancreatic β-cells lose their ability to secrete sufficient insulin, sometimes requiring external insulin therapy (14–18).

Insulin resistance and pancreatic β-cell dysfunction in T2D are driven by glucotoxicity (19), lipotoxicity, oxidative stress (20), and chronic inflammation. Persistent hyperglycemia (glucotoxicity) triggers oxidative stress, mitochondrial dysfunction, and endoplasmic reticulum (ER) stress in pancreatic β-cells, impairing their insulin secretion capacity (21). Simultaneously, lipotoxicity, caused by an excess accumulation of free fatty acids in non-adipose tissues such as the liver and skeletal muscle, interferes with insulin signaling pathways, further worsening insulin resistance (13,20). Additionally, adipose tissue secretes pro-inflammatory cytokines such as Tumor Necrosis Factor alpha (TNF-α), interleukin 6 (IL-6), and C-reactive protein (CRP), which impair insulin sensitivity and contribute to β-cell apoptosis (22,23). This inflammatory response, coupled with oxidative damage, accelerates pancreatic β-cell exhaustion and progressively reduces insulin production.

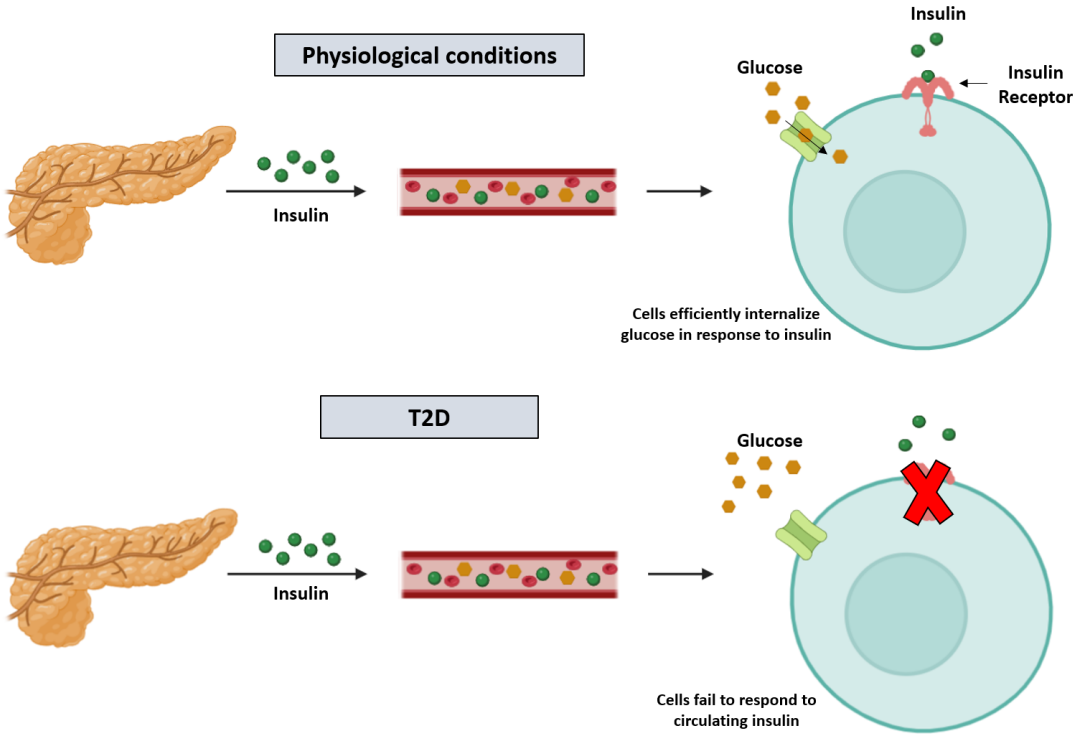

Figure 4: Comparison of insulin action in healthy and insulin-resistant conditions. In physiological conditions (top), insulin binds to its receptor, allowing glucose uptake into the cell. In T2D (bottom), insulin resistance occurs; insulin signaling is impaired, preventing effective glucose entry. This figure was created using *Biorender.*

Prolonged high blood sugar levels over the years contribute to severe complications, including retinopathy, nephropathy, neuropathy, and cardiovascular diseases, significantly increasing patient mortality (13,18,23).

The treatment of T2D begins with lifestyle changes, such as diet and exercise, while advances in pharmacotherapy have shown promising effects on glycemic control and improved cardiovascular outcomes. However, prevention remains the most effective strategy, with the possibility of remission in some cases through intensive lifestyle interventions (13).

3.3 Pancreas

3.3.1 Structure of Pancreas

The human pancreas is a retroperitoneal organ of the upper abdomen that, on average, weighs in the range of 100-150 g and measures 15-25 cm in length. It is anatomically connected with other abdominal organs including the spleen, stomach, duodenum and colon. The pancreas is a dual-function organ, regulating digestion through the exocrine system and blood glucose levels through the endocrine system (24).

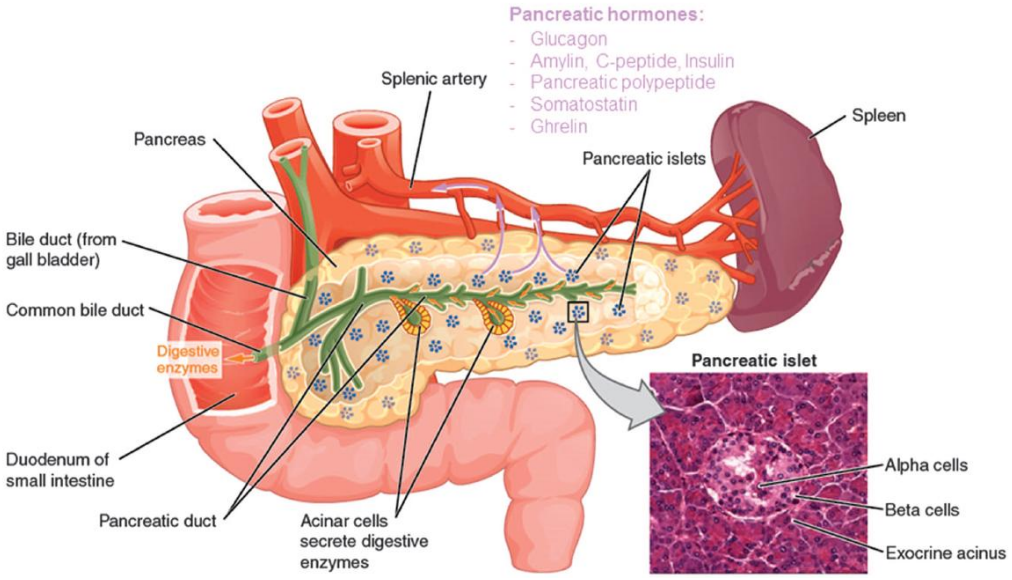

Figure 5: Anatomical organization of the human pancreas. The exocrine function of the pancreas is mediated by acinar cells that secrete digestive enzymes into the upper small intestine via the pancreatic duct. Its endocrine function involves the secretion of various hormones from different cell types within the pancreatic islets of Langerhans. Taken from (1).

Exocrine pancreas: The exocrine portion makes up about 98% of the total pancreatic volume (25) and consists of acinar and ductal cells. Acinar cells are organized into lobules called acini, and their main function is to synthesize and secrete hydrolytic

enzymes such as amylase, lipase and proteases for digestion. Ductal cells secrete sodium bicarbonate, which helps neutralize gastric acid in the duodenum and create and optimal environment for enzyme activity (26). These secretions flow into small intercalated ducts, which merge into larger intralobular ducts, eventually forming the main pancreatic duct. This duct connects with the common bile duct before releasing pancreatic juice into the duodenum (24,27).

Endocrine pancreas: The endocrine pancreas is responsible for the production and secretion of hormones that regulate intermediate metabolism. The hormones are released directly into the bloodstream, and they play a crucial role in controlling blood glucose levels and other metabolic functions. The endocrine pancreas is made up of islets of Langerhans, which are embedded within the exocrine pancreas (1,24).

3.3.2 Islets of Langerhans

The endocrine portion represents only 1-2% of the total pancreatic mass. Its cells are clustered together, forming islets of Langerhans (28). In 1869, Paul Langerhans was the first to describe these cell groups, although he was unable to determinate their function at time (29). Each of the several million islets in the human pancreas has its own vasculature, receiving more than 15% of the pancreas blood supply, and comprises approximately 2,000 endocrine hormone-producing cells (30,31). These cells are classified into five types: alpha, beta, delta, gamma, and epsilon cells, each responsible for secreting different hormones that regulate glucose homeostasis and metabolism (1,31).

- **Beta-cells (β):** β-cells are 50-70% of human islet cells and up to 80% of mouse islet cells (25). Their primary function is to synthesize and secrete insulin, it is a key hypoglycemic hormone that regulates blood glucose levels by facilitating glucose uptake into the cells (32).
- **Alpha-cells (α):** The second largest cell population of the islet, accounting for 20-40% of the total cell population in humans and 10-20% in mice (25). α-cell produces glucagon, the main hormone responsible for raising blood glucose levels and serving as the first line of defense against hypoglycemia (33).
- **Delta-cells (δ):** They represent 5% and 10% of the total endocrine cells in mouse and human islets respectively (34). δ-cells release somatostatin, a hormone that regulates glucose homeostasis by inhibiting the secretion of both glucagon and insulin (35).
- **Gamma-cells (γ):** These cells constitute approximately 3-5% of the islet and are responsible for producing and secreting pancreatic polypeptide (PP). Its release

is strongly stimulated by protein- and fat-rich meals. PP is a potent anorexigenic hormone, playing a crucial role in reducing appetite and modulating food intake (36,37). Additionally, PP inhibits glucagon release during low-glucose conditions (38).

- **Epsilon-cells (ε):** Representing less than 1% of the islet cells and secretes ghrelin, which is considered a "hunger hormone" that stimulates appetite. Despite their small population, ε-cells play important roles in regulating other endocrine cells. Ghrelin contributes to increase blood glucose levels by suppressing insulin.

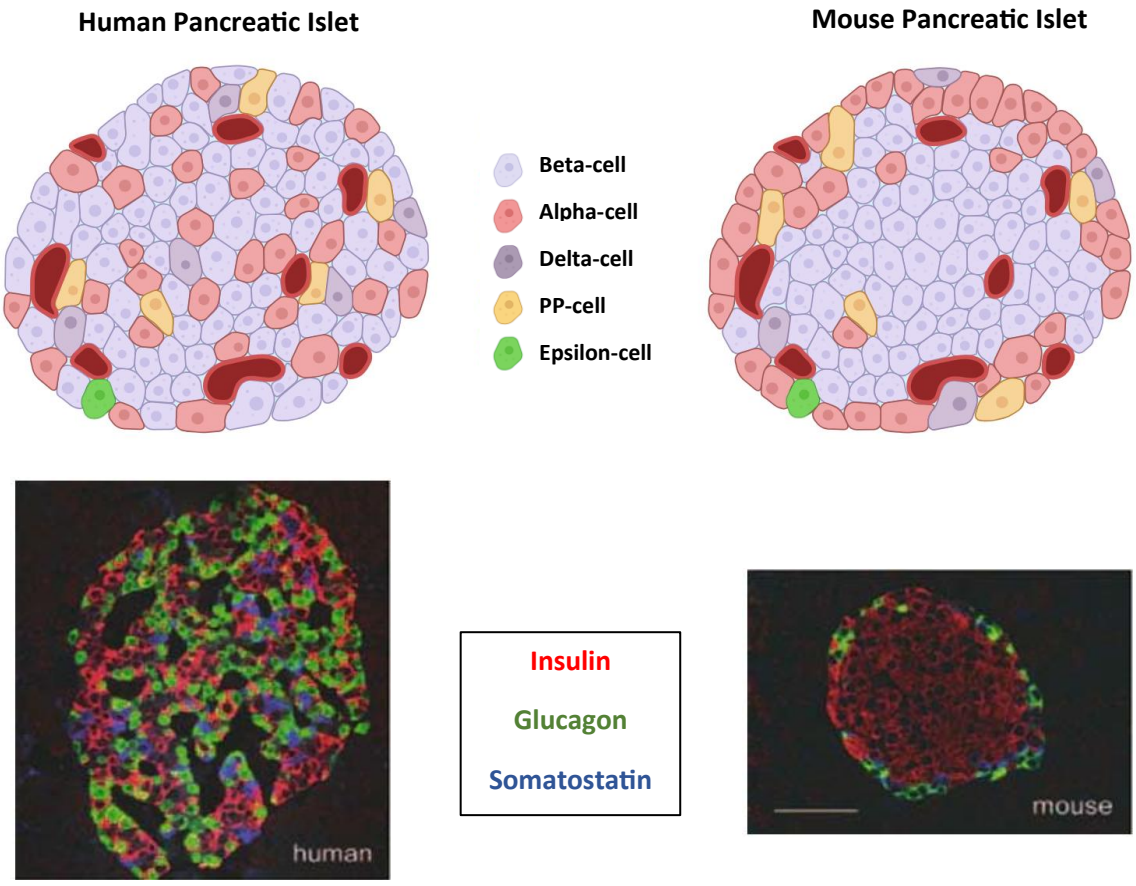

Figure 6: Architecture of human and mouse pancreatic islet. The image is adapted from (24).

The spatial organization of cells within the islet differs between humans and mice. In mouse islets, β-cells are predominantly located in the central core, while the other cell types are positioned at the periphery, forming a mantle (25). In humans, however, non-β-cells are not restricted to the periphery but are instead dispersed throughout the islet (25,34,39) (**Figure 6**). This arrangement may allow α-cells to more effectively influence β-cell function, even at low glucose concentrations, a regulatory mechanism that appears to be less efficient or absent in mouse islets (25,39).

3.4 β-cell

3.4.1 β-cell development:

The development of pancreatic β-cells is a highly regulated process that begins early in embryogenesis and continues through postnatal life. Pancreas development occurs in three major stages in mice: the **primary transition** (E9.5–E12.5), which involves the thickening of the endoderm and formation of dorsal and ventral pancreatic buds, containing multipotent pancreatic progenitors capable of differentiating into endocrine, exocrine, and ductal cells (40,41). The **secondary transition** (E12.5–birth) is characterized by the emergence of endocrine progenitors expressing *Neurogenin3 (Ngn3*), which delaminate from the epithelium and give rise to five distinct endocrine cell types: α, β, δ, PP, and ε cells (42–44) (**Figure 7**).

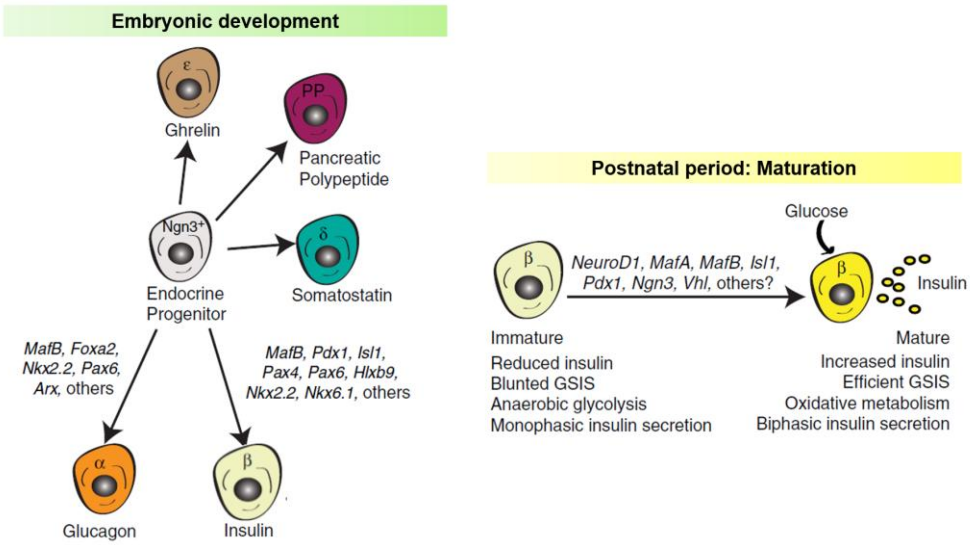

Figure 7: Embryonic and postnatal development of pancreatic endocrine cells. The image is adapted from (43).

β-cell differentiation is governed by key transcription factors such as *Ngn3*, *Pdx1, Nkx6.1, Nkx2.2, Pax6, Foxa2*, and *MafA*, which orchestrate the lineage commitment and their maturation (45). While fetal β-cells appear early during the secondary transition, they are initially immature and have limited ability to synthesize and secrete insulin. After birth, β-cells mature rapidly in response to new energy demands (41).

During this maturation process, β-cells undergo changes in gene expression, including increased levels of insulin-related genes such as *Ins2, Glut2, Glucokinase, and PCSK1/3,* which are expressed at much lower levels in neonatal cells compared to adults (46). Critical transcription factors, including *Pdx1, NeuroD1*, and *MafA*, regulate insulin production and secretion, ensuring proper β-cell function. Their dysfunction can impair insulin secretion and lead to diabetes (47).

The proper maturation of β-cells is vital for maintaining glucose homeostasis, and their dysfunction or loss is a hallmark of diabetes. Understanding β-cell maturation is key to developing therapeutic strategies, such as stem cell-based approaches or reprogramming techniques, aimed at treating diabetes (40,41,44,45,48).

3.4.2 Insulin biosynthesis

First discovered by Frederik Banting and Charles Best in 1921, insulin is a 51-amino-acid peptide hormone essential for glucose homeostasis, metabolism, and cell growth It is produced by pancreatic β-cells in response to elevated glucose levels (49).

The human insulin gene, *INS* (rodents have two: *ins1* and *ins2*), is located on chromosome 11 (50). It consists of three exons and two introns. Only exons 2 and 3 encode mature insulin, while exon 1 contains a 5′ untranslated region with a regulatory role in insulin expression (51). The transcription of *INS* is controlled by upstream enhancer elements that bind key transcription factors, including PAX6 (52), PDX1 (53), MafA (54), and NeuroD1 (55), along with several coregulators. These transcription factors regulate insulin expression by binding to the enhancer region (−340 to −91) (56). Additionally, insulin can promote its own transcription through an autocrine mechanism that influences enhancer-mediated activation (57).

During biosynthesis **(Figure 8),** the insulin gene is transcribed into mRNA with the aid of various transcription factors. The translation of preproinsulin occurs at the cytosolic surface of the ER, and the protein is translocated into the ER (51). Inside the ER, the signal peptide is cleaved by peptidase, forming proinsulin, which folds in the ER lumen, establishing three evolutionarily conserved disulfide bonds essential for insulin's structure (58). Properly folded proinsulin exits the ER and moves to the Golgi apparatus, where it is sorted and packaged into secretory vesicles (59).

Within these vesicles, prohormone convertases 1/3 and 2 (PC1/3 and PC2) and carboxypeptidase excises the C-peptide, producing mature insulin. Stored as zinc-stabilized hexamers, insulin remains in the secretory vesicles of pancreatic β-cells until the β-cell receives stimuli triggering exocytosis (51,59).

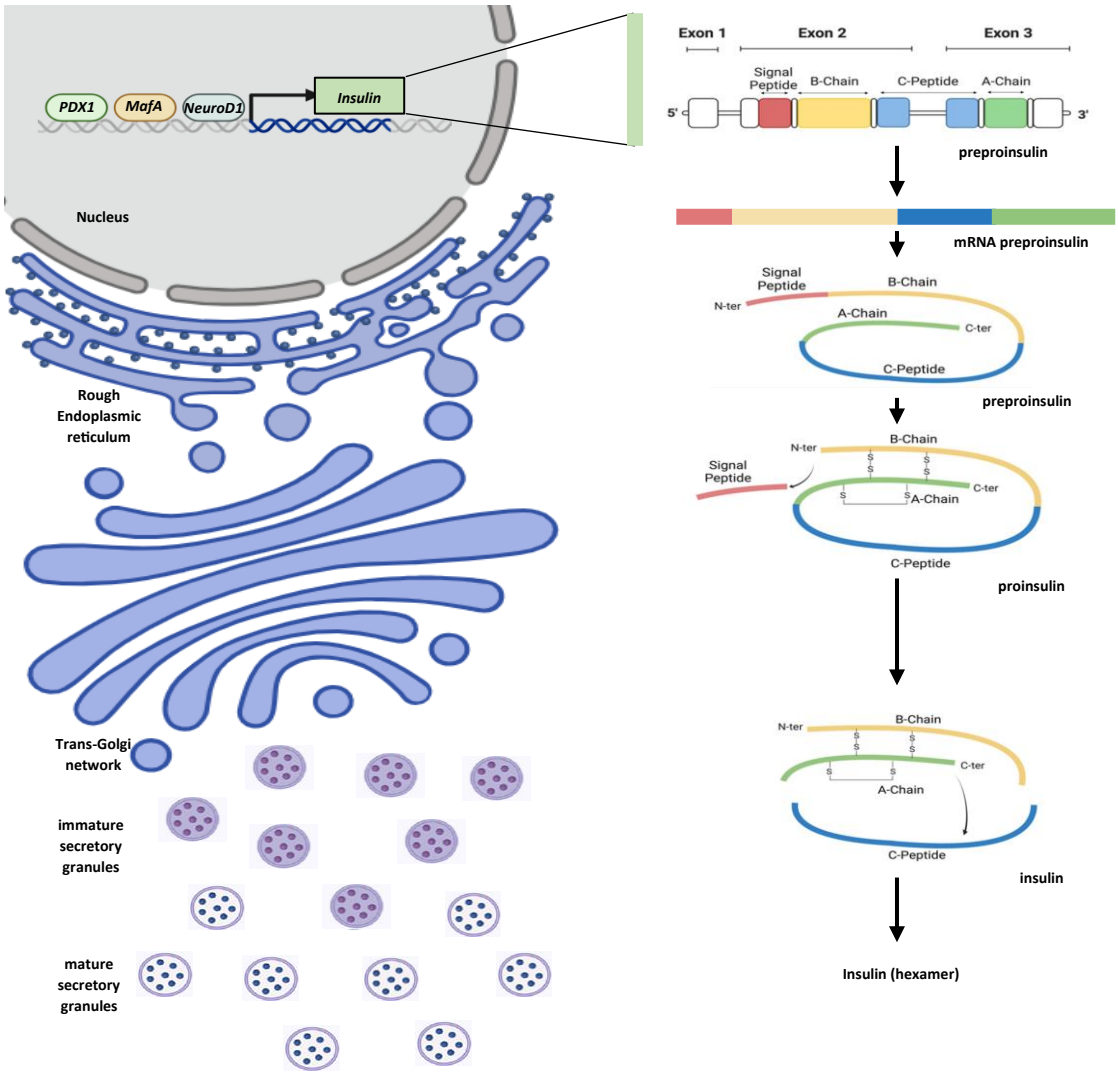

Figure 8: Insulin biosynthesis: Insulin maturation along the granule secretory pathway. The image is adapted from (51).

3.4.3 Insulin secretion

Glucose sensing and calcium dynamics in insulin secretion

The primary physiological stimulus for insulin secretion is the postprandial increase in circulating glucose concentration, a process known as glucose-stimulated insulin secretion (GSIS) (32). Pancreatic β-cells act as glucose sensors due to the presence of glucose transporters (GLUT) in their plasma membranes. Glucose enters mainly via the GLUT2 transporter, whereas in humans, GLUT1 has also been implicated in this process (60,61). These transporters exhibit distinct kinetic properties: GLUT1 operates efficiently at glucose concentrations of 1-3 mM, while GLUT2 functions at 15-20 mM (62).

Once inside the β-cells, glucose is rapidly phosphorylated by glucokinase (GK) to generate glucose-6-phosphate, which, through glycolysis, produces pyruvate. Pyruvate enters the mitochondria, where the tricarboxylic acid (TCA) cycle promotes the export of protons (H+) from the mitochondrial matrix via the electron transport chain, leading to

adenosine triphosphate (ATP) generation from adenosine diphosphate (ADP) by ATP synthase. This process increases the ATP/ADP ratio, which inhibits ATP-sensitive potassium (K_{ATP}) channels (formed by two subunits: SUR1 and Kir6.2). The closure of these channels leads to membrane depolarization (approximately -50 mV) (63,64). This activates voltage-dependent Ca^{2+} channels (VDCC), allowing Ca^{2+} influx into the cell (65). The resulting Ca^{2+} influx completes the signaling cascade, leading to insulin release (**Figure 9**) (66).

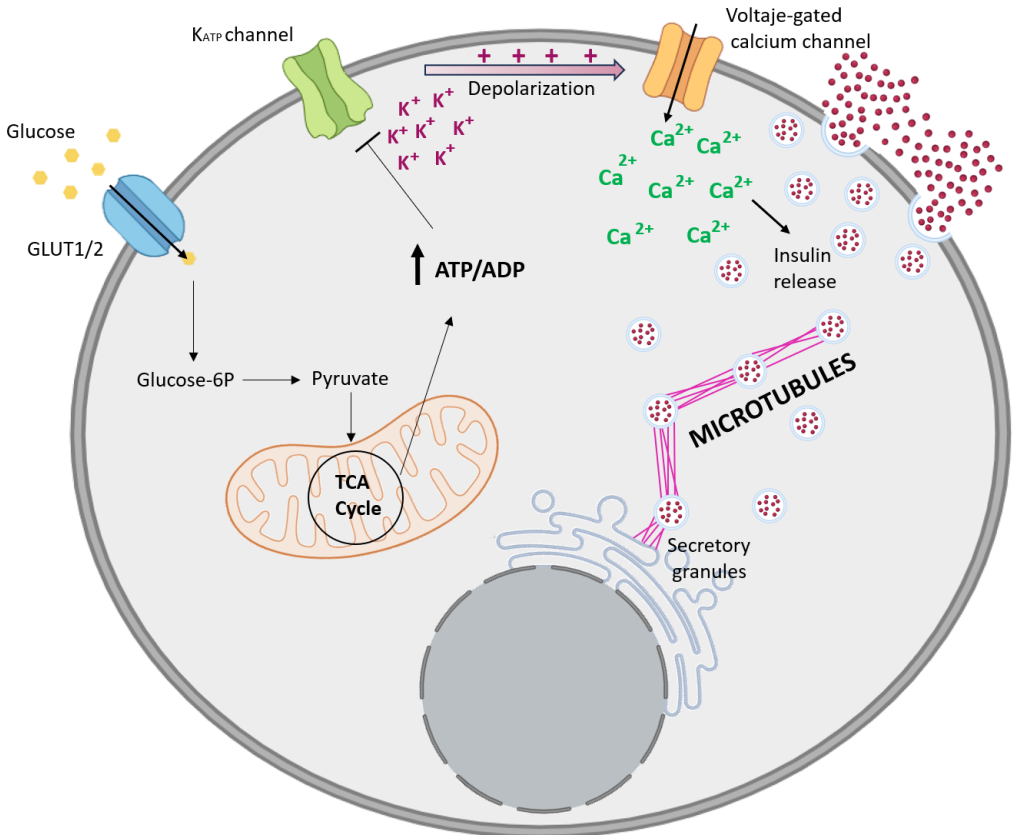

Figure 9: Mechanism of GSIS in pancreatic β-cell. This figure was created using *Biorender.*

The rise in cytosolic Ca^{2+} is tightly regulated by transport mechanisms, including the plasma membrane Ca^{2+} ATPase (PMCA), which pumps Ca^{2+} out of the cell, and the sarco-endoplasmic reticulum Ca2+ ATPase (SERCA), which sequesters Ca^{2+} into the ER (50). These mechanisms of regulation ensure that Ca^{2+} oscillations persist.

Oscillatory Ca^{2+} signaling is essential for coordinating insulin secretion among β-cells within the pancreatic islets (67). This synchronization is facilitated by connexin 36 (Cx36), a gap junction protein that allows intercellular electrical and metabolic coupling (68). Communication between cells contributes to the phenomenon of insulin secretory oscillations, which occurs with a periodicity of 5-10 minutes (min) in healthy humans (69).

Biphasic pattern of insulin release

Each pancreatic β-cell contains more than 10,000 insulin-containing secretory granules, but only 2% of them are ultimately released (70,71). These granules are functionally divided into two distinct pools: the readily releasable pool (RRP), which comprises less than 5% of the total and is in close proximity to the plasma membrane, within approximately 20 nm (72); and the reserve pool (RP), which contains the majority of granules and is stored farther away from the membrane (70).

Upon glucose stimulation, granules from the RRP are rapidly released, giving rise to the first phase of insulin secretion (72). Insulin secretion follows a biphasic pattern. The second phase is slower, more sustained, and results from the mobilization and translocation of granules from the RP to the RRP in response to continued glucose stimulation (70,73,74). This recruitment is essential to maintain insulin release over time and is tightly regulated by intracellular signaling pathways and cytoskeletal dynamics.

Intracellular trafficking of insulin granules

Insulin granules are transported along the cytoskeleton from the trans-Golgi network to the cell periphery, a process tightly regulated by both microtubules and actin filaments (75–78). These structures not only provide mechanical support but also direct granule movement and availability (79). In β-cells, microtubules emerge from the Golgi and form a dense, non-radial meshwork throughout the cytoplasm, acting as tracks for granule trafficking to the plasma membrane (76,80,81). Importantly, this network is dynamic: elevated glucose levels trigger microtubule depolymerization, facilitating granule access to exocytic sites and enhancing insulin secretion (82).

Actin filaments, which form a dynamic cortical network beneath the plasma membrane, also play a crucial role in the final steps of insulin granule release. Actin filaments regulate the docking and fusion of granules with the plasma membrane, ensuring that insulin is secreted efficiently upon stimulation (83,84). Initially, actin filaments serve as a physical barrier, preventing granules from accessing the membrane. However, upon glucose stimulation, actin undergoes remodeling, allowing the release of insulin granules to the exterior (85,86) **(Figure 10).**

Therefore, the cooperative interplay between microtubules and actin filaments is essential for the proper localization of granules and their eventual exocytosis.

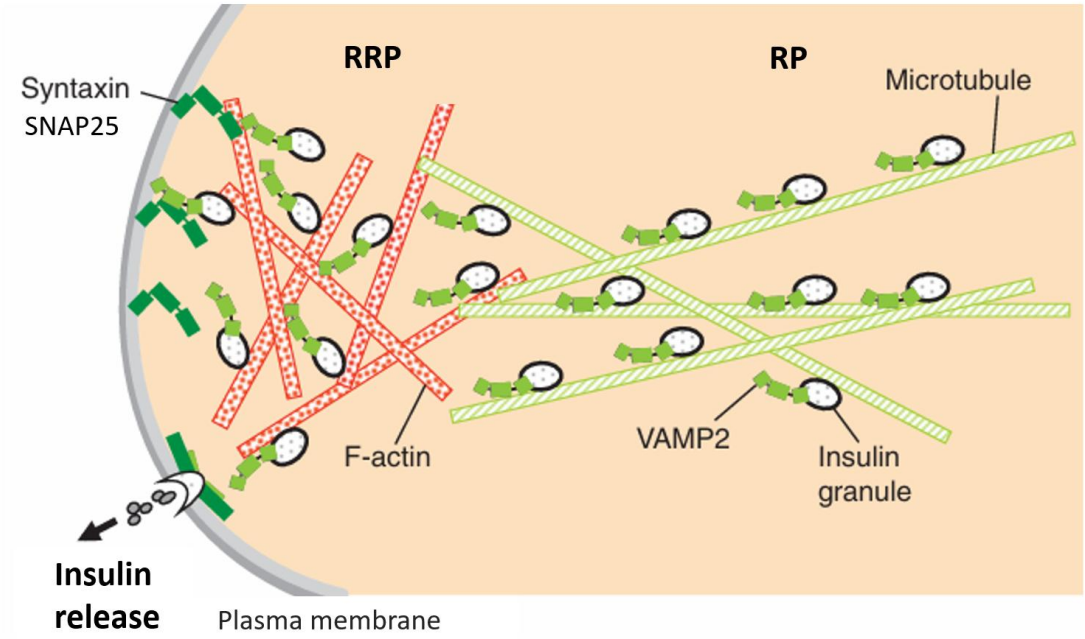

Figure 10: Mechanisms of biphasic insulin-granule exocytosis: Role of the cytoskeleton, small GTPases and SNARE proteins (syntaxin, SNAP-25, VAMP-2). The image is adapted from (85).

Insulin exocytosis

Once insulin granules reach the plasma membrane, they undergo exocytosis to release their contents towards the extracellular space. This process is driven by a highly conserved molecular machinery driven by Soluble N-ethylmaleimide-sensitive factor Attachment Protein Receptors (SNARE), which mediate the precise docking and fusion of granule and plasma membranes. Specifically, the v-SNARE VAMP2 is located on the granule membrane, while the t-SNAREs syntaxin-1A and SNAP-25 reside on the plasma membrane. Upon stimulation, these proteins form a stable ternary complex that brings the membranes into proximity, facilitating their fusion and allowing insulin release (87,88) **(Figure 11).**

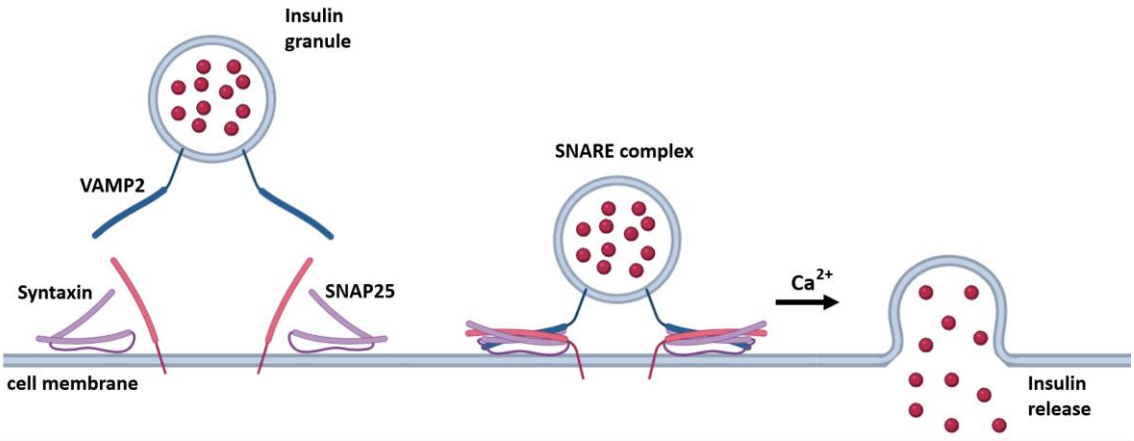

Figure 11: Formation of SNARE proteins complex. This figure was created using *Biorender.*

3.4.4 Other activators of insulin secretion

While glucose is the primary stimulus for insulin secretion, other factors can enhance or modulate this process. Paracrine signals from neighboring α- and δ-cells exert an important control on insulin secretion (50); Neurotransmitters such as acetylcholine, acting through muscarinic receptors, potentiate insulin release via phospholipase C (PLC) activation and Ca^{2+} mobilization (89). Incretin hormones like glucagon-like peptide-1 (GLP-1) and glucose-dependent insulinotropic peptide (GIP) amplify insulin secretion by increasing cAMP levels and enhancing Ca^{2+} influx (90,91). Additionally, amino acids, particularly leucine and arginine, serve as metabolic activators of insulin secretion by modulating intracellular ATP production and K_{ATP} channel activity (92,93).

3.5 Paracrine communication

The main pancreatic islet cells: α, β, and δ, secrete hormones that can regulate glucose homeostasis and energy metabolism by entering the bloodstream. These hormones also have local effects on neighboring cells within the islet through a process known as paracrine signaling, ensuring a coordinated response to fluctuations in glucose levels. (94–96).

β-cells, in addition to secreting insulin, can release other signaling molecules such as gamma-aminobutyric acid (GABA), zinc ions (Zn^{2+}), ATP, serotonin (5-hydroxytryptamine, 5-HT), and urocortin-3 (UCN3), which modulate the activity of neighboring α- and δ- cells. Insulin, 5-HT (97), and GABA (98) inhibit glucagon release from α-cells. In contrast, insulin and UCN3 stimulate δ-cells (94,99). α-cells, in turn, enhance glucose stimulated insulin secretion (GSIS) primarily by releasing glucagon, but also through other peptides such as GLP-1 (96,100,101). δ-cells secrete somatostatin, a potent inhibitor of both insulin and glucagon secretion, helping to prevent excessive secretions by the islet cells (94,102) **(Figure 12).**

Disruptions in these intra-islet cell interactions contribute to the glucose dysregulation observed in diabetes. (94,102,103).

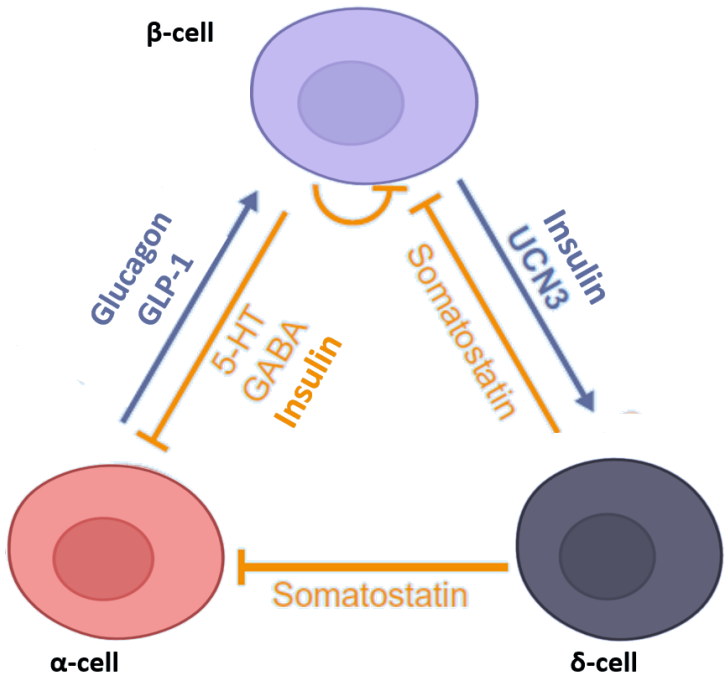

Figure 12: Paracrine regulation within the pancreatic islet. The interaction between β, α, and δ cells is illustrated. Orange arrows indicate inhibition, while blue arrows indicate activation. The image is adapted from (94).

3.5.1 Glucagon signaling in β-cell: Mechanisms and intracellular pathways

Glucagon is a hormone produced by α-cells whose primary physiological function is to maintain euglycemia through its action on the liver, promoting glycogenolysis and gluconeogenesis. In addition to its systemic role, glucagon exerts important paracrine effects within the islet, regulating the function and survival of islet endocrine cells (104,105). It is well established that glucagon enhances insulin secretion through a paracrine mechanism acting on β-cells, mediated primarily by the glucagon receptor (GcgR) (106) and also by the GLP-1 receptor (GLP-1R) (96,107), particularly under conditions of high glucose conditions (96). Both receptors belong to the family of G-protein coupled receptors.

Upon activation, GcgR and GLP-1R predominantly couple to the Gs proteins, stimulating adenylyl cyclase and increasing cAMP levels. The rise in cAMP activates protein kinase A (PKA) and exchange proteins directly activated by cAMP (EPAC) (108,109), which together enhance calcium influx and promotes insulin secretion (110,111).

Beyond insulin secretion, glucagon signaling also regulates the expression of insulin transcription genes. Specifically, cAMP response element-binding protein (CREB) is phosphorylated at serine 133 by PKA (112), inducing a conformational change that enables its translocation to the nucleus. There, phosphorylated CREB (pCREB) binds to the cAMP response element (CRE) and recruits the co-activator CREB-binding protein

(CBP) (113), leading to the transcription of genes involved in β-cell survival, proliferation, and insulin biosynthesis (114).

EPAC also plays a key role in this signaling cascade by acting as a guanine nucleotide exchange factor (GEF) for the small GTPase Rap1. Upon cAMP binding, EPAC undergoes a conformational change that enables it to catalyze the exchange of guanosine diphosphate (GDP) for guanosine triphosphate (GTP) on Rap1 (115). Activated Rap1-GTP initiates downstream signaling pathways, notably the MAPK/ERK cascade, further supporting β-cell function by promoting gene transcription related to insulin biosynthesis and cell proliferation (109,116). Some studies suggest that extracellular signal-regulated kinase (ERK) activation may occur through PKA-dependent mechanisms (117). Additionally, β-arrestin-dependent signaling triggered by G-protein-coupled receptors (GPCR) activation can scaffold MAPK cascade components, promoting sustained ERK signaling (118,119) (**Figure 13**).

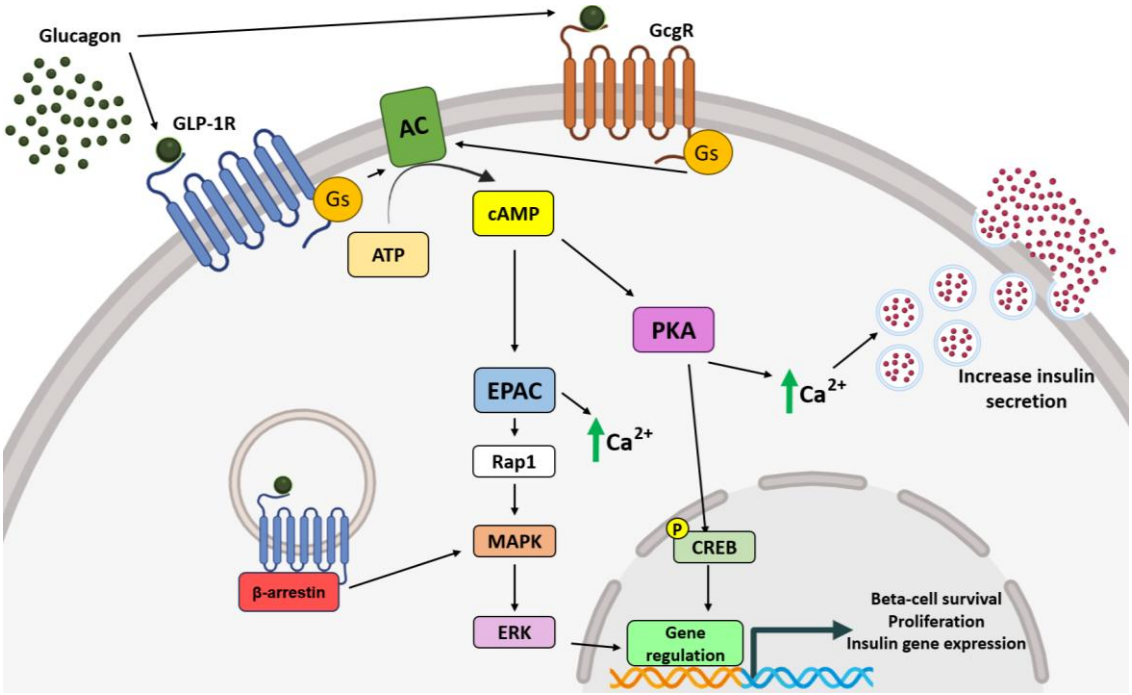

Figure 13: Glucagon signaling pathway in β-cell. This figure was created using *Biorender.*

While GcgR signaling in β-cells is well characterized through its coupling to G alpha subunit of the stimulatory G protein (Gαs), evidence for its coupling to Gαq in these cells remains limited. In other cell types, such as hepatocytes, GcgR has been shown to activate the PLC pathway via Gαq, leading to the generation of Inositol 1,4,5-trisphosphate (IP_3) and diacylglycerol (DAG), and subsequent activation of protein kinase C (PKC) (120). However, conclusive studies confirming this signaling route in pancreatic β-cells are still lacking.

3.6 Insulin-degrading enzyme

Insulin-degrading enzyme (IDE) is a highly conserved, zinc-dependent metalloendopeptidase. It is ubiquitously expressed in both insulin-responsive and non-responsive tissues, indicating that its physiological relevance extends far beyond insulin metabolism (119,120). The gene encoding IDE (*Ide*) shows remarkable evolutionary conservation, having been identified in diverse organisms ranging from bacteria to eukaryotes. This high degree of sequence preservation across species highlights the enzyme's functional importance and supports the idea of conserved biological roles maintained throughout evolution (121).

Historically referred to as "insulinase," IDE was initially characterized by its capacity to degrade insulin into smaller peptide fragments (122). Since then, research has significantly expanded our understanding of IDE, revealing a broader substrate repertoire and its involvement in multiple physiological and pathological processes.

3.6.1 Structure and localization

IDE is synthesized as a single polypeptide consisting of 1019 amino acids, with a molecular weight of approximately 110 kDa. Its gene is located on chromosome 10 in humans and chromosome 19 in mice (121,123).

The enzyme assembles as a stable homodimer, although it can also exist in a dynamic equilibrium between monomers, dimers, and tetramers (124). Each IDE monomer is composed of four homologous domains (1-4). Domains 1 and 2 make up the N-terminal portion of the protein (IDE-N), while domains 3 and 4 form the C-terminal portion (IDE-C). These two halves are connected by a 28-amino acid loop that contributes to the formation of a closed chamber where catalysis occurs. In the IDE dimer, the interface between monomers involves 18 residues from domains 3 and 4 (119,125) **(Figure 14).**

The catalytic site of IDE is located within domain 1 and features a Zn^{2+} ion coordinated by two histidines (His108 and His112) and one glutamate (Glu189) (119,126). Additionally, Glu111 plays a key catalytic role by activating a water molecule that acts as a nucleophile to mediate peptide bond hydrolysis. Although the active site is entirely within the IDE-N domain, IDE-C is essential for correct substrate recognition and positioning during catalysis (119,120).

The overall structure of IDE resembles a clamshell, with IDE-N and IDE-C forming a closed catalytic chamber just large enough to encapsulate peptide substrates. This configuration underlies its preference for intermediate-sized peptides (~20–40 amino

acids) and its unique substrate specificity, which is influenced more by the tertiary structure than by the primary amino acid sequence (119).

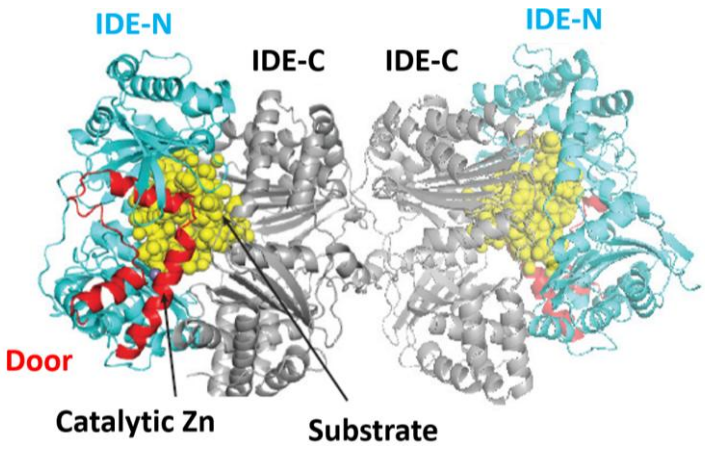

Figure 14. Homodimer structure of IDE. The N-terminal (IDE-N, blue) and C-terminal (IDE-C, gray) domains form two halves of a catalytic chamber. The substrate (yellow) is enclosed within this chamber, along with the catalytic zinc ion. The red region represents the "door" subdomain, which regulates substrate access. The image is adapted from (127).

During its catalytic cycle, IDE alternates between an open and a closed conformation (**Figure 15**). In the open state, substrates can enter the catalytic site and degradation products can be released. In the closed state, proteolysis occurs within the internal chamber (127,128).

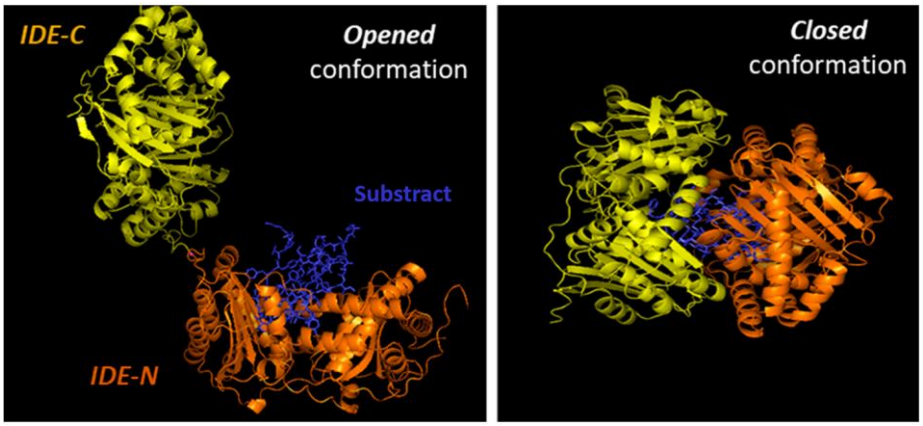

Figure 15: Cartoon illustrating the binding of substract by IDE. IDE is in an equilibrium between "opened" and "closed" conformational states. In the absence of a substrate (e.g., insulin), IDE is preferentially in the closed conformation. IDE must adopt the open conformation for substrates to enter the internal chamber, whereas the protease must assume the closed conformation for proteolysis to occurred. Release of the cleave products requires a return to the open conformation. The image is adapted from (119).

IDE is ubiquitously expressed across tissues and cell types. The subcellular localization of IDE is mainly cytosolic (129,130) but it has been reported to be present in several other subcellular compartments, as endosomes (131,132), peroxisomes (133), mitochondria (134), plasma membrane (135,136) and exosomes (137).

3.6.2 Proteolytic and non-proteolytic functions

Insulin is one of IDE's most well-characterized substrates, binding with high affinity (Km ~0.1 μM) (119). In addition, IDE also degrades other biologically active peptides, with lower affinity, such as glucagon (138,139), somatostatin (140), amylin (141), and amyloid-β (Aβ) (142,143) among others, supporting the multifunctional role of IDE in both metabolic and neurodegenerative contexts.

Beyond its proteolytic functions, IDE performs several non-proteolytic roles. It interacts with androgen and glucocorticoid receptors, enhancing their deoxyribonucleic acid (DNA) binding (144). IDE also interacts with cytoskeletal components like vimentin and nestin, which regulate the turnover and subcellular localization of proteins and peptides (145). In addition, IDE interacts with Sirtuin 4 (SIRT4), a mitochondrial protein that modulates insulin secretion (146), and α-synuclein (147). It has been shown to co-localize with Sorting Nexin 5 (SNX5), a protein involved in intracellular trafficking and insulin sensitivity regulation in kidneys (148). Some authors also propose that IDE has regulatory functions related to proteasome activity (149,150), and roles in growth and development, further expanding its functional repertoire (151).

3.6.3 The relationship between IDE and T2D

The implication of IDE in the pathophysiology of T2D has attracted increasing attention in recent years. Genetic polymorphisms in the *Ide* gene have been associated with impaired insulin metabolism and increased T2D risk (i.e., decreased insulin secretion, insulin sensitivity and hepatic insulin degradation) (152–156).

Elevated circulating levels of IDE have been observated in individuals with T2D and metabolic syndrome. Moreover, these levels have positively correlated with triglycerides, insulin, and C-peptide, whereas an inverse correlation has been reported with HDL-cholesterol (157). At the hepatic level, *Pivovarova and colleagues*, showed decreased hepatic *Ide* expression in subjects with T2D (158). This decrease in hepatic IDE expression and activity were linked to reduced insulin clearance and elevated plasma insulin levels (159). In contrast, *Villa-Pérez et al.* demonstrated that liver-specific *Ide* ablation (L-IDE-KO) in mice leads to normal plasma insulin levels and insulin clearance, although they showed insulin resistance (160).

Similar alterations have been identified in adipose tissue, where decreased IDE activity was found in adipocytes from both pre-diabetic and diabetic individuals (161). In the pancreas, IDE levels are reduced in β-cells of patients with T2D, a finding that may explain, at least in part, the β-cell dysfunction characteristic of the disease, as reported by *Fernández-Díaz* and colaborators (162).

Together, these findings demonstrate that IDE dysregulation occurs in several key tissues involved in glucose metabolism and may contribute to the development and progression of T2D. Further supporting this notion, the Goto-Kakizaki rat, a non-obese model of T2D, carries two coding mutations in the *Ide* gene, reinforcing its contribution to diabetes susceptibility (163).

3.6.4 Models of IDE deficiency

To better understand the role of IDE, several experimental models involving its ablation have been developed.

In 2003, the first study to characterize the phenotype of global IDE deficiency (IDE-KO) revealed that mice lacking IDE developed pronounced glucose intolerance, insulin resistance, and hyperinsulinemia by six months of age (164). In 2011, *Abdul-Hayan* confirmed and expanded these observations, reporting persistent glucose intolerance, fasting hyperinsulinemia, and insulin resistance in IDE-KO mice, supporting the idea that IDE deficiency contributes to progressive metabolic dysfunction (165).

In 2013, additional evidence demonstrated that GSIS in IDE-KO mice was impaired, likely due to defective replenishment of the releasable insulin granule pool. Moreover, a significant reduction in tubulin content was observed in β-cells of IDE-deficient mice, suggesting disrupted cytoskeletal dynamics. Interestingly, an inverse correlation between α-synuclein and IDE levels was found in β-cells of both IDE-KO mice and T2D patients, pointing to a potential link between IDE and protein aggregation pathways that may underlie β-cell dysfunction (166).

In the liver, tissue-specific deletion of IDE (L-IDE-KO) resulted in hepatic insulin resistance and glucose intolerance, particularly under high-fat diet conditions. Notably, these changes occur despite preserved insulin clearance, suggesting that hepatic IDE plays a role in insulin action independent of its degradative function (160). Conversely, hepatic overexpression of IDE improves glucose tolerance and enhances insulin sensitivity in obese mouse models, supporting its potential as a therapeutic target (167).

Models of IDE deficiency in pancreatic β-cells

Mice with β-cell-specific deletion of IDE (B-IDE-KO) showed constitutive insulin secretion and elevated plasma C-peptide levels, reflecting persistent insulin release. This phenotype is associated with increased GLUT1 expression and downregulation of genes related to β-cell maturation and insulin granule exocytosis, suggesting a role for IDE in maintaining β-cell identity and function. Despite normal glucose homeostasis, these mice developed hepatic insulin resistance, likely due to chronic hyperinsulinemia. These

findings support a non-proteolytic role of IDE in regulating insulin secretion and preserving β-cell maturity (168).

Models of IDE deficiency in pancreatic alpha-cells

Mice with α-cell-specific deletion of IDE (A-IDE-KO) develop hyperglucagonemia and hyperinsulinemia, along with hepatic glucagon resistance and α-cell hyperplasia. These alterations are linked to the inability of IDE-deficient α-cells to suppress glucagon secretion under high glucose levels or insulin inhibitory action. Additionally, α-synuclein aggregation and impaired primary cilia formation suggest cytoskeletal and signaling defects. Overall, these findings highlight a non-proteolytic role for IDE in regulating α-cell function and glucagon homeostasis, potentially contributing to T2D via chronic hyperglucagonemia (169).

3.6.5 IDE as a potential therapeutic target for T2D

Since its discovery, IDE has been investigated as a potential therapeutic target for T2D, based on the hypothesis that inhibition of insulin degradation could enhance and prolong insulin signaling. Early non-specific inhibitors, such as bacitracin and 1,10-phenanthroline, showed limited efficacy due to their poor selectivity and off-target effects (170–172). In response, more selective small-molecule inhibitors were developed, including Ii1, BDM41367, BDM44768, and the cyclic peptide 6bK. However, preclinical results have showed conflicting effects on glucose tolerance and insulin sensitivity (120).

Among these, 6bK has emerged as one of the most promising inhibitors. It is a cyclic peptide that blocks substrate access to the catalytic cleft. Studies have showed that 6bK improves oral glucose tolerance and reduces blood glucose levels in diet-induced obese mice. Nevertheless, when glucose was administered intraperitoneally, 6bK unexpectedly caused glucose intolerance, highlighting the complexity and context-dependence of IDE inhibition (171,173).

In addition, two other inhibitors, NTE-1 and NTE-2, were characterized. These compounds bind to the substrate anchoring site in the IDE-N domain. Both improved oral glucose tolerance in obese mice but did not produce significant changes in insulin tolerance (120).

These controversial results, along with altered IDE expression in T2D patients, have shifted focus toward activating IDE instead of inhibiting it. Recent studies have identified several promising activators, including Ia1, Ia2, and BDM35899 (174,175). Other compounds like resveratrol and carnosine show substrate-specific effects but have limitations due to poor bioavailability or toxicity (176,177).

Notably, we demonstrated that the Pre-Implantation Factor (PIF), embryo peptide that inhibits rejection by the mother in the first stage of pregnancy, enhances insulin secretion through IDE activation in pancreatic β-cells, improving glucose tolerance in diabetic mice (178,179). These findings suggest that IDE activation could be a promising therapeutic strategy for T2D.

3.7 The microtubule cytoskeleton

Microtubules are one of the three main components of the cytoskeleton in eukaryotic cells, along with actin filaments and intermediate filaments (180,181). They play essential roles in a wide range of cellular processes. For instance, microtubules form the mitotic spindle, the structure responsible for chromosome segregation during cell division (182). They also serve as the structural core of cilia and flagella, making them key elements for cell motility and function (183). In addition to these structural functions, microtubules serve as intracellular tracks for motor proteins that transport organelles, vesicles, and other cellular components (184), and they are crucial for maintaining cell organization by positioning organelles and establishing cell polarity (180).

3.7.1 Structure and dynamics of microtubules

Microtubules are formed by the polymerization of α- and β-tubulin heterodimers into long structures called protofilaments **(Figure 16)**. Typically, 13 protofilaments associate laterally to form a hollow, cylindrical tube. This organization creates structural polarity: the plus end, where β-tubulin is exposed, exhibits faster growth, while the minus end, with exposed α-tubulin, grows more slowly, is more stable and often anchored at the microtubule organizing center (MTOC) (180,184).

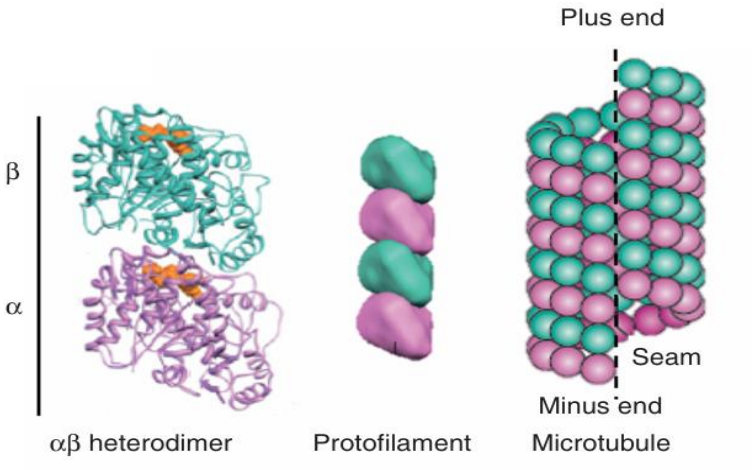

Figure 16: Microtubule structure. Image taken from (191).

Microtubule assembly begins with nucleation, a rate-limiting and energetically unfavorable process that depends on high local tubulin concentrations (185). This step is facilitated by the γ-tubulin ring complex (γ-TuRC), which acts as a scaffold for αβ-tubulin addition (186). In most cells, nucleation occurs at MTOCs, giving rise to a radial microtubule network that supports intracellular organization and polarity. Notably, in pancreatic β-cells, microtubule nucleation predominantly occurs at the Golgi apparatus, contributing to their specialized architecture (81).

A key feature of microtubules is their dynamic instability, they constantly switch between phases of growth and shrinkage, especially at the plus end (180,187). This behavior is controlled by the GTP molecule bound to β-tubulin. When tubulin dimers are added to the growing microtubule, β-tubulin carries GTP. After being incorporated into the microtubule, this GTP is slowly converted to GDP (188,189) **(Figure 17).**

As long as there is a “GTP cap” at the end, the microtubule stays stable and can keep growing. But if this cap is lost, because GTP is hydrolyzed faster than new dimers are added, the microtubule becomes unstable and rapidly breaks down, a process called catastrophe. Growth can start again if new GTP-tubulin dimers are added in time, which is known as rescue (190).

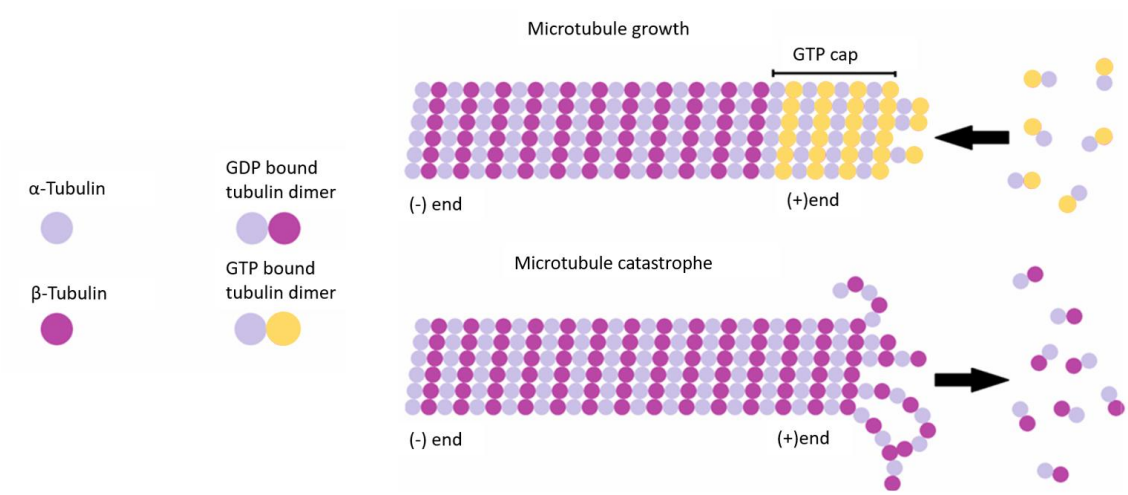

Figure 17: Schematic representation of microtubule formation and dynamic instability. Microtubules are composed of α- and β-tubulin heterodimers assembled into a hollow cylindrical structure. They elongate by the addition of GTP-bound dimers at the plus (+) end, forming a GTP cap that stabilizes the microtubule. Loss of this GTP cap triggers rapid depolymerization, or shrinkage, of the microtubule. The image is adapted from (180).

This GTP/GDP cycle is essential for the function of microtubules, allowing them to quickly reorganize and adapt to the needs of the cell, such as during cell division, transport of materials, and maintenance of cell shape.

3.7.2 Microtubule-binding proteins (MTBPs)

Microtubule-binding proteins (MTBPs) are a diverse group of proteins that interact with microtubules to regulate their stability, organization, and dynamics. Among them, microtubule-associated proteins (MAPs) represent a well-characterized subgroup that bind along the microtubule lattice and often act as stabilizers. MTBPs can be classified into different functional categories, including stabilizers, destabilizers, capping proteins, and bundling or cross-linking proteins. In addition to their structural roles, some MTBPs function as motor proteins involved in intracellular transport, while others interact with different cytoskeletal components or contribute to cellular processes such as signal transduction, translation, and metabolism (180).

Stabilizers: Enhance microtubule polymerization or inhibit depolymerization, often by cross-linking protofilaments. This group includes classical MAPs (tau, MAP2, MAP4) (191), STOP proteins (192), and members of the doublecortin and endothelial-monocyte activating polypeptide (EMAP) families (193).

Destabilizers: Promote microtubule disassembly through different mechanisms. Sequestering free tubulin (e.g., stathmin) (194), targeting microtubule ends, tip-destabilizing, such as kinesin-13 (195) or severing proteins like katanin and spastin, which cut microtubules into fragments, generating new ends that lack protective GTP caps and therefore leading to rapid depolymerization (196,197).

Capping proteins. Bind to microtubule ends, blocking growth or shrinkage. γ-TuRC caps and nucleates minus ends (186), while proteins like calmodulin-regulated spectrin-associated proteins (CAMSAPs) can associate with minus ends and stabilize them to varying degrees (180).

Bundlers cross-linkers: facilitate lateral interactions between microtubules, organizing their arrangement. For instance, MAP65/Ase1/PRC1 bundle antiparallel microtubules during mitosis (198).

Cytoskeletal integrators: Connect microtubules to actin or intermediate filaments, coordinating functions like cytokinesis and polarity. These include Adenomatous Polyposis Coli (APC), plakins, formins, myosin-10, and Tau (199,200)**.**

Other associated proteins include motor proteins (e.g., kinesin, dynein), motor modulators (e.g., tau), membrane linkers (e.g., CLIMP63), and metabolic enzymes, which can affect microtubule behavior, linking cytoskeletal dynamics to cellular metabolism (180).

MTBPs also differ by localization: some bind along the microtubule lattice, while others target dynamic ends, plus-end tracking proteins (+TIPs), like EB1, track growing plus ends, whereas proteins like CAMSAPs bind to minus ends (201).

3.7.3 Regulation of microtubule dynamics by environmental factors and drugs

Microtubule dynamics are highly sensitive to environmental changes and various drugs. Factors such as low tubulin concentration, cold temperatures, or high Ca^{2+} levels can induce rapid depolymerization. The microtubule state can also be manipulated by small molecules; agents like taxol promote microtubule assembly and stabilize them (202), while drugs like nocodazole and colchicine destabilize microtubules. This ability to alter microtubule dynamics is crucial in some medical treatments, and ongoing research aims to develop new compounds that specifically target microtubule (203). In addition, there is increasing focus on drugs that target MTBPs.

Due to their essential role in cell division, microtubules have become prominent pharmacological targets in cancer therapy. Many chemotherapeutic agents exert their effects by disrupting microtubule dynamics, thereby blocking mitosis and triggering apoptosis in rapidly dividing tumor cells. Among the most widely used are taxanes (e.g., paclitaxel), which stabilize microtubules and prevent their disassembly, and vinca alkaloids (e.g., vincristine), which inhibit tubulin polymerization. Despite their efficacy, these drugs can also affect normal proliferating cells and may lead to drug resistance. Nevertheless, microtubule-targeting agents remain a cornerstone of modern anticancer therapies (204).

3.7.4 Microtubules undergo posttranslational modifications

Microtubules are subject to a range of post-translational modifications (PTMs) that generate a so-called "tubulin code," which modulates microtubule behavior and influences interactions with MAPs and motor proteins (205,206).

One of the most well-characterized PTMs is **acetylation**, which involves the addition of an acetyl group to lysine 40 (K40) of α-tubulin (207). This modification occurs on the luminal side of the microtubule and is catalyzed by α-tubulin acetyltransferase 1 (αTAT1) (208,209), while it is reversed primarily by the histone deacetylase HDAC6 (210). Acetylation is associated with increased microtubule stability and longevity, and is particularly enriched in stable structures such as cilia and axons, where it supports structural integrity (211,212).

Other stabilizing PTMs include **polyamination**, catalyzed by transglutaminases, which add polyamines to glutamine residues on tubulin. This modification is especially abundant in neuronal axons and testes, where it enhances microtubule stability under depolymerizing conditions (213). **Detyrosination** also contributes to microtubule stabilization. In this modification, the C-terminal tyrosine of β-tubulin is removed after incorporation into microtubules by an unidentified carboxypeptidase. This is reversible via tubulin tyrosine ligase (TTL), unless further processing leads to D2-tubulin, an irreversible form that disrupts recycling and alters motor protein binding (214–216). **Tyrosinated** tubulin is generally associated with dynamic microtubules, whereas detyrosinated tubulin accumulates in stable ones, influencing interactions with motor proteins and +TIPs (217).

Similarly, **polyglutamylation** and **polyglycylation** involve the reversible addition of glutamate or glycine chains to specific glutamate residues on the C-terminal tails of α- and β-tubulin (205,218). These modifications are particularly enriched in cilia and flagella, where they modulate the interaction between microtubules and axonemal structures (219,220).

Lipid-based and ubiquitin-like modifications also modulate microtubule function. **Palmitoylation** at Cys376 of α-tubulin alters membrane interactions (221), while **ubiquitylation** promotes tubulin degradation and has been linked to neurodegenerative disease and flagellar disassembly (222). **Sumoylation** influences trafficking and neuronal functions (223).

Phosphorylation, occurring on serine, threonine, or tyrosine residues, is critical during mitosis and cellular stress, and can affect MAP binding (235). Notably, phosphorylation sites often overlap with those used by other PTMs, such as **O-linked glycosylation** (224), which involves the enzymatic addition of carbohydrates to serine or threonine residues. A key variant, **O-GlcNAcylation**, adds N-acetylglucosamine (GlcNAc) and is dynamically regulated by O-GlcNAc transferase (OGT) and O-GlcNAcase (OGA). In tubulin, this modification reduces heterodimerization and impairs polymerization (225). Excessive O-GlcNAcylation in pancreatic β-cells disrupts glucose homeostasis, indicating that this modification can contribute to cellular dysfunction (226).

In contrast, **non-enzymatic glycation** occurs under hyperglycemic conditions when glucose reacts with amino acids. This pathological modification has been linked to diabetes and, in axons, can denature tubulin and depolymerize microtubules, contributing to diabetic neuropathy (227).

Tubulin PTMs are complex, and they are regulated in a cell-specific way, affecting microtubule dynamics, cell function, and disease progression.

3.7.5 Microtubules in insulin secretion and diabetes

Microtubules are key components of the cytoskeleton that support both the structural organization and specialized functions of pancreatic β-cells. Unlike the classic radial arrangement observed in many other cell types, the microtubule network in β-cells is predominantly non-radial. This is because most microtubules originate from the Golgi apparatus rather than the centrosome, (Golgi-derived microtubules, (GDMTs) (228,229). This contributes to the complex architecture of the β-cell microtubule network. Moreover, these microtubules are highly stables (230).

β-cells show notable heterogeneity in microtubule organization, which parallels differences in their metabolic activity, insulin content, and glucose responsiveness (231). It is required to further explore local microtubules organization and its functional implications across different β-cell subtypes.

The microtubule network in β-cells is dynamically regulated in response to glucose, allowing these cells to rapidly adapt to metabolic demands. Under low-glucose conditions, microtubules are notably stable; however, upon glucose stimulation, they undergo rapid remodeling characterized by both depolymerization of existing filaments and polymerization of new ones (76,82,232). This turnover begins within min of glucose exposure and is largely mediated by Tau protein hyperphosphorylation via glucose-activated kinases, leading to Tau dissociation from microtubules. When Tau becomes hyperphosphorylated, it detaches from the microtubules (230). Notably, this process might involve katanin-mediated severing, as Tau is known to protect microtubules from this mechanism (228,233).

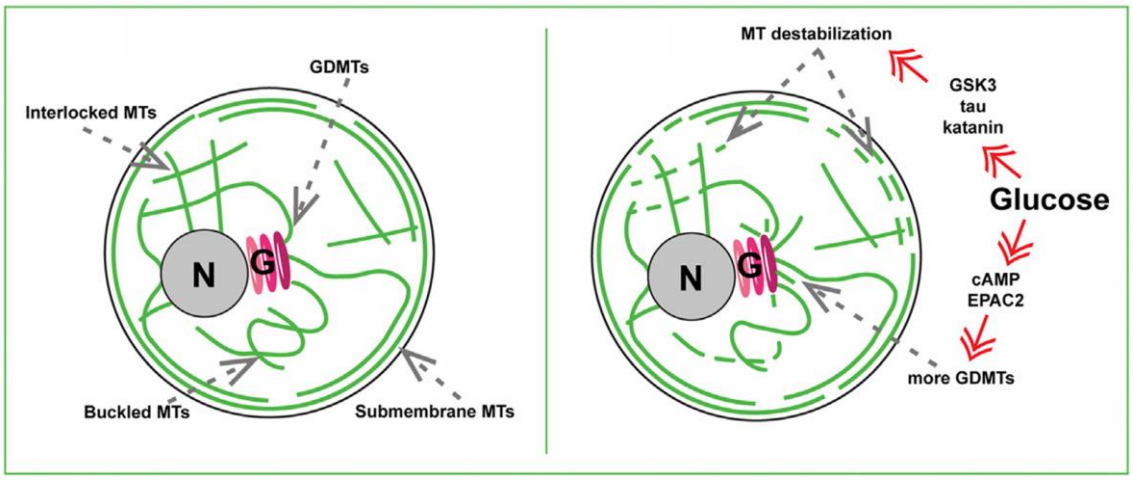

Figure 18: High-glucose triggered microtubules remodeling via two signaling axes. Taken from (228).

Concurrently, glucose stimulation also promotes nucleation at the Golgi apparatus and accelerates growth at the microtubules plus-ends. Interestingly, the pathways regulating microtubules disassembly and reassembly are distinct: depolymerization relies on ATP and kinases, while polymerization at the Golgi is driven by cAMP and EPAC2 (234). This dual regulation indicates that microtubules remodeling is finely tuned by separated metabolic pathways, allowing selective modulation of microtubules subsets during insulin secretion.

In diabetic models, dysfunctional β-cells exhibit an abnormal increase in microtubule density, which may contribute to impaired insulin secretion (82). These findings suggest that targeting the cytoskeletal network could be a promising therapeutic approach, with microtubule-targeting agents potentially repurposed for diabetes treatment.

3.8 Primary cilia

3.8.1 Primary cilia structure:

Primary cilia are sensory organelles on vertebrate cell surfaces that detect external stimuli and trigger intracellular signaling (235). They regulate key pathways like Hedgehog, Wnt, and platelet-derived growth Factor (PDGF), playing a crucial role in cell proliferation, differentiation, tissue development, and metabolic homeostasis (236).

Structurally, primary cilia are built around a microtubule-based core known as the axoneme, which is composed of α- and β-tubulin heterodimers. The axoneme typically follows a “9+0” arrangement, consisting of nine outer microtubule doublets and lacking the central pair of microtubules, which makes these cilia non-motile (237). In contrast, motile cilia display a “9+2” organization that enables movement (238). The axoneme is anchored to the cell by the basal body, a key role in initiating ciliogenesis and organizing microtubule growth. The basal body is composed of nine triplet microtubules arranged circumferentially and maintains the transition zone, a selective barrier that regulates protein trafficking between the axoneme and the cytoplasm. The basal body is connected to the membrane through transitional fibers. The entire ciliary structure is surrounded by a specialized membrane enriched with signaling receptors, channels, and other molecules, enabling the cilium to function as a cellular antenna (235) **(Figure 19)**.

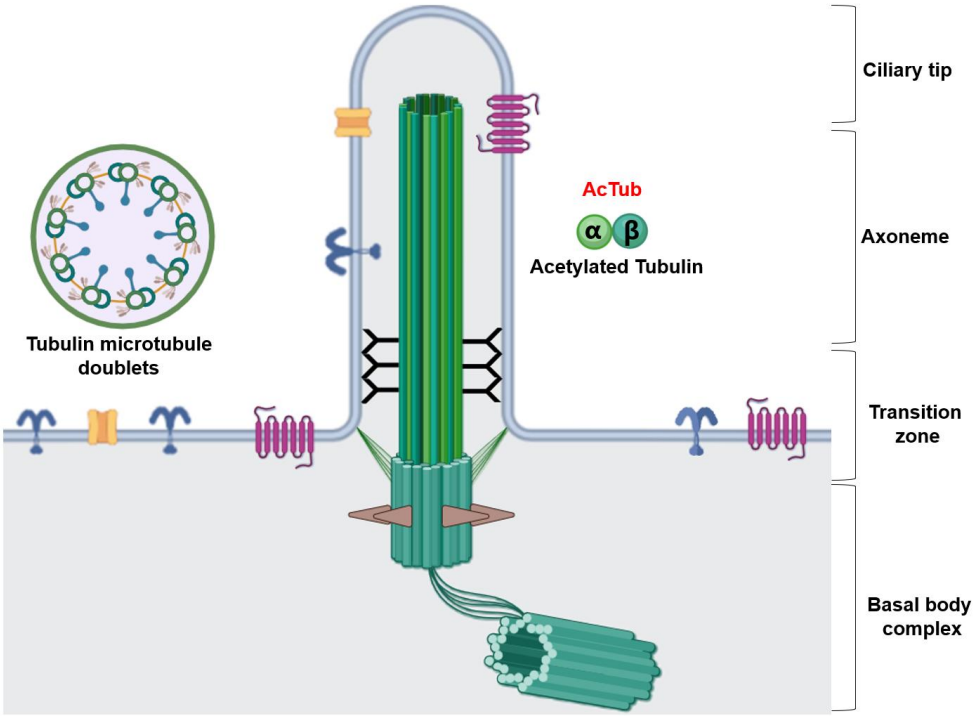

Figure 19. Structure of primary cilium. Schematic diagram of a typical non-motile primary cilium.

Tubulin forming the axoneme undergoes several post-translational modifications, such as acetylation and glutamylation, which enhance microtubule stability and play a regulatory role in ciliary signaling (211,212). Notably, acetylated tubulin is commonly used as a reliable marker for the visualization of primary cilia in immunofluorescence staining. Arl13b, a small GTPase of the ARF family, is also widely used as a ciliary marker and plays a critical role in ciliogenesis. A key feature of ciliary function is intraflagellar transport (IFT), a bidirectional trafficking system that moves protein complexes along the axoneme (239). Specifically, IFT88 plays a crucial role in this process, and its loss leads to defective ciliogenesis and the absence of primary cilia (240).

Ciliary integrity is also tightly coupled to the cell cycle: primary cilia are assembled during G0/G1, contributing to polarity and differentiation, and they are resorbed prior to mitosis (241).

Defects in primary cilia are linked to a variety of inherited developmental and degenerative diseases, known as ciliopathies, affecting multiple organs (235).

3.8.2 Primary cilia functions in pancreas β-cells

Primary cilium is found in differentiated endocrine α-, β-, and δ-cells (242). In pancreatic β-cells, the primary cilium plays a central role in maintaining proper function, identity, and organization. These antenna-like organelles coordinate key signaling pathways, such as fibroblast growth factor (FGF), Hedgehog (Hh), Wnt, TGF-β, and Notch, that are

essential for pancreatic development and endocrine regulation (243). Specifically, in β-cells, the cilium senses extracellular cues and integrates signals that regulate insulin secretion and β-cell fate. For example, ciliary Hh signaling modulates insulin gene expression and secretion, preserves β-cell identity, and protects against cytokine- and ER stress-induced apoptosis (244–246).

Disruption of ciliogenesis, such as deletion of Kif3a, a gene essential for intraflagellar transport, leads to reduced β-cell proliferation and defective GSIS (247). Similarly, knockout of the transcription factor Rfx3 results in shortened or absent cilia, reduced β-cell mass, and impaired glucose tolerance (248). Complete loss of cilia, as observed in IFT88-deficient β-cells, leads to impaired GSIS and dedifferentiation, further confirming the necessity of intact primary cilia for β-cell maturation and functional competence. Furthermore, the absence of β-cell cilia also disrupts circulating levels of glucagon and somatostatin, suggesting that primary cilia regulate glucose homeostasis through islet paracrine interactions (249). Indeed, recent evidence shows that somatostatin triggers local cAMP and Ca^{2+} signaling within primary cilia to modulate β-cell responses to paracrine cues (250).

In addition, deletion of LKB1 (STK11), a kinase that regulates cilia positioning, does not affect ciliogenesis per se, but causes mislocalized cilia. This misorientation leads to β-cell hypertrophy via mechanistic target of rapamycin (mTOR) activation, insulin hypersecretion, and loss of polarity. LKB1-deficient mice display pancreatic defects that resemble those of cilia-deficient models, emphasizing the role of ciliary orientation in coordinating insulin release and maintaining islet architecture (251).

Altogether, these findings highlight the primary cilium as a key structural and signaling hub in β-cells, required for proper development, identity maintenance, and glucose-responsive insulin secretion.

3.8.3 Ciliopathies and T2D

Ciliopathies are genetic disorders caused by ciliary dysfunction. Two well-known examples, Alström syndrome (ALMS) (252) and Bardet-Biedl syndrome (BBS)(253,254), are both associated with obesity and pancreatic islet dysfunction, yet they present distinct β-cell phenotypes. In individuals with ALMS, early-onset T2D is commonly observed due to impaired glucose sensing and defective insulin secretion by β-cells. ALMS1 deficiency has been associated with reduced β-cell proliferation and increased apoptosis, contributing to β-cell failure in Alström syndrome (252). In contrast, the loss of BBS proteins, critical for trafficking signaling receptors to the cilium, disrupts insulin signaling and impairs β-cell differentiation (247,253).

Support to this link between primary cilia and diabetes also comes from T2D animal models. For instance, in the *Goto-Kakizaki* rat, a threefold reduction in primary cilia in β-cells has been reported, along with misexpression of ciliary and basal body-related genes (255). Similarly, the *ob/ob* mouse model of obesity and diabetes shows dysregulation of these same genes in pancreatic islets (256). Importantly, recent evidence indicates that in individuals with type 2 diabetes, the length of primary cilia in pancreatic islets is reduced, further supporting a link between ciliary dysfunction and β-cell impairment (250).

Together, these findings point to the primary cilium as a key regulator of β-cell identity, proliferation, and insulin secretion. A deeper understanding of how ciliary signaling intersects with endocrine regulation could open the door to novel therapeutic strategies aimed at preserving β-cell function and glucose homeostasis in diabetes.

3.8.4 Primary cilia and IDE

As previously described in the section on IDE-deficient models, IDE deficiency in pancreatic β-cells (B-IDE-KO) leads to impaired insulin secretion and downregulation of genes involved in β-cell maturation and insulin granule exocytosis, resulting in chronic hyperinsulinemia and hepatic insulin resistance (168). These phenotypes closely resemble those observed in cilia-deficient β-cells, which exhibit impaired glucose-stimulated insulin secretion, dedifferentiation, and reduced β-cell mass (247–249). Notably, in pancreatic β-cells from individuals with diabetes, both IDE expression and primary cilium length have been observed to decrease (162,250), further supporting a potential link between IDE, ciliary structure, and β-cell dysfunction.

Supporting a more direct regulatory role, IDE deletion in α-cells (A-IDE-KO) causes tubulin disorganization and a marked reduction in primary cilia, accompanied by increased proliferation and altered glucagon secretion (169). These findings indicate that IDE can regulate cytoskeletal dynamics and ciliary structure, which in turn may influence β-cell function and overall islet hormone coordination.

Collectively, these observations underscore the role of IDE in preserving endocrine cell function, cytoskeletal organization, and ciliary integrity. The convergence of phenotypes in IDE- and cilia-deficient cells supports a model where IDE helps coordinate islet hormone secretion and glucose homeostasis, pointing to cytoskeletal and ciliary pathways as potential therapeutic targets in diabetes.

HYPOTHESIS AND AIMS

4. HYPOTHESIS AND AIMS

Hypothesis

General:

Physiological levels of IDE are required to preserve β-cell function by maintaining cytoskeletal organization and primary cilium integrity.

Specific:

1. Physiological levels of IDE are required to maintain proper β-cell metabolism and function.
2. IDE regulates the dynamics of the tubulin cytoskeleton in pancreatic β-cells.
3. IDE controls the formation and maintenance of the primary cilium.
4. IDE modulates β-cell paracrine signaling through the regulation of ciliary function.

Aims

The main aim of this study is to elucidate the physiological role of IDE in pancreatic β-cell function, focusing on its regulation of cytoskeletal organization and primary cilium integrity. This general aim can be divided into the following specific objectives:

1. To study the impact of partial IDE loss in cellular metabolism and β-cell function.
2. To investigate how IDE regulates the dynamics of the tubulin cytoskeleton in pancreatic β-cells under conditions of inhibition and secretion.
3. To determine the role of IDE in the formation and maintenance of the primary cilium.
4. To assess how IDE influences β-cell paracrine signaling through the modulation of ciliary function.

MATERIALS AND METHODS

5. MATERIAL AND METHODS

5.1 Experimental animals

5.1.1 Animal facilities

The experimental procedures were approved by the University of Valladolid Research Animal Ethical Committee and the JCyL authorities (Protocol No. #5003931), adhering to the European Guidelines for the Care and Use of Mammals in Research (European Commission Directive 86/609/CEE and Spanish Royal Decree 1201/2005).

Rodents were housed in ventilated cages enriched with cotton bedding on a cycle of 12 h of light, 12 h of darkness cycle at the animal facility of the University of Valladolid (UVa, Spain). Mice were fed standard rodent chow diet and water *ad libitum*.

5.1.2 Rodent models

A.) B-IDE-KO mice

Breeding strategies of β-cell specific IDE knockout mice

The Cre/LoxP recombination system was used to generate β-cell-specific IDE knockout mice. Homozygous mice with a floxed *Ide* gene were kindly provided by Dr. Malcom Leissring (165) from University of California, Irvine, USA. These mice have loxP sites flanking *exon 3* of *Ide* gene. Exon 3 contains the catalytic site sequence, critical for the proteolytic activity of the enzyme. *Insulin-Cre* mice were kindly provided by Dr. Herrera (257) from University of Geneva, Switzerland. This transgene expresses *Cre* recombinase under the control of the insulin promoter, which is active in pancreatic β-cells.

To generate β-cell specific IDE knockout mice, *Insulin-Cre* mice were crossed with $Ide^{flox/flox}$ mice. Cre-LoxP recombination results in the deletion of *exon 3* of the *Ide* gene, causing a frameshift with two stop codons in *exon 4* and therefore, an early termination of translation. Thus, we obtained our experimental litter $Ide^{flox/flox}$; Ins-Cre/+, named hereafter B-IDE-KO, heterozygotes $Ide^{flox/+}$; *Ins-Cre/+* named B-IDE-HT, and their controls $Ide^{flox/flox}$; +/+ or $Ide^{flox/+;}$ +/+ named B-IDE-WT **(Figure 20).**

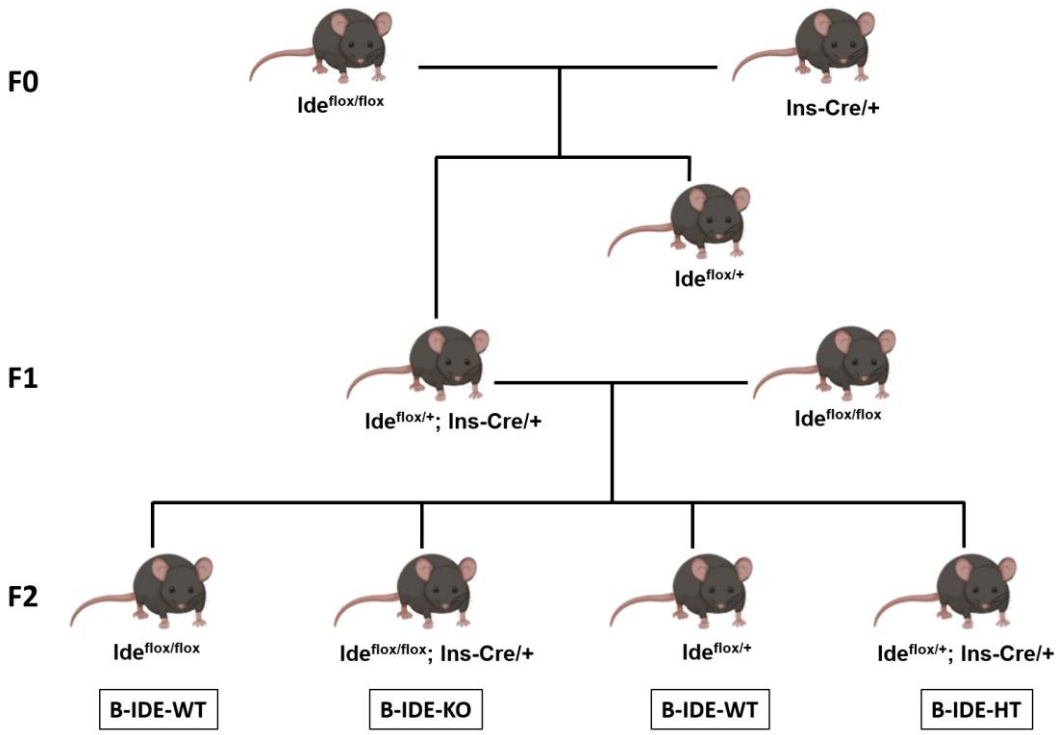

Figure 20: Breading strategy for generating B-IDE-KO mice colony.

B.) Mouse genotyping

To genotype B-IDE-KO mice colony, PCRs were performed with genomic DNA extracted from mice tail snips of ~0.2 cm using QuickExtract™ DNA Extraction Solution (Epicentre, EEUU). Tails were incubated in 50 µL of QuickExtract™ solution at 65ºC for 8 min, followed by 2 min incubation at 98 ºC in a thermo-block. For the PCR reaction, master mix was prepared with the following components for a final volume of 40 µl: 8 µL Buffer Reaction Mix (Bioline, UK), 0.2 µL Primer Forward (Metabion, Germany), 0.2 µL Primer Reverse (Metabion, Germany), 0.25 µL My Taq DNA Polymerase (Bioline, UK), 30.35 µL of nuclease free water, and 1 µL of DNA sample.

Genes analyzed by PCR were: *Ide*$^{flox/flox}$ and *Ins-Cre.* Primer sequences and the sizes of resulted amplicons were detailed in **Table1**

Primer/Target gene	Sequence (5´- 3´)	pb
Flox_Ide_F	AAC TGC CAC CTG TCC AAT CC	WT Ide: 480
Flox_Ide_R	CTC AGG GAT ACA ATG CGT GC	Ide$^{flox/flox}$: 650
Ins-Cre_F	TAA GGC TAA GTA GAG GTG T	473
Ins-Cre_R	TCC ATG GTG ATA CAA GGG AC	

Table 1: Primer sequences used for B-IDE-KO mice genotyping

PCR products were mixed with loading buffer for DNA (Bioline, UK), loaded on 2% agarose gel and electrophoresed in TBE buffer (89 mM Tris-HCl, pH 7.6, 89 mM boric

acid and 2 mM EDTA). The gel was stained with SYBRTH Safe DNA Gel Stain (Invitrogen, USA) and the bands were visualized by an ultraviolet transilluminator showing the three kinds of genotypes obtained in our mouse colony **(Figure 21).**

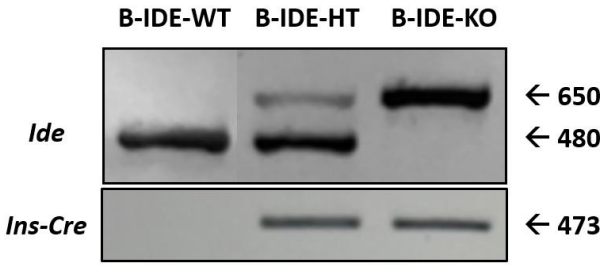

Figure 21: Representative image of PCRs results for mice genotyping. WT (wild type); B-IDE-HT (heterozygous); B-IDE-KO (β-cell specific IDE-knockout mouse).

C.) Mice metabolic characterization

Metabolic characterization was performed on both male and female mice at 6 months of age.

- Body weight

Body weight was monitored at 6 months old using a digital weight scale (Adam Equipment, USA)

- Blood glucose

Blood glucose levels were measured directly from cut tails tips using the Breeze2 Glucometer (Bayer, Germany). Blood glucose measurements were performed in mice under fasting (6 or 16 h without food), and after glucose overload (IP-GTT).

- Intra-peritoneal glucose tolerance test (IPGTT)

For the assessment of glucose tolerance, we performed intra-peritoneal glucose tolerance test (IPGTT). Mice were fasted for 16 h from 18 p.m. to 9 a.m. 2 g/kg glucose body weight was injected into the intraperitoneal cavity. Blood glucose levels were measured at different time points: 0, 15, 30, 60 and 120 min after glucose injection.

- Blood sampling and plasma collection

Plasma samples were obtained by direct blood flow from tail tip collecting the blood with Microvette®, a capillary tube coated with potassium-EDTA (Sarstedt, Germany). Then, blood samples were centrifuged at 1,200 *g* for 10 min at 4ºC to obtain and collect plasma fraction.

5.2 Rodent pancreatic islet isolation and culture

Rodents were euthanized by cervical dislocation. Islets were isolated by pancreatic duct perfusion with 3 mL per mouse of a solution of Collagenase V (1,000U/mL) (Sigma, USA) in “isolation buffer” (115 mM NaCl; 10 mM $NaHCO_3$; 5 mM KCl; 1.1 mM $MgCl_2$; 25 mM HEPES; 1.2 mM NaH_2PO_4; 2.5 mM $CaCl_2$; 5.5 mM Glucose; 0.1% BSA; pH 7.4).

Once perfused, the pancreas was digested in a 50 mL tube in a stationary bath at 37ºC for 14 min. The digestion process was stopped by the addition of 10 mL of isolation buffer and keeping it cold until collection. Islet isolation is a process through which islets are separated out of exocrine tissue. For GSIS it requires picking up islets one by one using pipets under a stereo microscope to preserve islet function. Freshly isolated islets were left to recover in isolation buffer for 2 h at 37°C in an incubator.

Islets were cultured in RPMI 1640 medium supplemented with 2 mM L-glutamine, 5.5 mM D-glucose, 10% FBS, 100 U/mL penicillin, and 100 µg/mL streptomycin. The islets were maintained at 37 °C with 5% CO_2 in a humidified atmosphere.

5.3 Cell Cultures

5.3.1 Cell lines

A.) Ins1E cell line culture

The rat insulinoma cell line. Ins1E derived from the parental cell line Ins-1 were donated by *Dr. Pierre Maechler* (University of Geneva, Switzerland). This cell type has the ability to secrete insulin in response to glucose overload. Cells were grown in RPMI 1640 Glutamax (GIBCO, USA) 11 Mm Glucose, 10 mM Hepes (Invitrogen Ltd, Europe), 50 µM β-mercaptoethanol (Sigma-Aldrich, USA), 1 mM Sodium Pyruvate (Invitrogen Ltd, Europe), 5% fetal bovine serum (FBS) (Gibco, USA) and 1% Penicillin-Streptomycin (Invitrogen Ltd, Europe) at 37°C and 5% CO_2 in a humidified atmosphere to 80% confluence.

B.) Min6 cell line culture

Min6 cells are a line of insulin-producing β-cells derived from mice insulinoma. This cell line was originally established by *Dr. Jun-ichi Miyazaki* and colleagues at Osaka University in 1990. Cells were grown in Dulbecco's modified eagle medium (4.5 g/L glucose) (GIBCO, USA) supplemented with 15% FBS (Gibco, USA), 1% Penicillin-Streptomycin (Invitrogen Ltd, Europe), 1 mM Sodium Pyruvate (Invitrogen Ltd, Europe)

and 50 µM β-Mercaptoethanol (Sigma-Aldrich, USA) at 37°C and 5% CO_2 in a humidified atmosphere to 80% confluence.

5.3.2 Different approaches for proteins knock-down

A.) Generation shRNA-IDE line in Ins1E and Min6 cells.

To study the effect of stable IDE silencing on β-cells phenotype, Ins1E and Min6 were transduced with a lentiviral vector of an IDE-specific short hairpin silencing RNA (shRNA) in parallel with an empty vector, therefore generating the Ins1E-shIDE, Min6-shIDE and Ins1E and Min6-Control lines.

Afterwards, Ins1E and Min6 cells were subjected to puromycin selection of stably infected cells and after that, cultured as mentioned above. Gene silencing efficiency was assessed by RT-qPCR and western blotting.

The vector used was pGreenPuro™ shRNA Cloning and Expression Lentivector (System Biosciences, USA). The pGreenPuro™ vector is an improved third generation of HIV-based expression lentivector. It contains a puromycin resistance gene to enable drug selection of target cells stably expressing the shRNA, and a copGFP gene, that works as a fluorescent reporter for the transduced cells. A map of the pGreenPuro™ vector is shown in **Figure 22.**

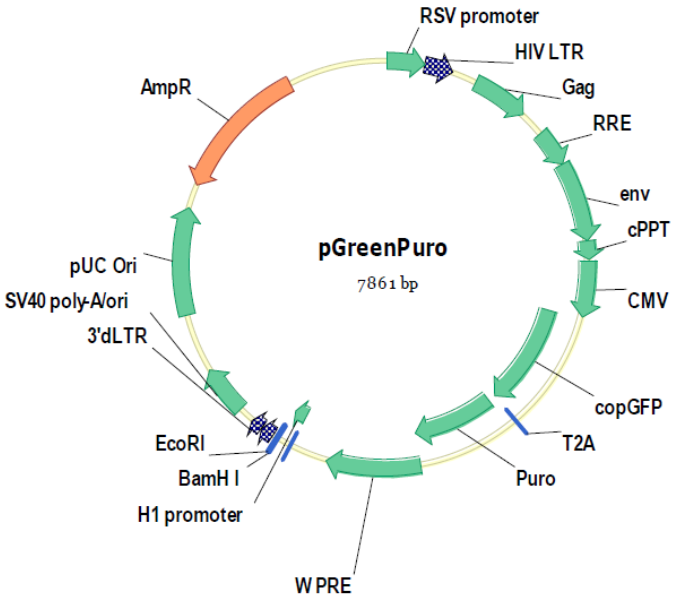

Figure 22: Map and features of pGreenPuro™ Vector (258).

The target sequence within the coding region of the IDE gene was selected based on pre-designed constructs provided by the manufacturer. This sequence, comprising both sense and antisense strands, was designed according to the manufacturer's template to form a stem-loop structure upon transcription. The oligonucleotide sequence selected is

shown in **Table 2.** The sequence is referred to as p25, as it is located in exon 25 of the IDE gene.

p25 Forward sequence
5´- GATCCCCCTTGTGAAGCCACACATTACTTCCTGTCAGATAATGTGTGGCTTCACAAGGGTTTTTG -3´
p25 Reverse sequence
5´- AATTCAAAAACCCTTGTGAAGCCACACATTATCTGACAGGAAGTAATGTGTGGCTTCACAAGGGG-3´

Table 2: Oligonucleotides sequences used for the lentiviral vector with initiator, sense, loop, antisense and terminator sequences highlighted.

B.) Generation shRNA-IFT88 in Min6

To study the effect of cilia silencing on β-cell phenotype, Min6 cells were transduced with an adenoviral vector encoding an IFT88-specific short hairpin RNA (shRNA), kindly provided by Dr. Donald Scott's group at the Diabetes, Obesity, and Metabolism Institute (The Mount Sinai Medical Center, NY, USA).

For experiments, Min6 cells were seeded at a density of 4×10^5 cells per well in a 6-well plate and incubated for 24 hours (h). After confirming cell viability, cells were exposed to 800 µL of serum-free medium containing either control or shIFT88 adenovirus at a multiplicity of infection (MOI) of 200. Cells were incubated at 37°C for 2 h to allow transduction. The medium was then removed and replaced with complete culture medium. Cells were subsequently incubated for 48 h in a humidified incubator at 37°C with 5% CO_2. Gene knock-down efficiency was assessed by western blotting.

5.4 Pancreatic β-cell *in vitro* treatments

5.4.1 Glucose

Min6 cells were seeded on the cell culture 6-well plates at a density of $5x10^5$ cells per well (for western blot analysis) or in 18-well ibidi (81817, GmbH, Germany) at a density of $5x10^3$ cells per well (for immunostaining) and cultured for 72 h. Cells were then washed twice with glucose-free HEPES balanced salt solution (HBSS) 125 mM NaCl, 5.9 mM KCl, 25 mM HEPES, 1.7 mM $CaCl_2$, 1.26 mM $MgCl_2$, and 0.2 (v/v) bovine serum albumin (essentially fatty acid free), pH 7.4). Next, the cells were preincubated for 30 min at 37ºC in 3 mM glucose HBSS. Glucose treatment was performed via static incubation for 30 min in 4 mL (for western blot) or 100 µL (for immunostaining) of the same buffer containing 3.3 mM or 16 mM glucose respectively. These experiments were always performed triplicates. Six wells were used per condition: 3 wells were treated with 3.3 mM glucose and 3 wells treated with 16 mM glucose. After this incubation period, lysis

buffer was added to the samples for western blot analysis, and for the immunostaining analysis, the cells were fixed.

5.4.2 Glucagon

Min6 cells were seeded on the cell culture 6-well plates at a density of $5x10^5$ cells per well and cultured for 72 h, as previous described. The cells were then serum-starved (deprived of, FBS) for 18 h, followed by treatment with 200 nM glucagon (Sigma, USA) for 10 and 30 min. Proteins were subsequently collected to study the effects of glucagon.

5.5 β-cell function

β-cell function from our models were evaluated in vitro by glucose stimulated insulin secretion technique.

5.5.1 Glucose-stimulated insulin secretion (GSIS)

A.) Min6 cells

Min6 cells were seeded on cell culture 24-well plates at a density of 4 $x10^5$ cells per well for 72 h. Cells were then washed twice with glucose-free HEPES balanced salt solution (HBSS) 125 mM NaCl, 5.9 mM KCl, 25 mM HEPES, 1.7 mM $CaCl_2$, 1.26 mM $MgCl_2$, and 0.2% bovine serum albumin (essentially fatty acid free), pH 7.4). Next, the cells were preincubated for 30 min at 37ºC in 3.3 mM glucose HBSS. Insulin secretion was then stimulated by using, first a static incubation for 30 min in 1 mL of the same buffer containing 3.3 mM glucose, and afterwards with 1 mL of 16 mM glucose HBSS of 30 min. These experiments were always performed in triplicates, using three wells per condition: All wells were first treated with 3.3 mM glucose, followed by treatment with 16 mM glucose. After each incubation, 500 µL of the supernatants were collected. Secreted insulin was measured by Mouse Insulin ELISA (Mercodia, Sweden) **(Table 3).**

To determine DNA amount in treated cells, after insulin secretion, cells were incubated with 1.5% acid-ethanol buffer (1,5% HCl in 70% EtOH), overnight (O/N) and DNA was measured on NanoDrop® ND-1000 full spectrum spectrophotometer (Marshall Scientific, USA). Insulin secretion was normalized by DNA amount.

B.) Rodent islets

After isolation, the islets were maintained at 37 °C with 5% CO_2 in a humidified atmosphere O/N. The day after, to promote insulin secretion, groups of 5 islets were plated on cell culture inserts and incubated for one h in 500 µL of 3 mM glucose Krebs-Ringer buffer (140 mM NaCl, 4.5 mM KCl, 1 mM $MgCl_2$, 25 mM HEPES, 2.5 mM $CaCl_2$, 0.1% BSA), followed by 500 µL of 16 mM glucose Krebs-Ringer buffer for 1 h. After

incubation, we collected the supernatants and hormone secretion was analyzed by Insulin/Proinsulin ELISA kit (Mercodia, Sweden).

5.5.2 Glucagon-stimulated insulin secretion

A.) Min6 cells:

The exact same procedure as described in the previous section was performed (5.5.1 Min6), with the difference of including 200 nM glucagon (Sigma, USA) in high glucose (16 mM) concentration.

B.) Rodent islets

The exact same procedure as described in the previous section was performed (5.5.1 Rodent islets), with the difference of including 200 nM glucagon (Sigma, USA) in high glucose (16 mM) concentration.

5.6 Intracellular calcium signaling recordings

Ratiometric recording of intracellular calcium in intact islets

Following islet isolation, islets were allowed to recover for at least 1 h at 37°C in 1 mL of isolation buffer. Subsequently, 2 µL of a 2 mM stock solution of the fluorescent Ca^{2+} probe fura-2-AM (Molecular Probes, Netherlands), prepared in DMSO (Sigma, Germany) were added to achieve a final probe concentration of 4 µM (0.2% final DMSO). Islets were incubated for at least 2 h at RT in a humidified atmosphere continuously gassed with carbogen (95% O_2, 5% CO_2). During this incubation period, the lipophilic esterified form of the Ca^{2+} probe crosses the cell membrane and becomes trapped in the cytosol due to hydrolysis of the AM ester groups by intracellular esterases, which confers the molecule a negative charge.

Once loaded, islets were individually transferred to a thermostatically controlled recording chamber maintained at 37°C. The chamber floor consisted of a 24 mm coverslip pretreated with poly-L-lysine to immobilize the islet. During experiments, islets were continuously perfused at a flow rate of 1 mL/min using a peristaltic pump with a solution composed of (in mM): 120 NaCl, 5 KCl, 1.8 $NaHCO_3$, 1.1 $MgCl_2$, 2.5 $CaCl_2$, and 20 HEPES.

The chamber floor and perfusion system were mounted on an Axiovert 200 inverted microscope (Carl Zeiss, Germany) equipped with a recording system based on a xenon 2 filter wheel and shutter system (Sutter Instruments Co., USA) equipped with 340 nm and 380 nm filters (Omega Optics, Spain). The selected excitation light was reflected by

a dichroic mirror toward a 40X oil immersion Fluar objective with a numerical aperture (NA) of 1.3 (Carl Zeiss, Germany) to illuminate the sample.

The emitted fluorescence passed back through the objective and the dichroic mirror, then through a 510 nm emission filter (Omega Optics, Spain), and was finally captured and amplified by a high-resolution, wide dynamic range digital camera (ORCA C4742-95, Hamamatsu Photonics, Spain). Images were acquired at a frequency of 1 image every 2 seconds. Calcium signal monitoring and control of system components were managed using the Aquacosmos 2.0 software interface (Hamamatsu Photonics, Spain).

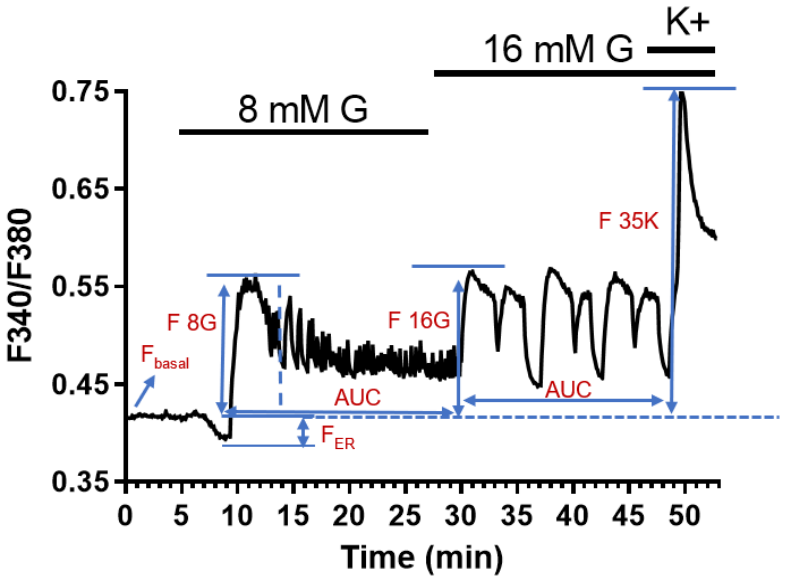

Figure 23. Analyzed parameters: Ca^{2+} record illustrating all the parameters that were measured: F_{basal}, basal fluorescence; F_{ER}, effect of Ca^{2+} sequestration in the ER; F 8 G, increase of fluorescence or amplitude of the first Ca^{2+} transient at 8 mM G; F 16 G, increase of fluorescence or amplitude of the first Ca^{2+} transient at 16 mM G; AUC, area under the curve during exposure to 8 mM G; AUC, area under the curve during 16 mM G; F35 K, amplitude of transient at 35 mM K^{+}.

Intracellular calcium concentration ($[Ca^{2+}]i$) variations were expressed as the ratio between the fluorescence emitted at 510 nm after excitation at 340 nm and that obtained after excitation at 380 nm (F340/F380). For each trace, the following parameters were quantified: the basal mean F340/F380 value at 3 mM glucose; the peak F340/F380 value (FPEAK) at 8 mM and 16 mM glucose, as well as after depolarization with 35 mM KCl, reflecting the amount of Ca^{2+} entering the cell during the initial transient response to each stimulus; the fluorescence increase (ΔF), calculated as (F340/F380 final – F340/F380 initial, with the initial value corresponding to 3 mM glucose); and the area under the curve per minute (AUC/min) at 8 mM and 16 mM glucose, estimating the overall Ca^{2+} increase during the entire stimulation period, which may be more representative of the calcium pool linked to insulin secretion. In addition, the ER fluorescence ratio (F_{ER}) was determined as an indirect index of endoplasmic reticulum Ca^{2+} uptake capacity,

calculated from the initial transient decrease (negative peak) observed immediately after switching from 3 to 8 mM glucose **(Figure 23).**

All these analyses, along with the statistical evaluation of the results, were performed using Origin v7.0552 software (OriginLab Corp, USA).

5.7 Enzyme-linked immunosorbent assay (ELISA)

To determine insulin levels in plasma or cell culture supernatants from GSIS, we used enzyme-linked immunosorbent assay (ELISA). ELISA kits used in this study are "sandwich" type, which means that this assay is composed by two highly specific antibodies that recognize two different epitopes in the same protein, providing high effectiveness and sensitivity in the recognition of the desired protein.

In our assays, wells are pre-coated with a first anti-antigen antibody. The sample containing the antigen is deposited inside these wells together with peroxidase-conjugated antibody and incubated 2 h. Thus, each molecule of antigen will be bound to an antibody in the base that retains it and a second antibody that label it. After that, wells are washed 6 times to remove unbound sample and enzyme labelled antibody. Then, the bound conjugate is detected by reaction with 3,3'-5,5'-tetramethylbenzidine (TMB) (incubation 30 min). The reaction is finally stopped by the addition of an acid stop solution, giving a colorimetric endpoint that is read spectrophotometrically at 450 nm (HEALES microplate reader, China). This process is summarized in **Figure 24.**

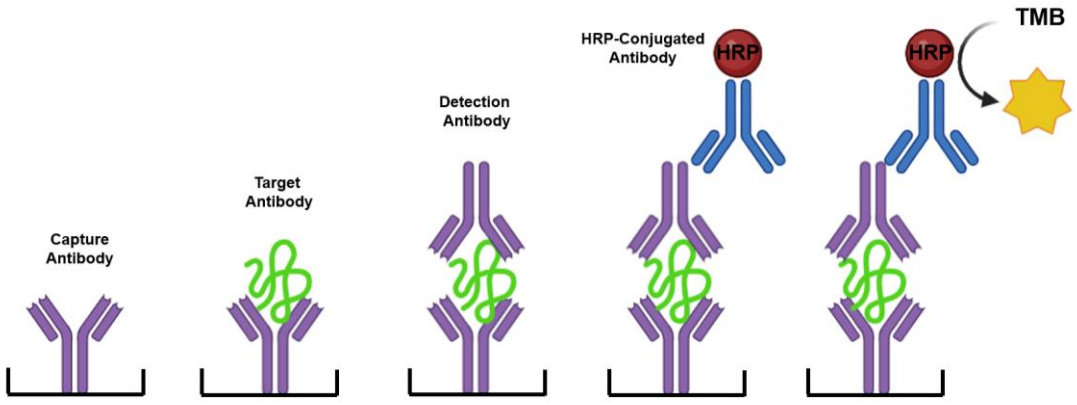

Figure 24. Illustration of an ELISA sandwich technique. Retrieved from LifeSpan Bioscience, Inc.

Sample	ELISA
Min6 supernatant	MOUSE INSULIN ELISA (Mercodia, #10-1247-01)
Islet supernatant	Ultra Sensitive Mouse Insulin ELISA Kit (Crystal Chem, #90080)

Table 3: ELISA kits used for insulin measurements.

5.8 Western Blot

5.8.1 Protein extraction and quantification

β-cells were washed three times with phosphate-puffered Saline (PBS). Then, cells were homogenized in 100 µL of cold assay buffer [125 mM Tris-HCl pH 6.8, 2% (m/v) sodium dodecyl sulfate (SDS) and 1 mM dithiothreitol (DTT)] supplemented with protease and phosphatase inhibitor cocktails (Sigma, USA) and 1 mM phenylmethylsulphonyl fluoride (PMSF; Merck Life Science, Spain).

Cells lysates were briefly sonicated, and protein content was quantified by the Micro BCA Kit (Thermo Scientific, USA). Protein extracts were mixed with LSB (Laemmli Sample Buffer: 60 mM Tris-Cl pH 6.8, 2% weight/volume (w/v) SDS, 10% (v/v) glycerol, 5% (v/v) β-mercaptoethanol, 0.01% (w/v) bromophenol blue) and heated at 100°C for 5 min to complete protein denaturation.

5.8.2 Protein electrophoresis and western blot

20 µg of solubilized proteins were separated by their molecular weight using 10% polyacrylamide gels under denaturing conditions (SDS-PAGE). Gel electrophoresis was carried out at 150 V in electrophoresis buffer (Biorad Laboratories, USA) and then transferred to PDVF (Polyvinylidene fluoride) Immobilon-P membranes (Millipore, USA) at 30 V O/N in transfer buffer (Biorad Laboratories, USA) at 4°C. Transferred membranes were incubated for 1 h at RT with blocking solution (PBS-0.1% (v/v) Tween 20 and 5% (w/v) (not-fat dry milk). Blots were incubated subsequently for 1 h at RT or O/N at 4ºC for the appropriate primary antibody in 10% blocking solution. Primary antibodies used and blot conditions are summarized in **Table 4**.

Afterwards, membranes were washed 3 times for 10 min with PBS-0.1% Tween 20 and incubated with the corresponding secondary antibodies conjugated with peroxidase in 10% blocking solution for 30 min at RT. Secondary antibodies are summarized in **Table 5.**

Membranes were washed 3 times with PBS-0.1% Tween 20, and peroxidase activity was visualized by the enhanced chemiluminescence kit Immun-Star WesternC (Bio-Rad, USA). Signals were detected by exposure to X-ray film to produce bands within the linear range. Bands were scanned at 600 pixels per inch with HP Scanjet G4010 (Hewlett-Packard, Spain) using HP Photosmart Premier 6.5 software (Hewlett Packard, Spain). The obtained images (negative) were converted to 32-bit format and inverted to generate an image for quantification. Band intensity was quantified with ImageJ software (NIH, USA). Each band was individually selected with a rectangular ROI selection, followed by

quantification of the peak area of the histograms obtained. Results were normalized to housekeeping protein on each membrane.

Antibody	Supplier	Reference	Dilution	Incubation time and ºC	Specie	Molecular weight
αβTubulin	Cell Signaling	2148	1:5000	1 h; R. T	Mouse	52 kDa
Acetylated tubulin	SIGMA	T6793	1:10000	1 h; R. T	Mouse	55 kDa
Arl13b	Neuromab	N295C166	1:1000	O/N; 4°C	Mouse	60 kDa
CREB	Cell Signaling	9197	1:2000	1 h; R. T	Rabbit	43 kDa
ERK 1/2 (p44/42 MAPK)	Cell Signaling	9102S	1:1000	1 h; R. T	Rabbit	42,44 kDa
GAPDH	Millipore	MAB374	1:200000	1 h; R. T	Mouse	37 kDa
Glucagon Receptor	Abcam	Ab75240	1:5000	1 h; R. T	Rabbit	54 kDa
IDE	Millipore	9210	1:40.000	1 h; R. T	Rabbit	110 kDa
Insulin Receptor β	Cell Signaling	3025	1:2000	O/N; 4°C	Rabbit	95 kDa
IFT88	Proteintech	13967-1-AP	1:10000	1 h; R. T	Rabbit	88 kDa
p84	Abcam	5E10	1:200000	O/N; 4°C	Mouse	80 kDa
p-PKA Substrate (RRXS*/T*)	Cell Signaling	9624	1:50000	O/N; 4°C	Rabbit	Smears
p-CREB (Ser133)	Cell Signaling	9198S	1:2000	O/N; 4°C	Rabbit	43 kDa
p-ERK (p-p44/42 MAPK)	Cell Signaling	9102S	1:1000	O/N; 4°C	Rabbit	42,44 kDa

Table 4: List of primary antibodies used for western blot.

Antibody	Supplier	Reference	Dilution	Incubation time and ºC	Specie
Anti-Rabbit Ig-G HRP	Jackson Immuno	711-035 152	1:20000	30 min; R. T	Rabbit
Anti-Mouse Ig-G HRP	GE Healthcare	A9310	1:5000	30 min; R. T	Mouse

Table 5: List of secondary antibodies used for western blot.

5.9 RT-PCR

5.9.1 RNA purification

Total ribonucleic acid (RNA) was purified from 2 x 10^{6} cells in culture using Trizol™ reagent (Invitrogen Life Technologies, USA). The cells were homogenized with 500 µL of Trizol and centrifuged 10 min at 4°C and 2800 *g* to remove undissolved samples. Next, 100 µL chloroform (PanReac AppliChem, Germany) is added to the supernatant to extract RNA and centrifuged 15 min at 4°C and 2800 *g*, which causes the formation of two phases by density difference: an organic phenolic phase containing DNA and denatured protein residues, and the upper aqueous phase containing RNA. Phase containing RNA is transferred to a new tube and added 250 µL of isopropanol (PanReac AppliChem, Germany) and centrifuged 10 min at 4°C and 2800 *g* to precipitate the RNA. After that, isopropanol is discarded and the pellet is washed in 75% ethanol and allowed to dry. Finally, the pellet was resuspended in 30 µL of DNAse/RNAse free H_2O.

Quantification of total RNA was performed by measuring ultraviolet absorbance on a NanoDrop® ND-1000 full spectrum spectrophotometer. Removal of any possible genomic DNA contamination was achieved by treating the samples with the RapidOut DNA removal kit (Thermo Scientific™, USA).

5.9.2 cDNA SYNTESIS

First strand of complementary DNA (cDNA) was synthesized using the iScriptTM cDNA Synthesis Kit (Bio Rad, USA), which is a highly sensitive reagent optimized for reliable cDNA synthesis for gene expression analysis using real-time reverse transcription quantitative PCR (RT-qPCR). The reverse transcription reaction was incubated in a thermal cycler (Thermo Scientific™, USA).

5.9.3 RT-PCR

Target gene mRNA and housekeeping mRNA levels were determined by real time quantitative PCR (qPCR) with TaqMan™ assays on a LightCycler™ 480 system. The qPCRs were performed on equal amounts of cDNA in triplicates for each biological sample, using Maxima Probe qPCR Master Mix (Thermo Scientific™, USA) for TaqMan™ assays **(Figure 25).**

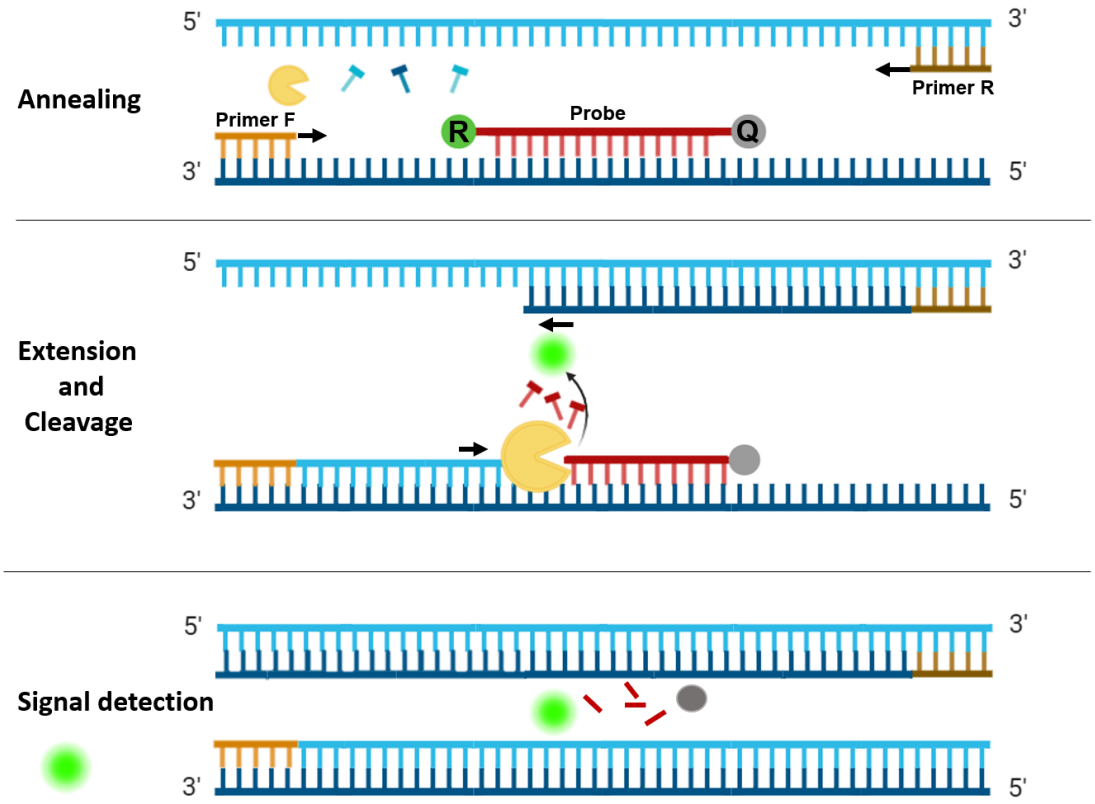

Figure 25: Detection workflows based on TaqMan

Data were analyzed using the 2 fit point absolute quantification protocol and setting the fluorescence threshold at 1.00. Target mRNA expression levels were normalized using the $2^{-\Delta\Delta Ct}$ relative quantification method (259) to the mRNA levels of the housekeeping gene for ribosomal protein L18 (*Rpl18*) as reported by our laboratory in previous studies (160,162,169). Primers and TaqMan™ probe sequences are shown in **Table 6** and **7**:

Gene ID	Description	Primers
Rpl18	Ribosomal protein L18	F: 5′-AAGACTGCCGTGGTTGTGTGG-3'; R: 5'-AGCCTTGAGGAGGATGCGACTC-3'; Probe: 5′-FAM TTCCCAAGCTGAAGGTGTGTGTGTGCA-BHQ1-3′.

Table 6: Primers and TaqManTM probe for gene expression assay for mouse Rpl18.

Gene ID	Description	TaqMan® Probe
Ide	Insulin-degrading enzyme	Mm00473077_m1
Insr	Insulin receptor	Mm01211875_m1
GcgR	Glucagon receptor	Mm00433546_m1

Table 7: List of TaqMan probes used in this study.

5.10 MTT Assay

To evaluate cell viability, cells were seeded in a 96-well plate at a density of 50,000 cells per well and allowed to adhere overnight in a humidified incubator at 37°C with 5% CO_2. The culture medium was changed after 24 h. After 48 h, 10 µL of MTT reagent (at a final concentration of 0.5 mg/mL) was added to each well and incubated for 3 h at 37°C in a 5% CO_2 atmosphere. Following incubation, the medium was carefully removed, and 100 µL of DMSO (Sigma, USA) was added to each well to dissolve the formazan crystals. Absorbance was measured at 570 nm using a microplate reader.

5.11 Cell Immunofluorescence (For confocal and STORM imagining)

To detect the presence of different proteins in β-cells, cells were seeded in ibidi chamber slide (µ-Slide 18 well, ibidi GmbH, Gräfelfing, Germany; Cat. No. 81816) at a density of 3,000 cells per well. Cells were fixed using three different buffers: extraction, fixation, and reducing buffers **(Table 8),** two of which contained glutaraldehyde (GA). Both the extraction and fixation buffers were pre-warmed in a 37°C water bath prior to use. Cells were incubated with 50 µL of extraction buffer for 40 seconds at 37°C in the incubator, followed by the addition of fixation buffer for 10 min at 37°C. Subsequently, cells were incubated with the reducing buffer for 7 min at RT followed by a washing step with PBS.

Fixation buffers		
*Extraction buffer:	0.25% v/v Triton X-100 and 0.1% GA in Pipes Ethylene Glycol Buffer (PEM, 80 mM Pipes (pH 6.9), 5 mM EDTA, 2 mM magnesium chloride ($MgCl_2$), and 10% (v/v) ethylene glycol).	To break the cell membranes and allow the extraction of proteins of cellular components.
**Fixation buffer:	0.25% v/v Triton X-100 and 0.5% GA in PEM.	To fix the cells and preserve their structure and components.
***Reducing buffer:	0.1% w/v. Mix 10 mg of NaBH4 into 10 mL of PBS. Make fresh.	To reduce disulfide bonds and facilitates protein visualization.

Table 8: Composition of extraction, fixation, and reducing buffers used for fixation of β-cells.

To prevent non-specific binding, cells were incubated for 1 h at RT with 50 µL of blocking solution, consisting of 5% normal goat serum (NGS), 0.1% Triton X-100, and an unconjugated affinity-purified F(ab) fragment anti-mouse IgG (1:100) in PBS. Following the blocking step, cells were incubated with 50 µL of the primary antibody solution

(prepared in blocking solution without Triton X-100) for 1 h at RT. The primary antibodies used are summarized in **Table 9.**

Antibody	Supplier	Reference	Dilution	Species
IDE	Millipore	AB9210	1:50	Rabbit
Tubulin A	Sigma-Aldrich	T9026	1:500	Mouse
Tubulin B	Sigma-Aldrich	T5293	1:250	Mouse
AcTub	Sigma-Aldrich	T6793	1:750	Mouse
GM130	Becton Dickinson	610823	1:100	Mouse

Table 9. Primary antibodies used for immunofluorescence.

Samples were washed three times with PBS to remove excess primary antibodies and subsequently incubated with the appropriate secondary antibody for 1 h at RT in the dark. Secondary antibodies used are also summarized in **Table 10.**

Antibody	Supplier	Reference	Dilution	Species
CF583	Biotum (Biozol)	20792-50 µL	1:100	Mouse
CF505	Biotum (Biozol)	20877-50 µL	1:100	Rabbit

Table 10. Secondary antibody used for immunofluorescence.

To ensure the complete removal of excess secondary antibodies, an additional washing step of five washed (5 min) with PBS was performed. Finally, cells were incubated with post-fixation buffer (4% PFA) for 10 min at RT in the dark and the images were acquired by STORM. In the case that the images were acquired using the confocal microscope, a Hoechst staining step was performed afterwards. This involved an 8-min incubation in the dark with 50 µL of 1:5000 Hoechst 33342 diluted in water, followed by three washes with water.

5.12 Histological studies

5.12.1 Pancreas dissection, fixation and paraffin embedding

We accessed by latero-longitudinal incision to the abdominal cavity of the animal and proceeded to the extraction of the pancreas. Once the pancreas was dissected, it was washed with PBS. After that, it was introduced in a histological cassette and immersed in 10% (v/v) neutral buffer formalin solution (Bio-Optica, Milano, Italy) O/N. After this fixation time, tissue was dehydrated, immersed in successive solutions of ethanol (Dávila Villalobos S.L., Spain) of increasing concentration from 70% (v/v) to 100% (v/v) dilution

and finally to absolute xylol (PanReac AppliChem, Germany) and then embedded into paraffin blocks. Once hardened, 5 µm pancreas serial sections were obtained from these blocks using a microtome. Sections were incubated at 56 °C overnight to favor the adherence of the sample to the slides. Polylisine treated slides were used to guarantee tissue adhesion.

5.12.2 Immunofluorescence of pancreatic sections

Slides containing 5 µm-thick pancreatic sections of B-IDE-colony were baked at 60ºC O/N. Then, slides were immersed twice in tissue clearing agent for 10 min each, and subsequently in ethanol baths of descending ethanol content, 100% (v/v) ethanol for 5 min, 90% (v/v) ethanol for 5 min, 70% (v/v) ethanol for 5 min, and 50% (v/v) ethanol for 5 min.

After rehydration in ethanol, slides were rinsed with deionized water. Antigen retrieval (Citrate buffer, pH 6, C9999, Sigma-Aldrich, USA) was performed in a pressure cooker for 20 min. Afterward, the slides were cooled for 10 min in an open container placed on ice, then transferred to RT in PBS-Tween. Slides were washed three times for 5 min in PBS-Tween, dried around the edges, and marked with a hydrophobic pen (PAP-pen).

Subsequently slides were incubated with 150 µL of Fab blocking solution (PBS + 5% goat serum + 1% Fab mouse blocking reagent) for 1 h at RT. Following this, slides were washed three times for 2 min each in PBS-Tween. Primary antibody staining was performed by applying 150 µL of primary antibody solution (PBS + 2% normal goat serum (NGS)) to each slide and incubating for 1 h at RT. The primary antibodies used are summarized in **Table 11.**

Antibody	Supplier	Reference	Dilution	Species
Insulin	Agilent Technologies	IS00230-2	1:10	Guinea Pig
Glucagon	Abcam	ab92517	1:1000	Rabbit
AcTub	Sigma-Aldrich	T6793	1:1200	Mouse

Table 11: List of primary antibodies used for inmmunofluorescence.

After primary antibody incubation, slides were washed three times for 5 min each in PBS-Tween. Secondary antibody staining was performed by applying 150 µL of secondary antibody solution and incubating for 30 min at RT in dark. The secondary antibodies used are summarized in **Table 12.**

Antibody	Supplier	Reference	Dilution	Species
AF488	Life Technologies	A11073	1:1000	Guinea Pig
AF647	Life Technologies	A21242	1:1000	Mouse
AF555	Life Technologies	A21430	1:1000	Rabbit

Table 12: List of secondary antibodies used for inmmunofluorescence.

Slides were washed three times for 5 min each in PBS-Tween to remove excess secondary antibodies. Slides were washed five times for 2 min each in distilled water to remove detergent. Nuclei were counterstained with Hoechst 33342 (1:10,000 Hoechst solution, diluted in water) and incubating for 8 min in the dark. Slides were then washed three times for 5 min each in distilled water. Finally, slides were mounted with a coverslipt (high precision 25 x 50 mm nº 1,5 H, #0107222, Marienfeld, Germany), two drops of ProLong Gold mounting medium (P36930, ThermoFisher, USA).

5.13 Microscopy

5.13.1 Stochastic Optical Reconstruction Microscopy (STORM)

To visualize cellular structures and proteins (IDE, cilia, Golgi and microtubules) with a resolution of 20-30 nm, we used STORM super-resolution microscopy. This technique allows us to surpass the diffraction limit of conventional optical microscopy. It is based on the stochastic activation and deactivation of fluorescent molecules to reconstruct an image with precise localization and high-resolution from many individual detections. Once the samples have been stained as indicated in section 5.11, we proceed to sample preparation and image acquisition.

Sample Preparation: Once the samples were immunostained as indicated, 100 µL of freshly-made BCubed imaging buffer (ONI, Oxford, UK) was applied to the sample. The imaging buffer is composed of glucose oxidase, catalase, and β-mercaptoethylamine (MEA) to achieve the stochastic activation and deactivation of fluorophores. Next, mount the coverslip containing the labeled cells on the magnetic sample holder and add 100 µL of the imaging buffer. Place the lid on and ensure there are no air bubbles between the imaging buffer and the lid. Clean the bottom of the sample with absolute ethanol.

Image acquisition and reconstruction: Single molecule data acquisition (SMLM) was conducted on the Nanoimager S running NimOS V.1.19.4 (ONI, Oxford, UK). The images were acquired using a 100X 1.4 NA objective lens (Olympus, Japan) and a sCMOS camera (Hamamatsu Orca Flash 4.0 V3, Japan). Each acquisition was conducted with

the exposure time set at 30 ms, with the temperature control enabled and set at 32°C. The 532 nm and 473 nm laser was used to image the proteins of interest. A total of 30,000 image frames were captured (10.000 per laser), using a high-sensitivity sCMOS CAMERA. The microscope was equipped with a 100x oil immersion objective (Olympus UPLXAPO100, Japan) with a numerical aperture (NA) of 1,4 and working distance of 0,13 mm. For image reconstruction, the NimOS processing software (from ONI) was used. Drift correction, localization filtering (to reduce background localizations) and some data analyses were performed in the cloud-based data analysis platform from the microscope manufacturer (CODI, ONI, Oxford, UK). Drift was corrected over all frames and included all localizations with photon count <30.000, SD of the point-spread function between 75 nm and 200 nm, estimated localization precision (SD) <15 nm. Localizations were excluded where the same emission event lasted more than 15 frames. **Figure 26** shows a representative STORM image of microtubules and the primary cilium.

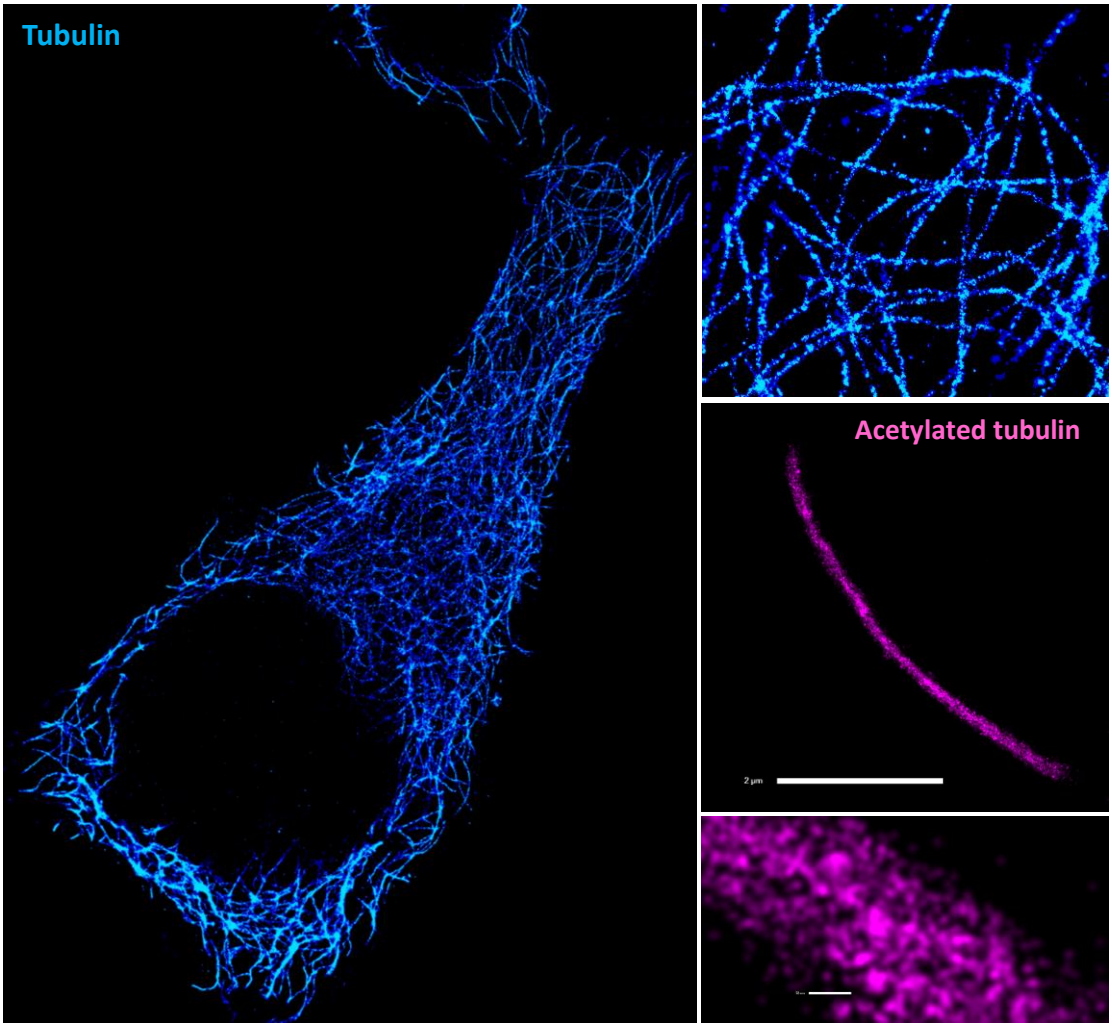

Figure 26: Representative image of Stochastic Optical Reconstruction Microscopy (STORM). Blue: Microtubules labeled with tubulin in fixed cells, showing the cytoskeletal organization with high resolution. Pink: Primary cilium stained with acetylated tubulin.

5.13.2 Confocal microscopy

The same ONI Nanoimager was also employed for confocal microscopy. The system was equipped with appropriate confocal filters to select specific excitation and emission wavelengths, ensuring optimal imaging conditions. A 100x oil immersion objective was used to acquire nine images at 0.5 µm intervals. The imaging setup included three chromatic channels: TRITC (558–625 nm) with a laser power of 90**,** GREEN (500–531 nm) with a laser power of 60, and DAPI (449–464 nm)**.** The exposure time per frame was 133.33 ms, with a frequency of 0.74 Hz**.**

The acquired confocal images were processed separately from the STORM data. Cilia were quantified using the free **ImageJ software** (NIH, USA) (260). Microtubule length and curvature were measured using the **Skeleton** tool in ImageJ/Fiji. Colocalization analyses were conducted using the **JaCoB** (261) plugin in ImageJ/Fiji, applying both the Pearson correlation coefficient and the Manders overlap coefficient. Additionally, microtubule heatmaps were generated using **QuPath**.

5.13.3 Scanner

After the staining of sections from the B-IDE-KO mice pancreas, whole tissue sections were scanned by an Axio Scan.Z1 slide scanner (Zeiss, Jena, Germany) using a 20x/0.8 NA Plan-Apochromat (a = 0.55 mm) objective. Subsequently, sample analysis was performed using the QuPath software, an open source software for digital pathology (262).

Quantification of tissue, islet and cell detection

First, tissue area and islets were automatically identified based on average values of all channels for the labeled proteins (insulin and glucagon) using thresholding detection and machine learning. Information on the whole tissue sections, number of islets per section, as well as the total number of α- and β-cells was obtained. Independent workflows and settings for 1) tissue, 2) islet, and 3) cell detection are shown in the **Figure 27.**

First, for the tissue detection, the command *Pixel classification → Create thresholder* was used. After applying the *fill holes* function, the tissue was manually checked for the presence of artifacts. Then, a small ROI was created, and islets were recognized as a new class by *Pixel classification.* For this purpose, the command *Train pixel classifier* was used and new objects (islets) were created. Once the new islet classifier was saved, *Cell detection* was performed in the entire tissue sections. Cells were identified as areas

of staining above the background level, by applying optimized nucleus threshold, segmentation parameters *(Median filter radius and Sigma),* and cell expansion (263).

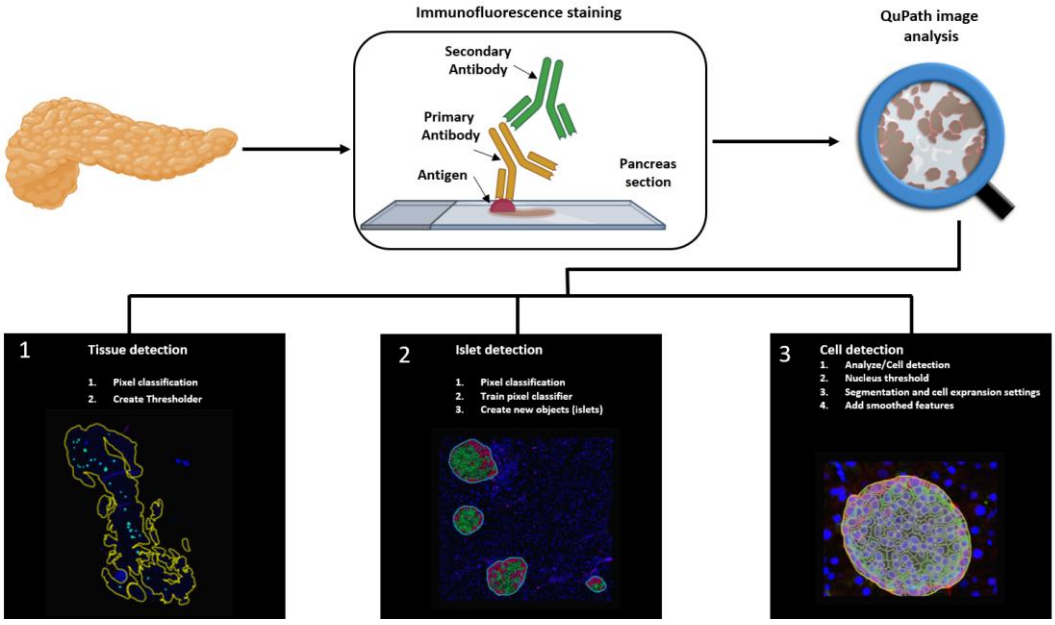

Figure 27 A: **Schematic illustration of the whole-slide image analysis workflow using QuPath.** Experimental method and image analysis. 1) Tissue was detected using an intensity thresholder based on average values of all channer for the labeled proteins. 2) Islets were created using pixel classifier and 3) cells were detected and smoothed features were added.

Endocrine cell detection and acetylated tubulin presence

Thresholding detection was applied to create unique classifiers for every staining combination due to fluorescence channel dependency. After islet detection, the path *Classify → Object classification → Create single measurement classifier tool* was applied to detect cells positive for insulin and glucagon **(Figure 27 B)** Cells were identified as areas of staining above the background level by applying optimized *Cell mean* intensity thresholds. Data on β- or α-cells were obtained by using insulin or glucagon positive cells as a reference. Acetylated tubulin threshold was also created. Annotation measurements were exported and information on islet size, cell composition and area of acetylated tubulin in each cell was obtained.

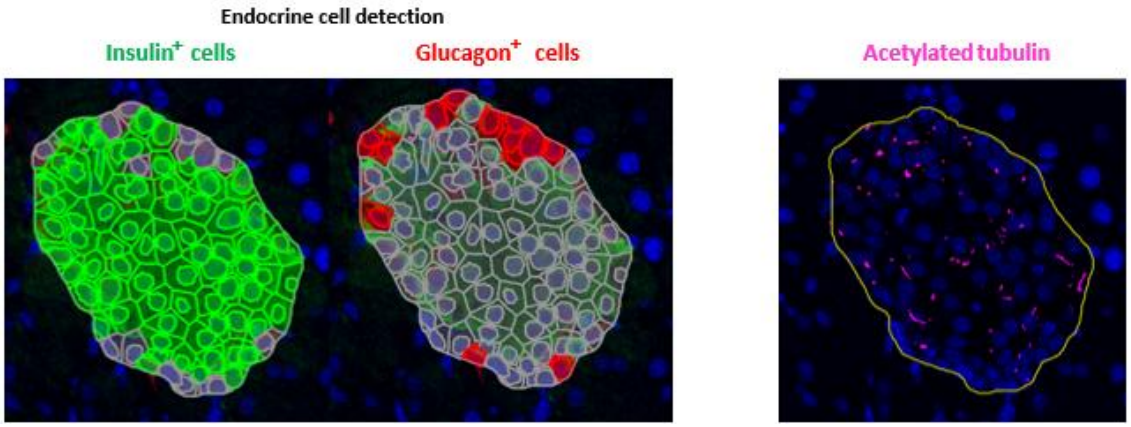

Figure 27 B: The single measurement classifier tool was employed to detect positive cells for the marker of interest. Cells were identified as areas of staining above the background level by applying optimized cell mean intensity thresholds.

5.14 STADISTICAL ANALYSIS

Statistical analysis of data was performed using GraphPad Prism Software 8.0 (CA, USA). Data are represented as the mean +/- the standard error of the media. To check the normality of distributions, we used Kolmogorov-Smirnov test. To analyze statistical differences between two sets of data, we used Student's t-test (parametric data) or Mann–Whitney U test (non-parametric data). Comparisons between more than two sets of data were done using one-way ANOVA or two-way ANOVA (two independent variables) for parametric data and Kruskal-Wallis test or Friedman´s test (two independent variables) for non-parametric data. Post hoc analyses were done using Bonferroni test (parametric data) or Durnett (nonparametric data). Statistically differences were considered significant at $p<0.05$.

Image analysis: Colocalization was assessed using the Pearson correlation coefficient, which measures the linear correlation between the intensity distributions of two channels and ranges from –1 (perfect negative correlation) to 1 (perfect positive correlation), with values near 0 indicating no correlation. The Manders overlap coefficient ranges from 0 to 1 and reflects the degree of spatial overlap between signals, where 0 indicates no overlap and 1 indicates complete colocalization.

RESULTS

6. RESULTS

IDE levels are reduced in β-cells from patients with T2D (162). For this reason, we considered important to investigate whether IDE is necessary for proper β-cell function. Because IDE was only partially decreased in β-cells of T2D patients we examine the role of IDE in a cellular model of partial IDE deficiency (Min6-shIDE and Ins1E-shIDE) (showing a 40–70% reduction). In addition, we decided to explore the physiological implications of partial IDE loss in β-cells using six-month-old B-IDE-HT mice.

In a previous study from our laboratory (168), the metabolic and functional profile of B-IDE-KO mice, which completely lack IDE in β-cells, was characterized in order to understand the role of IDE in these cells. This characterization was performed at six months of age and revealed several phenotypic alterations in both the metabolic *in vivo* characterization and in cell and function *ex vivo*, most importantly fasting hyperinsulinemia with normoglycemia, dysregulated glucose-stimulated insulin secretion, and reduced expression of β-cell maturity markers, indicative of insulin resistance and β-cell functional immaturity.

On the other hand, previous results from our laboratory in α-cells (A-IDE-KO) (169) suggest a potential role of IDE in cell proliferation and the regulation of the primary cilium, which is composed, among other proteins, of acetylated tubulin.

PART 1: CHARACTERIZATION OF B-IDE-HT AND B-IDE-KO MICE:

To further investigate this potential regulation of IDE in β-cells, we conducted a characterization study of pancreatic β-cells in these two models of IDE deficiency (B-IDE-KO and B-IDE-HT).

1.1 Metabolic characterization of B-IDE-HT mice

These initial metabolic characterization was only performed in B-IDE-HT mice, because B-IDE-KO mice were previously characterized (168).

We first assessed whether the body weight of B-IDE-HT mice differed from that of B-IDE-WT mice (control mice). No significant differences in body weight were observed at 6 months of age **(Figure 28).**

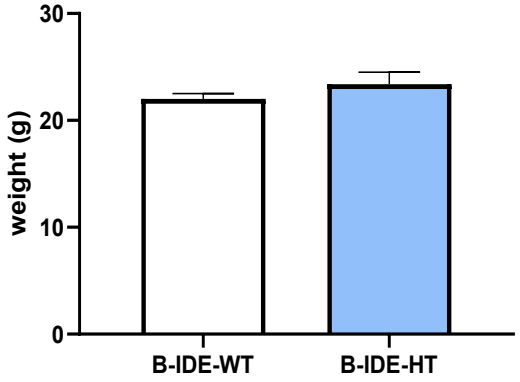

Figure 28: Body weight of B-IDE-WT and HT mice at 6 months. (n = 10 – 26 mice per genotype). Data are represented as mean ± SEM. Statistical analysis was performed using Student´s t-test.

In addition, blood glucose levels were measured under fasting conditions at 6 months of age. Fasting glucose levels at both 16 and 6 h were within the normal range, with no significant differences between the two groups **(Figure 29A - 29B).**

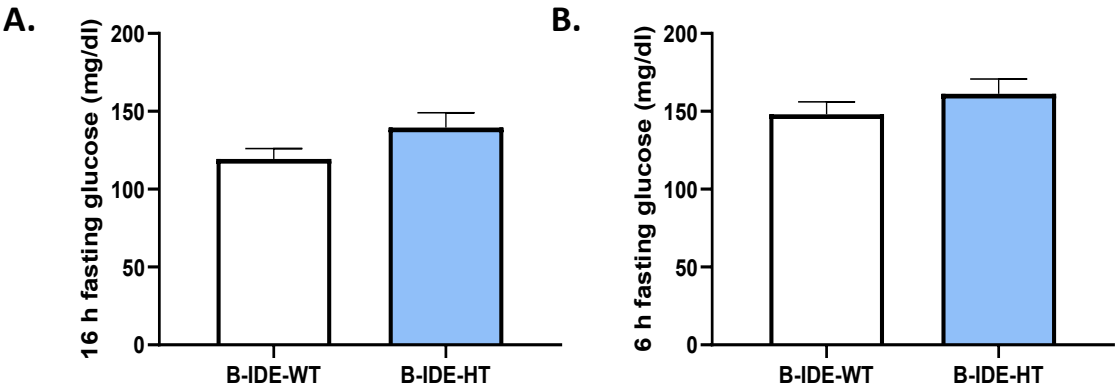

Figure 29: Circulating levels of glucose of B-IDE-HT mice at 6 months. A: Blood glucose levels under 16 h fasting conditions**. B:** Blood glucose levels under 6 h of fasting conditions. (n = 10 – 26 mice per genotype). Data are represented as mean ± SEM. Statistical analysis was performed using Student´s t-test.

To evaluate glucose homeostasis in B-IDE-HT mice, we performed an intraperitoneal glucose tolerance test (IPGTT) at 6 months of age. The results indicated normal glucose tolerance in B-IDE-HT mice **(Figure 30).**

In B-IDE-KO mice, significant increase in glycemia compared to WT was observed 15 min after glucose administration at 6 months of age, as previously reported (168). In this case, B-IDE-HT mice, showed a trend toward increased glycemia at 15 min, although it was not significantly different **(Figure 30 A).** Although, when analyzing the area under the curve (AUC), B-IDE-HT mice showed no differences with B-IDE-WT mice a **(Figure 30 B).**

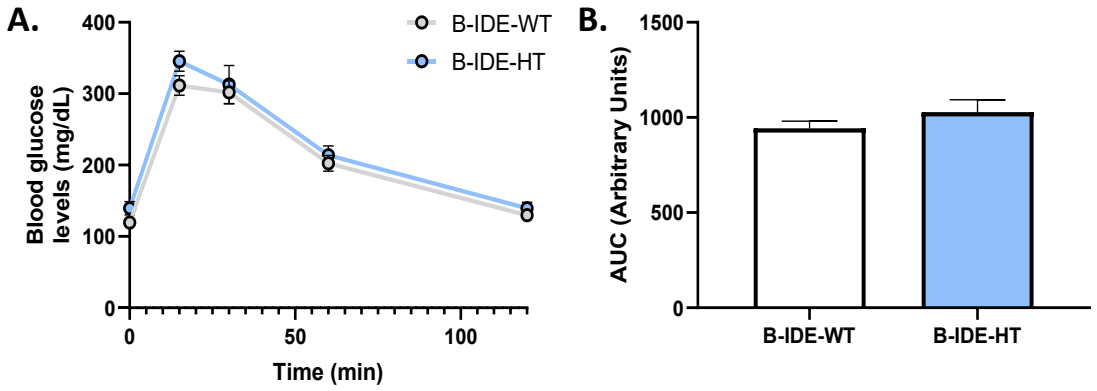

Figure 30: Intraperitoneal Glucose Tolerance Test at 6 months in B-IDE-HT mice. **A:** IP-GTT: Blood glucose levels after glucose challenge (2g/kg). **B:** Area under the curve (AUC) of A. (n = 10 – 26 mice per genotype). Data are represented as mean ± SEM. Statistical analysis was performed using Student´s t-test.

1.2 Functional characterization of B-IDE-HT mouse islets

To determine how partial loss of IDE affects insulin secretion, we isolated islets from B-IDE-HT mice and their controls, following the protocol described in the Materials and Methods section. GSIS assays revealed that B-IDE-HT islets exhibited an impaired insulin secretion in response to high glucose (**Figure 31A-B**), supporting the crucial role of IDE in maintaining proper β-cell function under high-glucose conditions.

We next investigated whether glucagon could further enhance insulin secretion in these islets. GSIS assays in the presence of glucagon showed that, although insulin secretion remained lower in B-IDE-HT islets compared to controls under high glucose, glucagon still exerted a positive effect in both groups (B-IDE-HT and control) **(Figure 31A and C).**

To explore whether the altered insulin secretion observed in B-IDE-HT mice is linked to impaired intracellular Ca^{2+} mobilization, a study of Ca^{2+} transport in response to glucose in the islets was conducted, comparing B-IDE-WT and B-IDE-HT mice. The fluorescence of Ca^{2+} entering the ER (F_{ER}) revealed a significant decrease in B-IDE-HT mice, suggesting reduced Ca^{2+} uptake and pointing to a defect in Ca^{2+} signaling originated from the ER.

In B-IDE-HT mice, in response to 8 mM glucose, a condition that typically triggers a massive Ca^{2+} influx for insulin secretion, the maximum peak of Ca^{2+} entering the cytoplasm was notably lower. A similar trend was observed in response to 16 mM glucose, though the reduction did not reach statistical significance, it was on the verge of being significant. When the cells were stimulated with high potassium (K^+) to fully depolarize the membrane and induce the release of granules independent of glucose,

B-IDE-HT mice showed a tendency toward reduced Ca^{2+} entry, but this difference was not statistically significant.

Finally, the area under the curve (AUC) at both 8 mM and 16 mM glucose was significantly lower in the heterozygous mice. Since the AUC directly correlates with the total Ca^{2+} influx, these results highlight impaired Ca^{2+} signaling in B-IDE-HT mice at both glucose concentrations, which ultimately contributes to reduced insulin secretion.

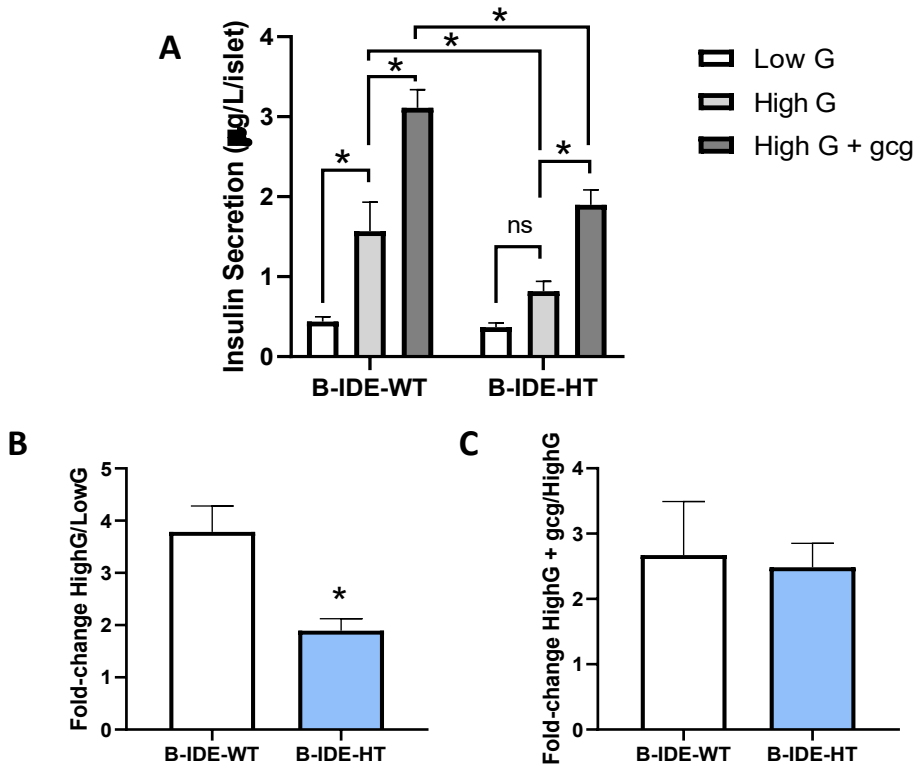

Figure 31. In vivo effects of partial genetic IDE ablation in pancreatic β-cells on insulin secretion at 6 months of age. A: Glucose-stimulated insulin secretion (GSIS) in islets from B-IDE-WT and B-IDE-HT mice under three conditions: 3 mM glucose, 16 mM glucose, and 16 mM glucose in the presence of 200 nM glucagon. (n = 3 mice per genotype, measured in triplicate). **B:** Fold-change in insulin secretion at high versus low glucose (HighG/LowG). **C:** Fold-change in insulin secretion at high glucose with glucagon versus high glucose (HighG+gcg/HighG). Data are presented as mean ± SEM.*$p < 0.05$ by two-way ANOVA (A) or unpaired Student's t-test (B and C).

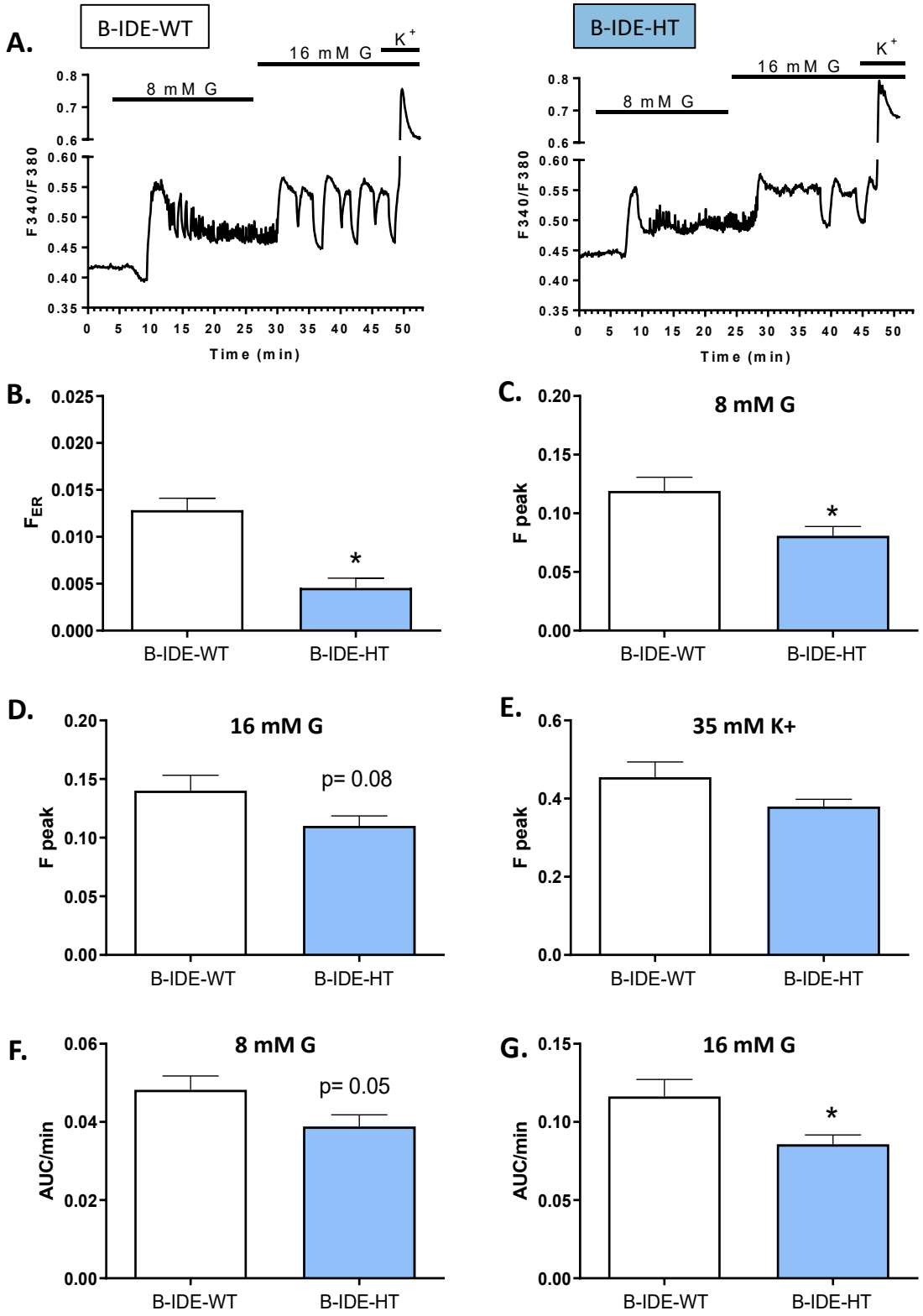

Figure 32. Intracellular calcium responses in pancreatic islets from B-IDE-WT and B-IDE-HT mice measured with Fura-2. **A:** Representative Ca^{2+} recordings in islets from B-IDE-WT and B-IDE-HT mice. **B:** ER fluorescence ratio (F_{ER}), reflecting Ca^{2+} uptake in the ER. **C-E:** Peak fluorescence ratios (F_{Peak}) in response to stimulation with 8 mM glucose (C), 16 mM glucose (D), and 35 mM KCl to induce membrane depolarization (E). **F-G:** Area under the curve (AUC) of the calcium response upon stimulation with 8 mM (F) and 16 mM (G) glucose. Statistical analysis was performed using Student's t-test; $p < 0.05$ was considered significant. Data are presented as mean ± SEM.

1.3 Morphometric characterization of B-IDE-HT and B-IDE-KO islets

To investigate whether IDE deficiency could contribute to changes in islet composition, pancreatic sections from B-IDE-HT, B-IDE-KO and B-IDE-WT (control) mice were analyzed using doble immunostaining for insulin and glucagon **(Figure 33A).**

The proportion of β- and α-cells within the islets was quantified for both groups of mice. The percentage of β-cells showed a slight increase in B-IDE-HT islets and a significant increase in B-IDE-KO islets **(Figure 33 B).** However, no differences were observed in the percentage of α-cells across these groups **(Figure 33 C).**

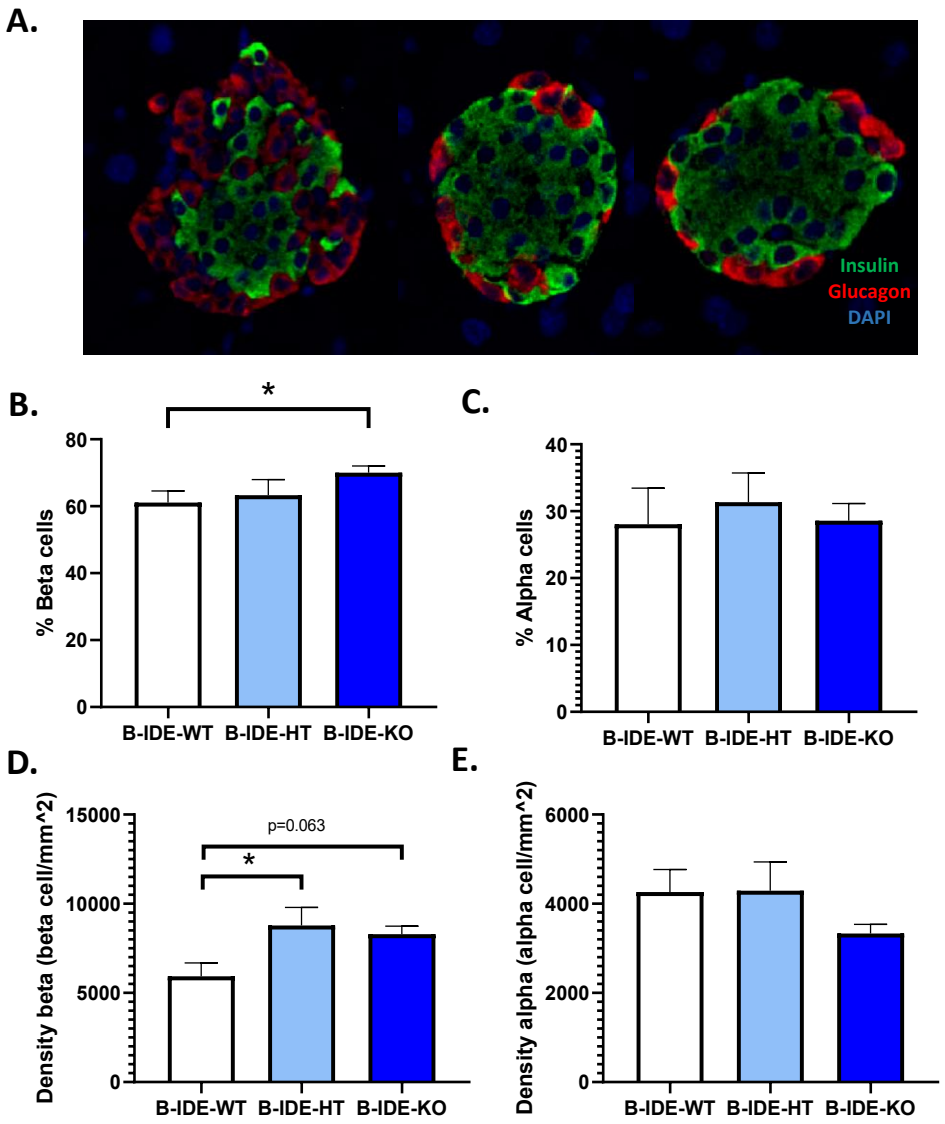

Figure 33: Islet characterization of β-cell specific insulin-degrading enzyme knockout (B-IDE-KO) and heterocigote (B-IDE-HT) mouse at 6 months of age. A: Representative image of islet staining for insulin (green), and glucagon (red). **B**: Percentage of β-cells in the islet. **C**: Percentage of alpha-cells in the islet. **D**: β-cell density in the islet. **E**: Alpha-cell density in the islet. (n = 6 B-IDE-WT, n = 5 B-IDE-HT, n = 6 B-IDE-KO). *p<0.05 by one-way ANOVA. Data are represented as mean ± SEM.

β-cell density, defined as the number of β-cells per islet area, was significantly higher in B-IDE-HT islets and showed a strong trend toward significance in B-IDE-KO islets **(Figure 33 D).** In contrast, α-cell density remained unchanged **(Figure 33 E).**

These findings suggest that IDE deficiency in β-cells may contribute to an increase in β-cell proliferation within the islet.

To further analyze the structural differences in pancreatic islets, we measured the area of α- and β-cells in B-IDE-HT and B-IDE-KO mice compared to their B-IDE-WT controls.

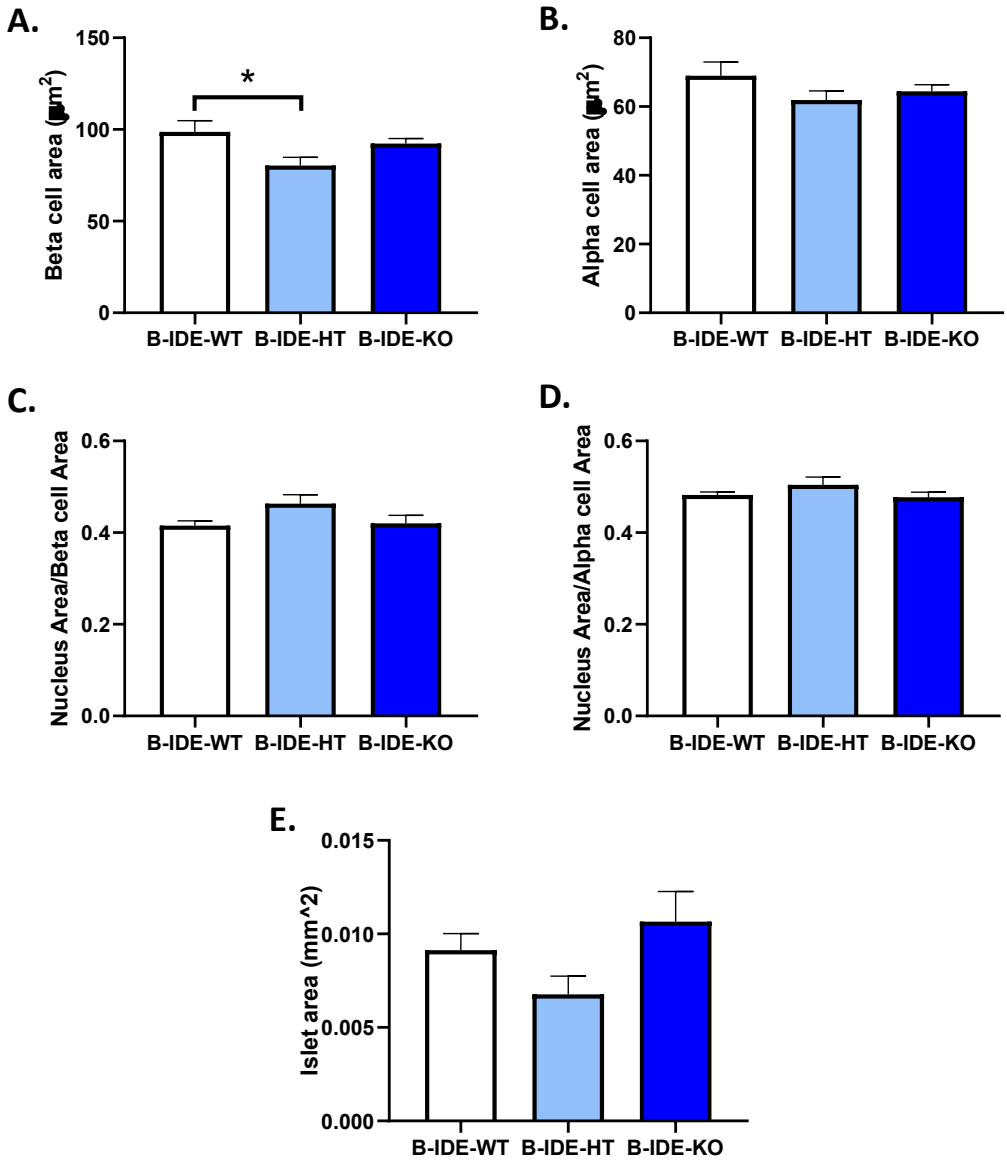

Figure 34: Cellular characterization of β-cell specific insulin-degrading enzyme knockout (B-IDE-KO) and heterocigote (B-IDE-HT) mouse at 6 months of age. A: β-cell area in the islet. B: α-cell area in the islet. **C:** Nucleus-to-cytoplasm area ratio in β-cells. **D:** Nucleus-to-cytoplasm area ratio in alfa-cells. **E:** Total islet area. (n = 6 B-IDE-WT, n = 5 B-IDE-HT, n = 6 B-IDE-KO). *p<0.05 by one-way ANOVA. Data are represented as mean ± SEM.

β-cell area was significantly reduced in B-IDE-HT mice compared to controls **(Figure 34 A).** A similar trend was observed in B-IDE-KO β-cell, although it did not reach statistical significance. These data, compared with the previous figure showing increased β-cell percentage and density, indicate that our β-cell-specific IDE-deficient mouse models have more β-cells overall, but individual cells are smaller. In contrast, no significant differences were found in α-cell area across the groups **(Figure 34 B).**

We also assessed the nuclear to cytoplasmic area ratio in both cell types. No significant differences were detected in β- **(Figure 34 C)** or α-cells **(Figure 34 D).**

Regarding islet size, B-IDE-HT mice exhibited a trend toward smaller islets compared to controls, but this difference was not statistically significant **(Figure 34 E).**

1.4 Study of primary cilia in B-IDE-HT and B-IDE-KO pancreata

To investigate whether IDE was regulating ciliogenesis, we quantified the number of cilia per cell and their length in both α- and β-cells of B-IDE-HT and B-IDE-KO mice compared to B-IDE-WT. Primary cilia were identified by acetylated tubulin staining, which appears in magenta, while insulin and glucagon were labeled in green and red, respectively **(Figure 35A).**

In β-cells, the number of cilia per cell was significantly reduced in B-IDE-HT mice, with an even greater reduction observed in B-IDE-KO mice **(Figure 35 A, B).** In α-cells, there was an almost significant reduction in the number of cilia per cell in both B-IDE-HT and B-IDE-KO mice, suggesting a potential impact of β-cell IDE loss on α-cell ciliation **(Figure 35 D).** However, no significant differences were observed in ciliary length between the groups in either β-cells **(Figure 35 C)** or α-cells **(Figure 35 E).**

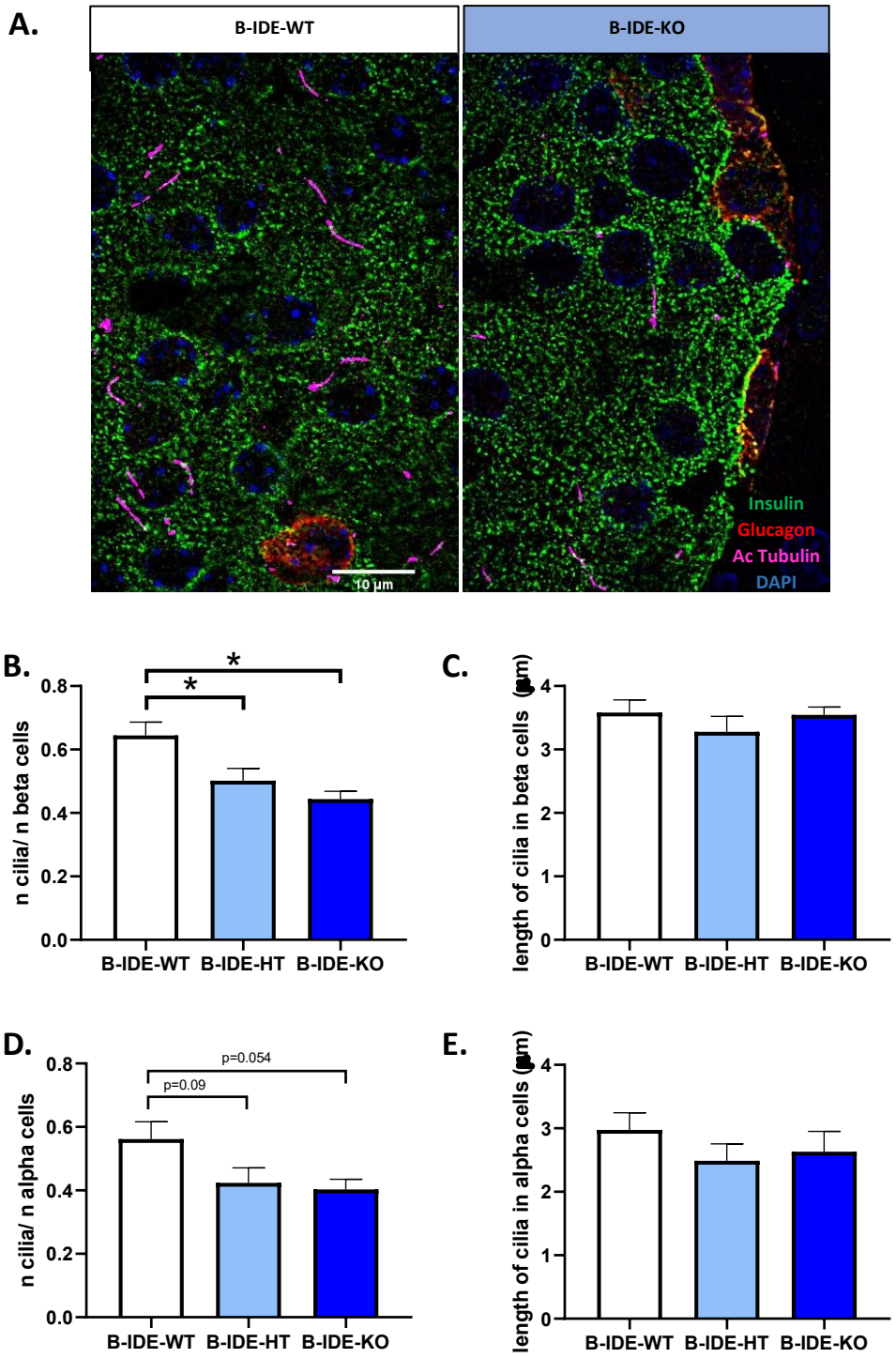

Figure 35: Cilia characterization of β-cell specific insulin-degrading enzyme knockout (B-IDE-KO) and heterocigote (B-IDE-HT) mouse homeostasis at 6 months of age. A: Representative confocal image of islet staining for cilia stained with acetylated tubulin (magenta), insulin (green), and glucagon (red). **B:** Quantification of average of number of cilia per β-cell. **C:** Quantification of β-cilia length. **D:** Quantification of average of number of cilia per α-cell. **E:** Quantification of α-cilia length (n = 5 B-IDE-WT, n = 5 B-IDE-HT, n = 5 B-IDE-KO). *p<0.05 by one-way ANOVA. Data are represented as mean ± SEM.

Summary of Findings Part 1

- **Metabolism:** Body weight is not altered in B-IDE-HT mice compared to controls. A slight increase in glucose levels was detected 15 min after IPGTT.
- **Islet function:** Insulin secretion in response to high glucose and glucagon was significantly impaired in B-IDE-HT β-cells relative to controls.
- **Calcium dynamics:** Altered Ca^{2+} mobilization in the endoplasmic reticulum and the cytoplasm at 8 mM and 16 mM glucose in B-IDE-HT β-cells, which may underlie their impaired insulin secretion.
- **Islet composition and structure:** Islets from B-IDE-KO and B-IDE-HT showed increased β-cell density, reduced β-cell area, and a trend toward smaller islets. No changes in α-cells were detected.
- **Primary cilia:** Significant reduction in the number of cilia in β-cells of B-IDE-HT and B-IDE-KO mice, compared to controls.

These data highlight the physiological relevance of IDE in β-cell function, islet composition, and primary cilium regulation.

PART 2: IDE-KNOCKDOWN IN BETA CELLS

Previous findings in the preclinical models of IDE loss of expression (A-IDE-KO, B-IDE-HT, and B-IDE-KO) suggest that IDE regulates both α- and β-cell function. Our hypothesis is that IDE exerts this regulation through the modulation of the primary cilium and the tubulin cytoskeleton, which may also influence the transport of insulin and glucagon receptors to the membrane, leading to dysregulation of the paracrine signaling in β-cells.

2.1 Generation and analysis of IDE knockdown in β-cells

To investigate more deeply the role of IDE in pancreatic β-cells, we generated several models of IDE knockdown in two β-cell lines: Ins1E and Min6. IDE depletion was performed using shRNA- technology as described in the Materials and Methods section. Our primary goal was to evaluate the effects of IDE depletion across different cellular models.

2.1.1 Generation and analysis of IDE-KD in Ins1E β-cell line: Ins1E-shRNA-IDE

To validate IDE knockdown in Ins1E cells, we first measured IDE protein levels by WB. There was a 40% IDE protein reduction in shRNA-IDE Ins1E cells compared to their control cells **(Figure 36 A, B).** These results indicate that IDE knockdown was effective.

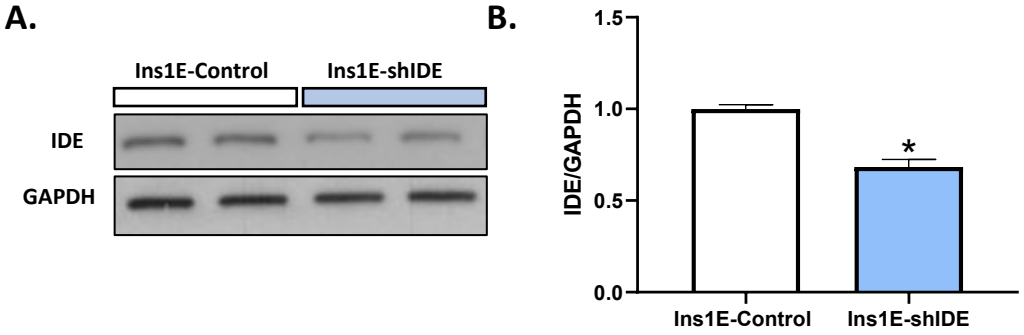

Figure 36: Protein levels of Ide in shRNA-IDE Ins1E cells. A: Representative WB of IDE levels in control and shRNA-IDE Ins1E cells. **B:** Quantification of IDE by WB. (N=3, in triplicates). *p<0.05 versus Control by Student's t-test. Data are presented as means ± SEM.

2.1.2 Generation and analysis of IDE-KD in the Min6 β-cell line: Min6-shRNA-IDE

For the study with Min6 cells, we used Min6-WT and Min6-shRNA-CTL cells as controls. Prior to their use, we verified that both behaved similarly. This validation was performed by comparing IDE knockdown levels in Min-shIDE cells **(Figure 37 A, B)** and functionally assessing GSIS **(Figure 37 C).** From here on, both Min6 (Min6-WT) and Min6-shRNA (Min6-shRNA-CTL) cells will be used as controls and they will be called Min6-Control in figures and text.

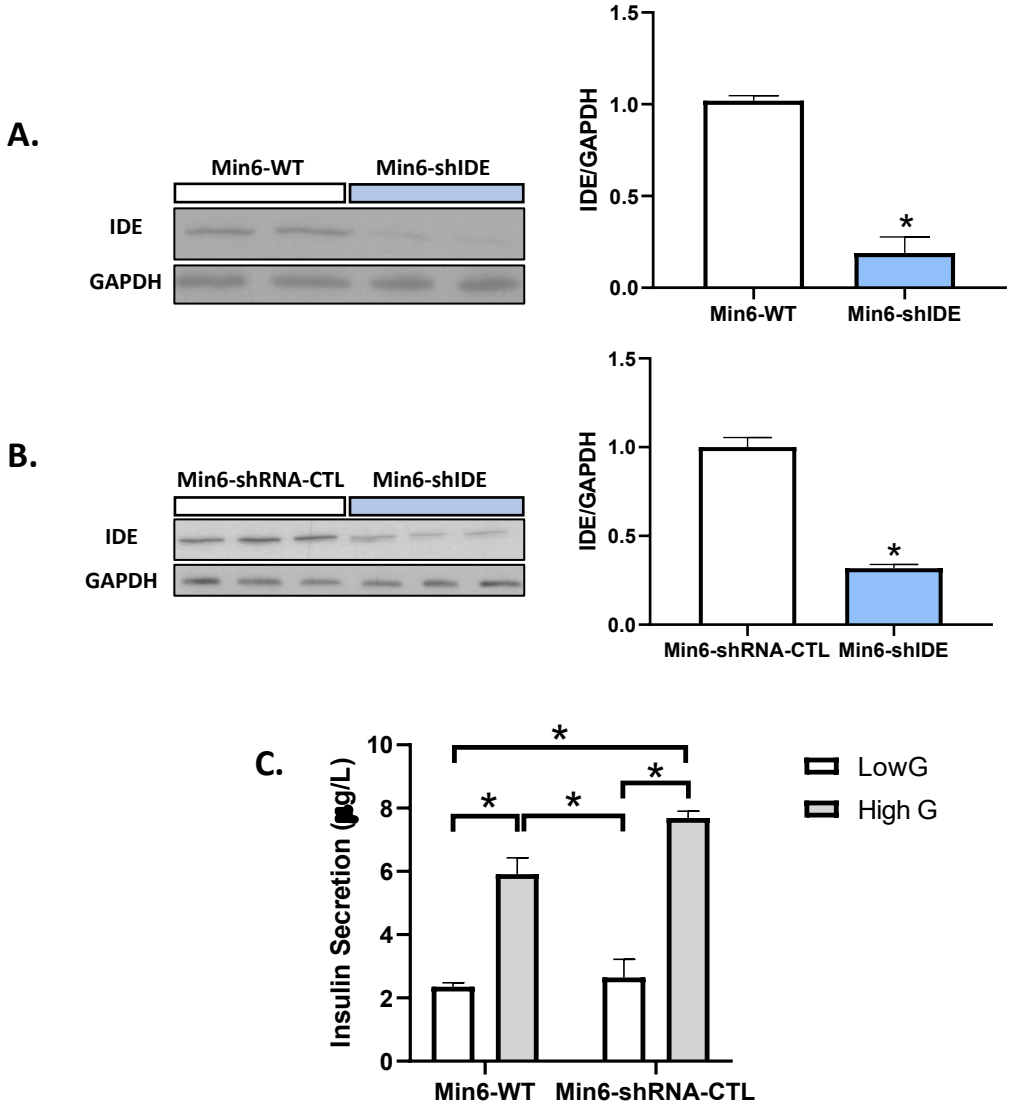

Figure 37: Validation of control cell lines and IDE knockdown in Min6 cells. **A:** Representative WB of IDE levels in WT and shIDE Min6 cells and quantification of IDE by WB. (N=3, in triplicates). **B:** Representative WB of IDE levels in Min6-shRNA-CTL and shIDE Min6 cells and quantification of IDE by WB. (N=3, in triplicates). **C:** Glucose-stimulated insulin secretion assays showed no functional differences between Min6-WT and Min6-shRNA-CTL cells, validating their use as interchangeable controls. *p<0.05 by two-way ANOVA and Student's t-test. Data are presented as means ± SEM.

We validated the reduction of IDE in Min6 cells. In this model, we achieved our highest knockdown efficiency, with a 70% reduction in IDE expression in shRNA-IDE compared to Min6-Control cells **(Figure 38 A, B),** which was sustained over time across multiple passages under puromycin selection pressure.

We also performed quantitative RT-qPCR to confirm IDE knockdown and observed a significant reduction of 60% in *Ide* mRNA levels in IDE-KD Min6-cells (Min6-shIDE) compared to their control cells **(Figure 38 C).**

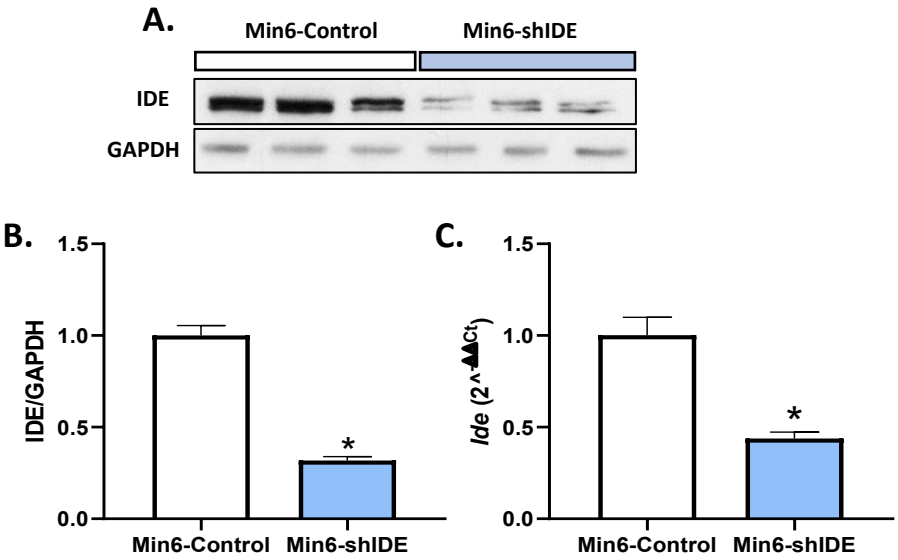

Figure 38: Protein and mRNA levels of Ide in shIDE Min6 cells. A: Representative WB of IDE levels in Control and shIDE Min6 cells. **B:** Quantification of IDE by WB. (N=3, in triplicates). **C:** Results of RT-quantitative PCR measurements of *Ide* expression in Control and shIDE Min6 cells. *p<0.05 versus Control by Student's t-test. Data are presented as means ± SEM.

To further validate the observed reduction in IDE levels and considering that this technique was widely used throughout our study, we performed immunostaining to confirm the decrease in IDE expression **(Figure 39).** We quantified the IDE-positive area relative to the total cell area in each image and observed an approximate 70% reduction in IDE levels in knockdown cells compared to controls **(Figure 39 C).**

In Min6-Control cells, IDE staining was more concentrated in a specific perinuclear region, with additional diffuse staining throughout the cytoplasm. In contrast, in Min6-shIDE cells, the intensity of perinuclear structures appeared to be maintained; however, IDE staining in the cytoplasm was significantly reduced, indicating an overall decrease in IDE expression **(Figure 39 A, B).**

With these results, we confirm that we have two effective IDE-KD models for our study.

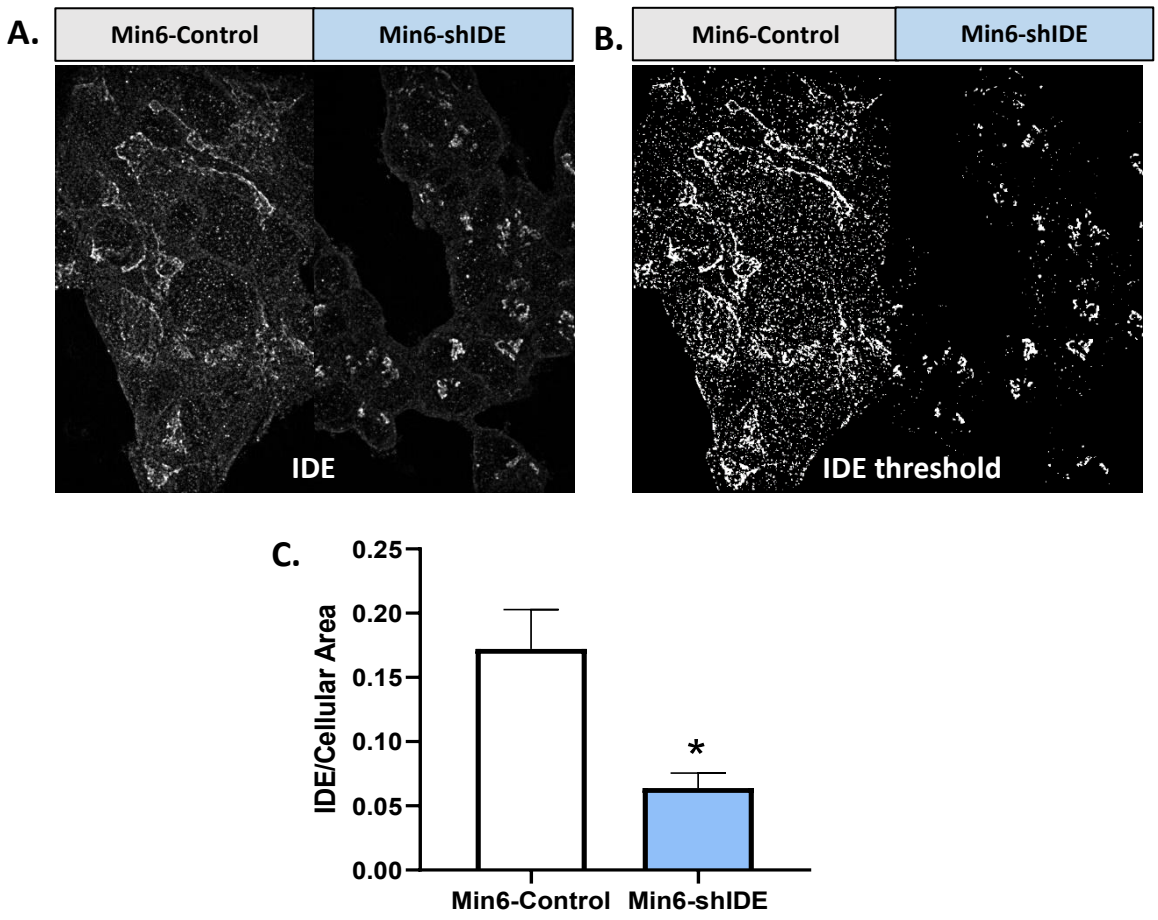

Figure 39. Analysis of IDE expression in Min6-Control and shIDE cells using confocal microscopy. **A:** Representative images of Min6-Control and Min6-shIDE stained for IDE. **B:** Threshold to segment the specific IDE signal. **C**: Quantification of the IDE-positive area/total cell area. (n = 8 images). *p<0.05 versus Control by Student´s t-test. Data are presented as means ± SEM.

2.2 Characterization of IDE-KD β-cells

2.2.1 Impact of IDE depletion on proliferation and viability of Min6-cells

To assess whether IDE depletion affects cell proliferation, we performed BrdU staining assay and quantified the number of BrdU-positive nuclei in the Min6-shIDE cells compared to its control **(Figure 40 A).** Although the results did not show a statistically significant difference, we observed a trend toward an increase in BrdU-positive cells upon IDE knockdown.

Additionally, to determine whether cell viability is affected when IDE levels are reduced, we conducted an MTT assay. Analysis of absorbance as an indicator of metabolic activity revealed no significant changes between Min6-shIDE cells and their respective controls **(Figure 40 B).** These findings indicate that IDE depletion does not impair cell viability under the conditions tested.

Overall, our data suggests that IDE knockdown does not have a strong impact on cell proliferation or viability in Min6 cells.

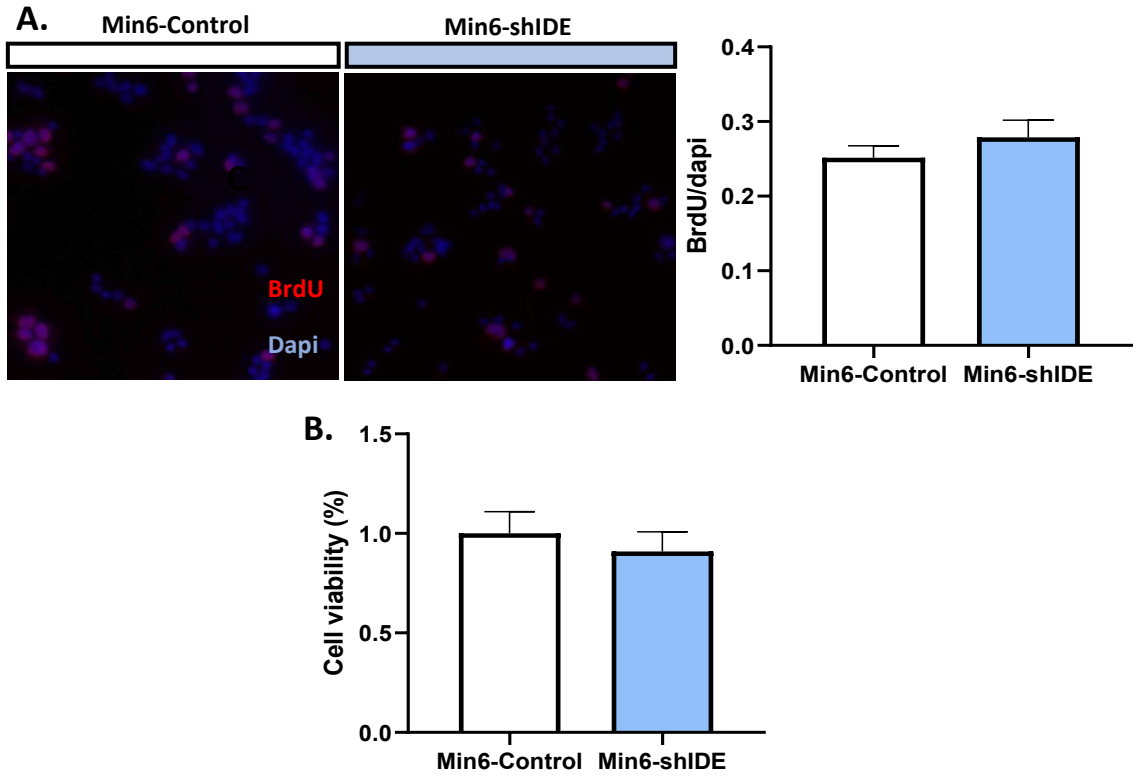

Figure 40. Proliferation and cell viability in shIDE Min6 cells. A: BrdU assay to assess cell proliferation in control and IDE-KD cells, with corresponding quantification (N=2, triplicates). **B:** MTT assay comparing cell viability between control and shIDE Min6 cells (N=5). Statistical analysis was performed using Student´s t-test. Data are presented as means ± SEM.

2.2.2 Glucose-stimulated insulin secretion in Min6-shIDE cells

To characterize these cell lines, we first assessed β-cell function by analyzing glucose-stimulated insulin secretion (GSIS). IDE suppression in β-cells resulted in a marked reduction of insulin secretion, particularly in response to glucose overload **(Figure 41).** These findings are consistent with the results obtained in B-IDE-HT islets. However, the fold change did not reach statistical significance, likely because Min6-shIDE cells already showed reduced basal secretion at low glucose, diminishing the relative difference at high glucose.

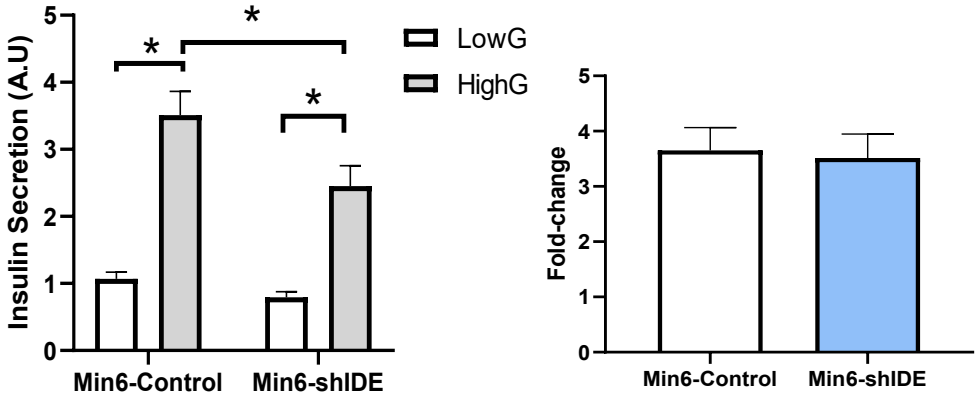

Figure 41: In vitro effects of IDE inhibition on insulin secretion in Min6 shIDE cells. Glucose-stimulated insulin-secretion in Min6 cell lines exposed to 3 mM glucose or 16 mM glucose and fold change of data. N=6 different experiments by triplicates. *p<0.05 by two-way ANOVA. Data are represented as mean ± SEM.

2.3 Regulation of the IDE–tubulin–primary cilium axis under stimulatory and inhibitory glucose conditions

In presence of high glucose, β-cells produce and secrete high levels of insulin to lower glucose concentrations and maintain glucose homeostasis. The tubulin cytoskeleton plays a key role in regulating insulin secretion. The primary cilium structure is based on microtubules that form the axoneme. Tubulin undergoes posttranslational modifications as acetylation to stabilize microtubules for ciliogenesis. Primary cilium facilitates communication with neighboring cells to support proper β-cell function. (76,253)

As demonstrated by earlier results in this thesis, IDE plays a crucial role in insulin secretion under high glucose conditions. To further investigate the role of IDE in regulating these proteins involved in β-cell function under glucose conditions, we performed an insulin secretion assay under low- and high-glucose conditions (3 and 16 mM glucose) in both control and IDE-KD β-cells. Additionally, we conducted various analyses to assess cytoskeletal and ciliary protein regulation, in conditions of insulin secretion (16 mM) and inhibition (3 mM).

2.3.1 Effect of glucose on IDE expression in β-cells

To investigate the role of IDE in pancreatic β-cell function, we detected IDE protein expression levels under low and high glucose concentrations. Interestingly, IDE expression was not regulated by glucose either in control conditions **(Figure 42 A)** or in IDE-depleted conditions (Ins1E-shIDE, **Figure 42 B).**

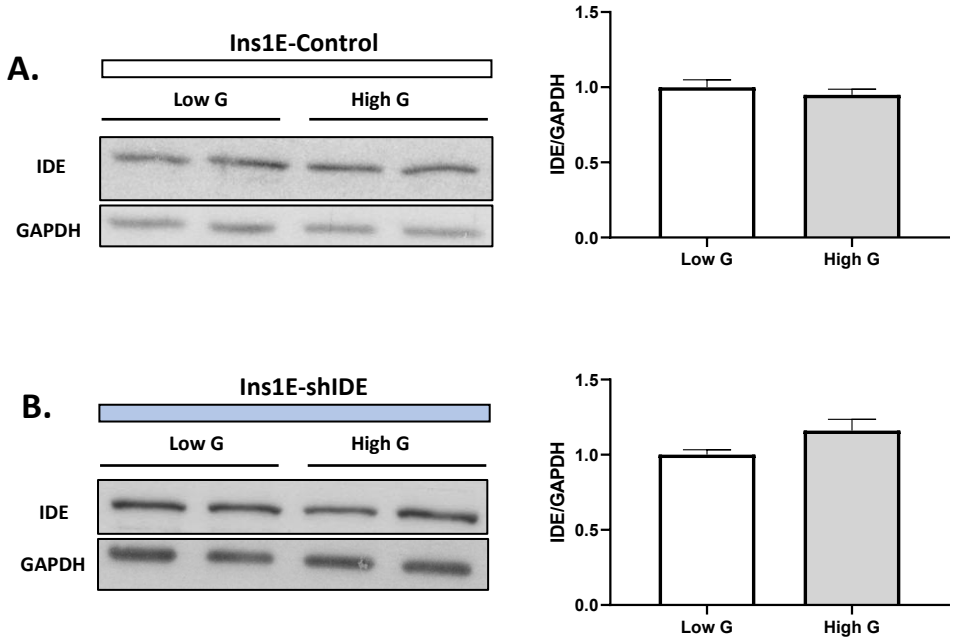

Figure 42: Protein levels of IDE in Ins1E-Control and shIDE under basal (Low G) and secretory (High G) conditions. A: Representative WB panel and quantification of IDE by WB in Ins1E control conditions. **B:** Representative WB panel and quantification of IDE by WB in Ins1E-shIDE. Statistical analysis was performed using Student´s t-test. Data are represented as mean ± SEM.

2.3.2 Impact of IDE depletion on cytoskeleton dynamics in β-cells under basal (low glucose) and secretory conditions (high glucose)

Tubulin cytoskeleton plays a crucial role in insulin secretion by β-cells (82). Previous results from our group have shown that IDE depletion drastically reduces tubulin levels in α-cells (169). Based on this, the objective of this section is to investigate the role of IDE in β-cells under both inhibitory and stimulatory insulin secretion states using Ins1E and Min6 cells.

A.) Impact of IDE depletion on tubulin levels in Ins1E cells under basal and secretory conditions

First, we analyzed tubulin levels in Ins1E-Control cells **(Figure 43 A, B)** under low-glucose conditions (3 mM), where insulin secretion is minimal, and high-glucose conditions (16 mM), when insulin secretion is elevated. Although no significant differences were observed, there was a tendency to reduced tubulin levels under high glucose. Additionally, we performed tubulin staining and generated heat maps from the acquired images by confocal microscope **(Figure 43 C).** An increased tubulin signal was observed at the cell periphery under high-glucose conditions, suggesting enhanced microtubule organization in regions where insulin granules are trafficking, supporting the idea of active vesicle transport and secretion.

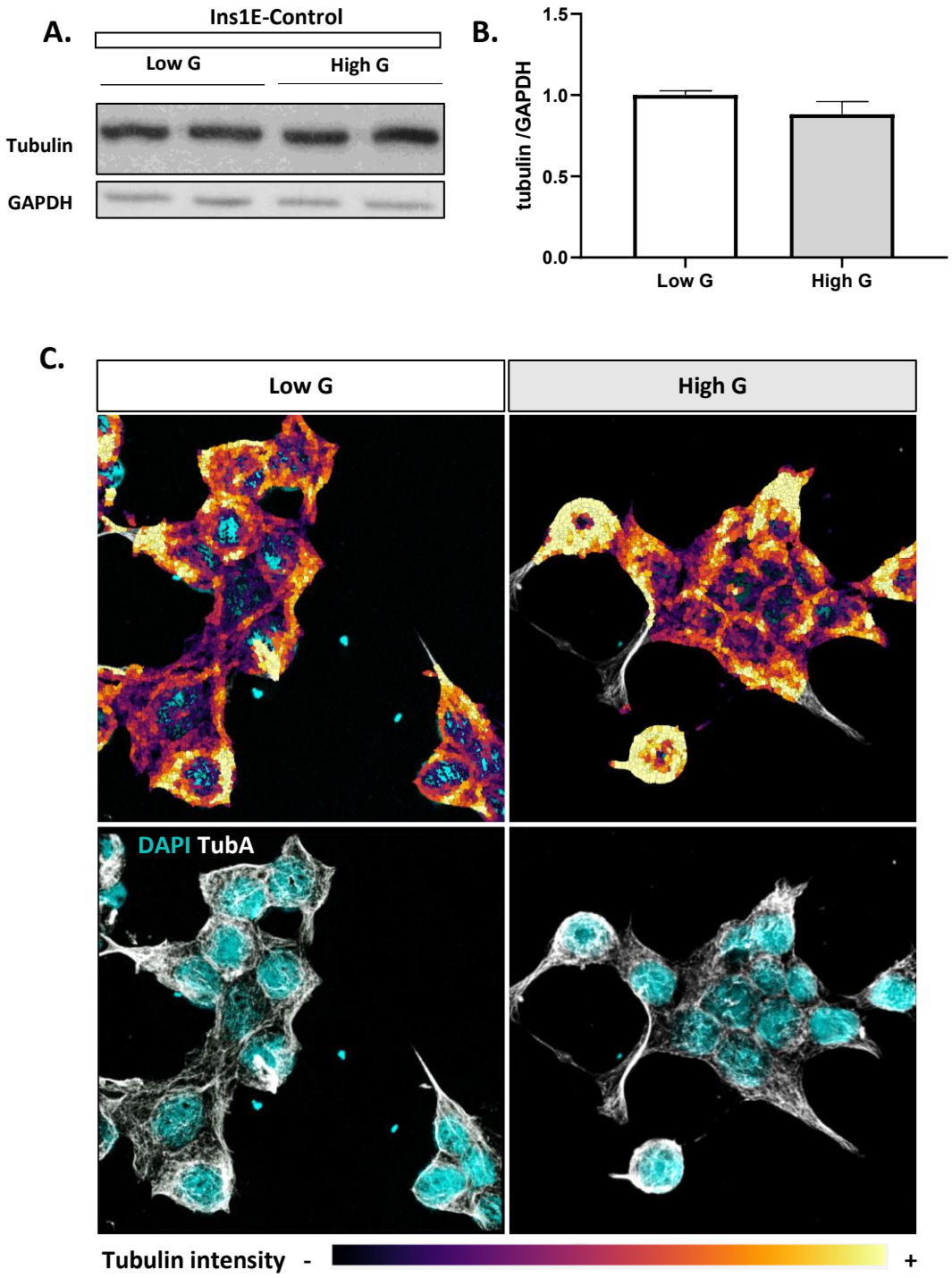

Figure 43: Tubulin protein levels stained by intensity in Control Ins1E cells under basal and secretory conditions. A: Representative WB panel of tubulin. **B**: Quantification of Tubulin by WB. (N=3, in duplicates). **C:** Tubulin intensity heatmap in Control Ins1E-cells. Statistical analysis was performed using Student´s t-test. Data are presented as means ± SEM.

We then conducted the same analysis in Ins1E-shIDE cells **(Figure 44).** In this case, when cells were treated with high glucose, tubulin levels significantly increased compared to Ins1E-shIDE cells under low-glucose conditions **(Figure 44 A, B).** Heat maps of tubulin cytoskeleton staining further confirmed these findings, showing not only

an increase in tubulin intensity but also a more concentrated distribution within the cytoplasm. This contrasts with Ins1E-Control cells under high-glucose conditions, where tubulin localization was more prominent at the periphery, likely facilitating insulin exocytosis. These results suggest that IDE plays a key role in tubulin regulation, particularly under high-glucose conditions in Ins1E cells.

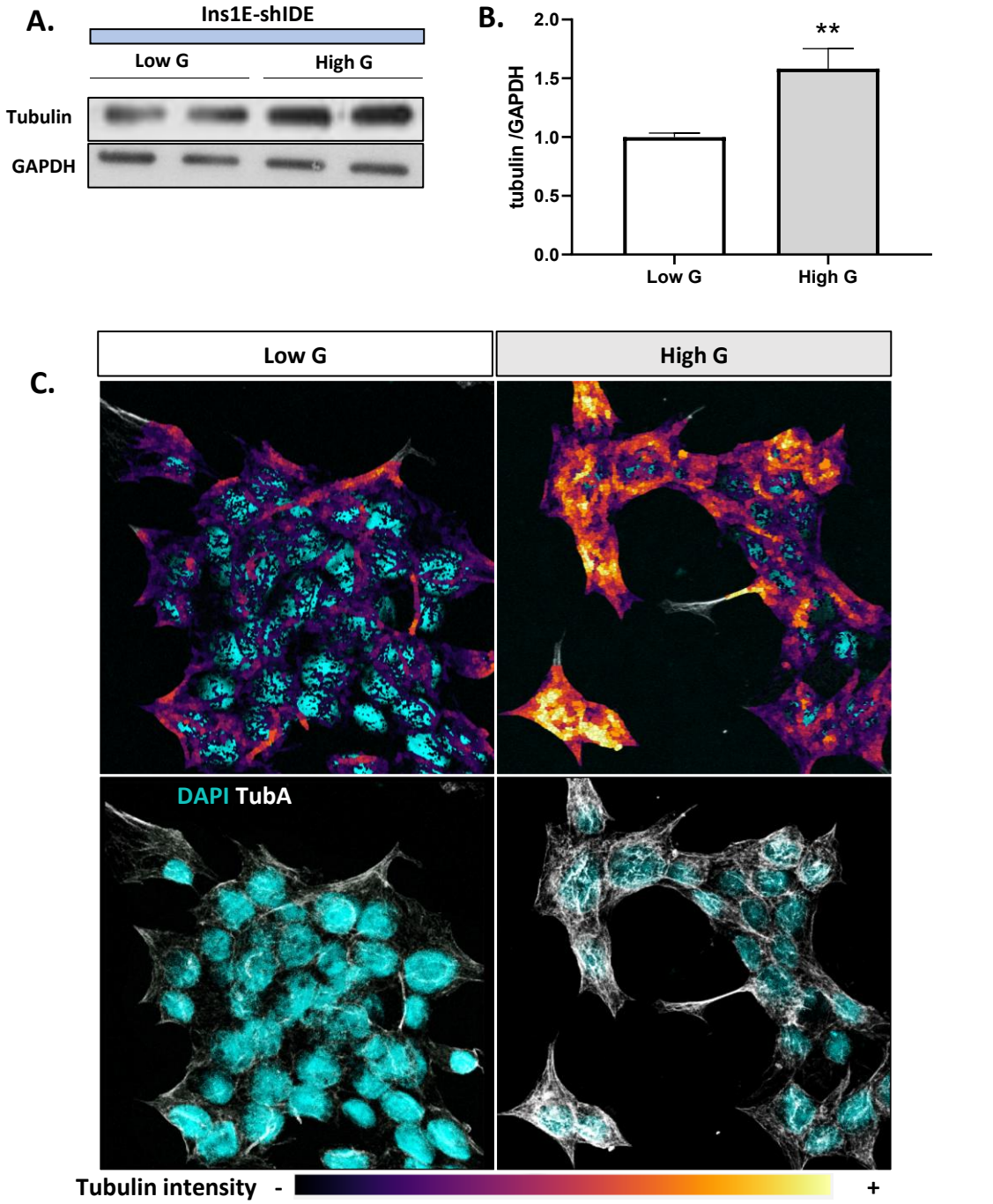

Figure 44: Tubulin protein levels stained by intensity in Ins1E-shIDE cells under basal and secretory conditions. A: Representative WB panel of tubulin. **B:** Quantification of tubulin by WB. (N=3, in duplicates). **C**: Tubulin intensity heatmap in Control Ins1E cells. **p<0.01 by Student´s t-test. Data are presented as means ± SEM.

B.) Impact of IDE depletion on tubulin levels in Min6-cells under basal and secretory conditions.

To validate these findings and investigate the role of IDE in tubulin regulation under glucose conditions, we repeated the same experiment in Min6 cells. In this case, both control and shIDE cells were subjected to low- and high-glucose treatments in parallel, allowing us to directly compare our results including IDE expression levels.

We analyzed tubulin protein levels in Min6-Control and Min6-shIDE cells under low- (3 mM) and high-glucose (16 mM) conditions **(Figure 45 A, B).** No significant differences were observed when comparing tubulin levels between glucose conditions within each group. However, an opposing trend in response to glucose was detected. In control cells, tubulin levels tended to decrease in response to high glucose, whereas in Min6-shIDE cells, tubulin levels showed a tendency to increase under high-glucose conditions. Showing a similar behavior than Ins1E cells.

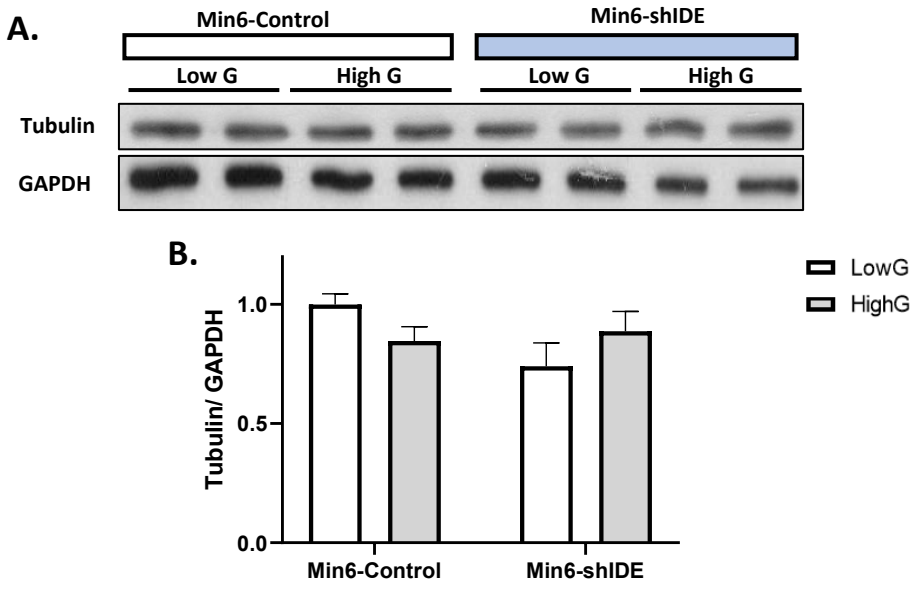

Figure 45: Protein levels of tubulin in Control and shIDE Min6 cells under basal (Low G) and secretory conditions (High G). A: Representative WB panel of tubulin. **B**: Quantification of Tubulin by WB. (N=3, in duplicates). Statistical analysis was performed using two-way ANOVA. Data are presented as means ± SEM.

Tubulin intensity analysis **(Figure 46)** from staining further supported these trends. In Min6-Control cells, tubulin intensity appeared slightly lower under high-glucose conditions compared to low glucose, although the difference was not significant **(Figure 46 B, C).** Additionally, the distribution of tubulin intensity under high glucose showed a shift toward the cell periphery **(Figure 46 A),** like what was observed in Ins1E-cells. In Min6-shIDE cells, we observed a significant increase in tubulin intensity under high glucose conditions **(Figure 46 B, C).** This increase was not only significant compared to low glucose in Min6-shIDE cells but also in comparison to all other conditions (low- and

high- glucose Min6-Control). Moreover, in this high glucose condition, tubulin remained highly concentrated in the cytoplasm **(Figure 46 A),** consistent with our observations in Ins1E-shIDE cells.

These results suggest that both cell models exhibit a similar response to IDE depletion under different glucose conditions. Overall, our findings indicate that IDE plays a role in regulating both the quantity and spatial distribution of tubulin in response to glucose levels.

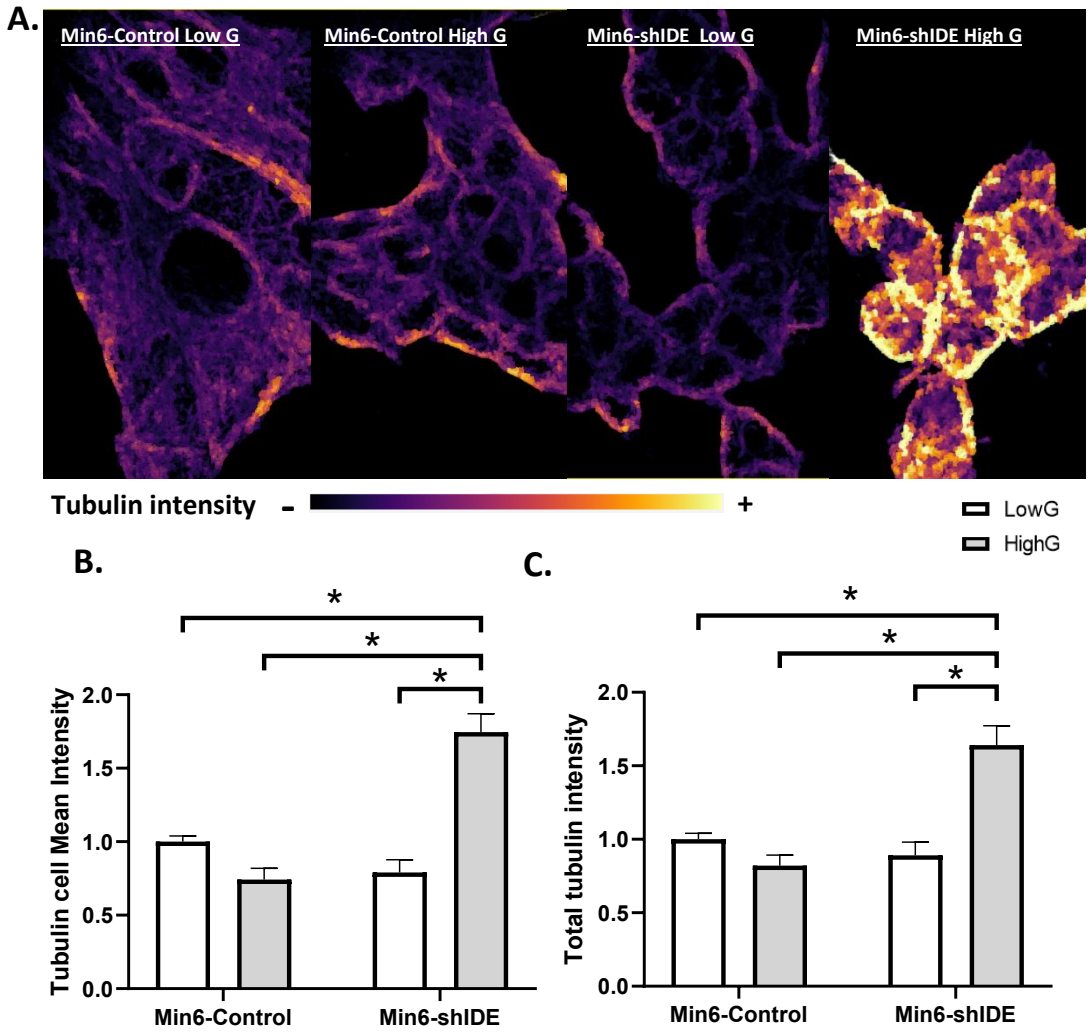

Figure 46. Tubulin intensity in Control and shIDE Min6 cells under basal (Low G) and secretory (High G) conditions. A. Representative heatmap images of tubulin. **B:** Quantification of average cellular tubulin intensity. **C**: Quantification of total tubulin intensity. (N=3, 6 images per N). *p<0.05 by two-way ANOVA. Data are presented as means ± SEM.

C.) Impact of IDE Depletion on tubulin cytoskeleton branching under basal and secretory conditions

To further investigate microtubule behavior under low- and high-glucose conditions in the presence or reduction of IDE, we analyzed microtubule length and curvature **(Figure 47).** In Min6-Control cells, high glucose induced a tendency to microtubule breakage, although this effect was not statistically significant. This trend became more pronounced and significant in Min6-shIDE cells under low- versus high-glucose conditions **(Figure 47 B).** Moreover, in Min6-shIDE cells, microtubule length under low-glucose conditions was significantly greater than in Min6-Control cells **(Figure 47 B).**

In addition, in Min6-shIDE cells under low glucose, microtubules tended to be more curved than in all other conditions, with a statistically significant difference compared to the corresponding control condition **(Figure 47 C).** The Euclidean distance represents the straight-line distance between the start and end points of a microtubule segment, while the branch length corresponds to the actual path the microtubule follows. A lower Euclidean-to-length ratio therefore reflects a curved trajectory.

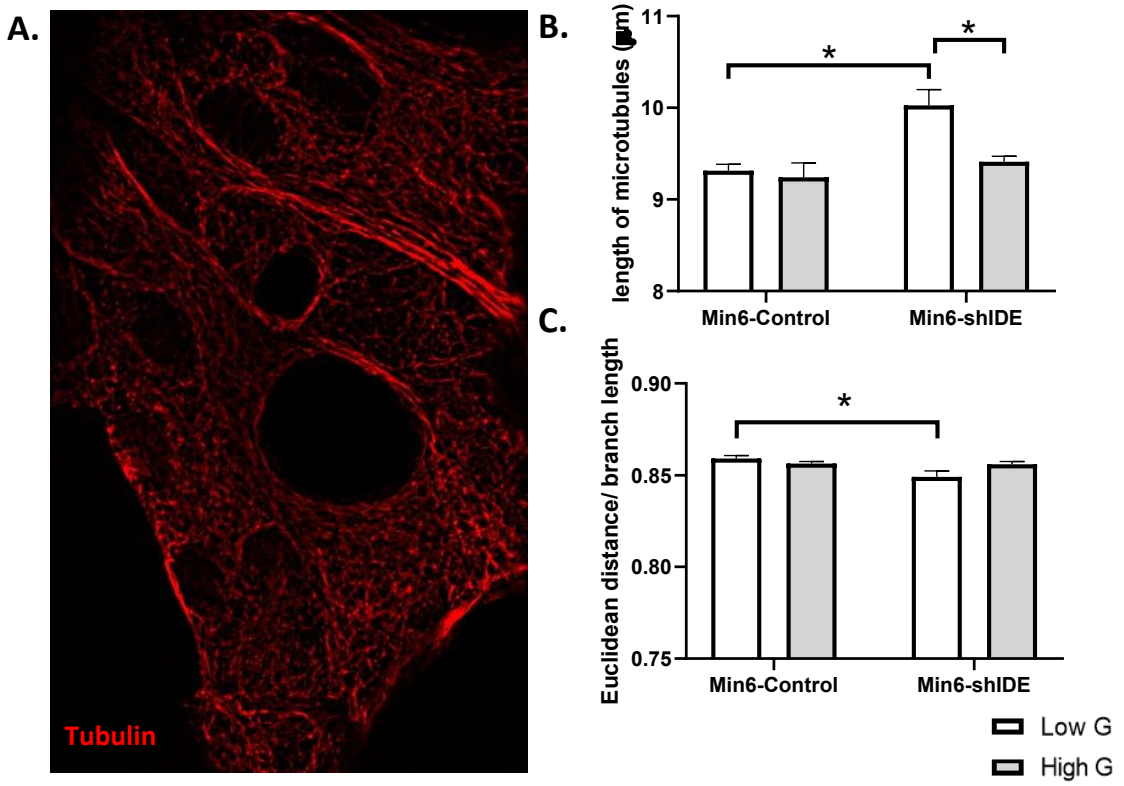

Figure 47. Analysis of microtubule dynamics in Min6-Control and shIDE cells under basal (Low G) and secretory (High G) conditions: A: Representative image of tubulin staining. **B:** Quantification of microtubule length under different conditions. **C:** Quantification of microtubule curvature, represented as the Euclidean distance/length ratio. (n = 8 images). *p < 0.05 by two-way ANOVA. Data are presented as means ± SEM.

D.) Effects of IDE depletion on tubulin-IDE colocalization under basal and secretory conditions

To elucidate how glucose regulates IDE, microtubules, and their interaction, we performed a colocalization analysis of tubulin and IDE under low- and high-glucose conditions.

We observed that in Min6-Control cells under both low- and high-glucose conditions, as well as in Min6-shIDE cells under high glucose, there were no significant differences in the fraction of tubulin colocalizing with IDE, as measured by Manders' coefficient (Tubulin/IDE). However, in Min6-shIDE cells under low glucose condition, colocalization was noticeably reduced compared to the other three conditions, showing a significant decrease relative to high glucose **(Figure 48 B).**

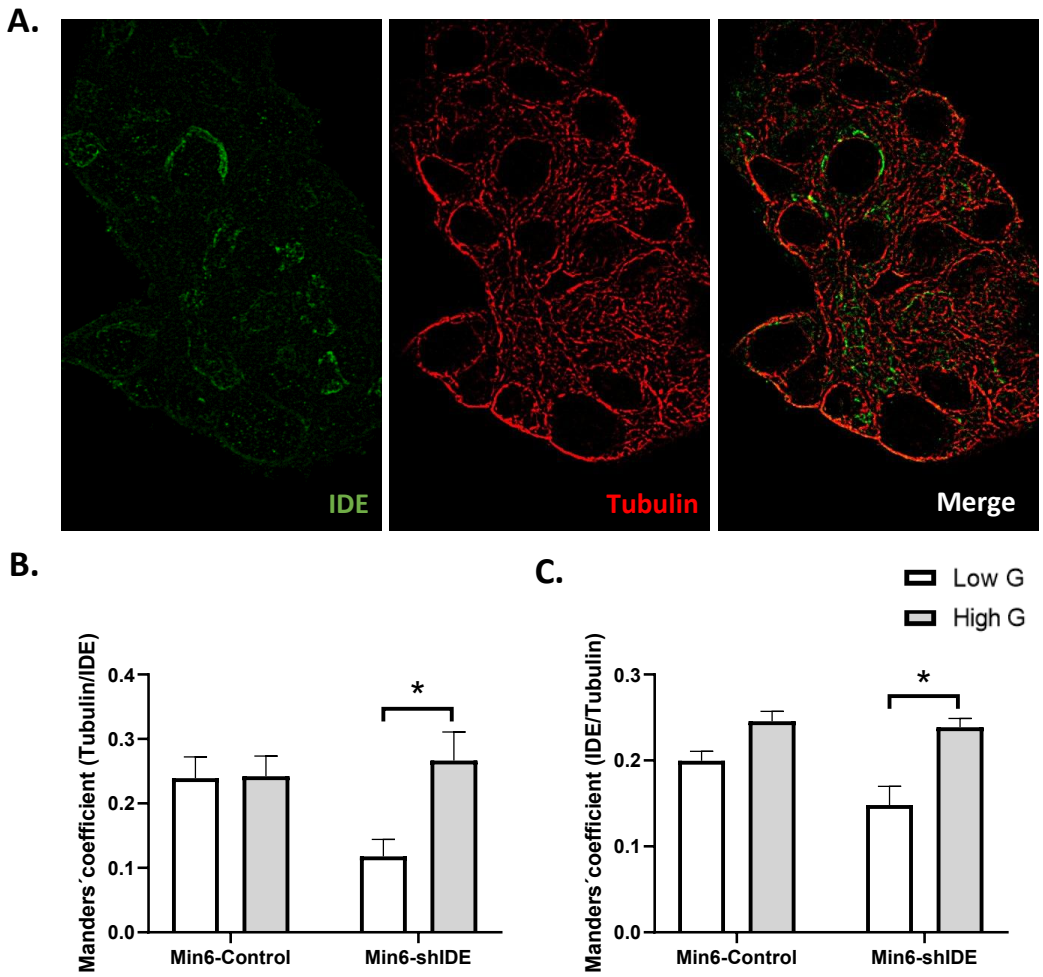

Figure 48. Analysis of microtubule dynamics and colocalization with IDE in Min6-Control and shIDE cells under basal (Low G) and secretory (High G) conditions. A: Representative image of tubulin and IDE staining. **B:** Quantification of colocalization using Manders' coefficient M1, representing the fraction of tubulin signal overlapping with IDE. **C:** Quantification of colocalization using Manders' coefficient M2, representing the fraction of IDE signal overlapping with tubulin. (n = 8 images from 2 independent experiments). *p < 0.05 by two-way ANOVA. Data are presented as means ± SEM.

When analyzing Manders' coefficient (IDE/Tubulin) (the fraction of IDE colocalizing with tubulin), we observed that high glucose increased this coefficient in both control and Min6-shIDE cells, indicating a greater proportion of IDE associated with microtubules. This difference was statistically significant in Min6-shIDE cells **(Figure 48 C).**

These results suggest a regulatory role for IDE in glucose-dependent microtubule dynamics.

2.3.3 Impact of IDE depletion on cilia β-cells under basal and secretory conditions

The primary cilium acts as a signaling antenna that regulates intercellular communication. Pancreatic islet cells are known to be ciliated (235). Previous findings from our laboratory have shown that alpha cells lacking IDE exhibit a reduction in both the number of cilia and the levels of acetylated tubulin (264). In B-IDE-KO and B-IDE-HT mice, we observed a decrease in the number of cilia compared with B-IDE-WT. Additionally, our unpublished results indicate that high glucose levels can also regulate these ciliary proteins in α-cells. Based on these findings, our objective was to investigate the effect of high glucose on the primary cilium in β-cells and to determine the possible role of IDE in this process.

A.) Impact of glucose and IDE depletion on cilia marker levels in Ins1E-cells

To explore the impact of high glucose on the β-cell cilium, we quantified the levels of some ciliary marker proteins (Arl13b and acetylated tubulin) in Ins1E-Control cells under low- (3 mM) and high-glucose (16 mM) conditions **(Figure 49).** While Arl13b showed a non-significant trend toward decreased levels in response to high glucose **(Figure 49 B),** acetylated tubulin exhibited a drastic reduction under these conditions **(Figure 49 C).**

In contrast, in Ins1E-shIDE cells, high glucose led to a trend toward increased Arl13b levels, while the decrease in acetylated tubulin was milder compared to that observed in control cells **(Figure 50).**

These findings suggest that IDE may play a role in the glucose-mediated regulation of at least some of the proteins that constitute the primary cilium.

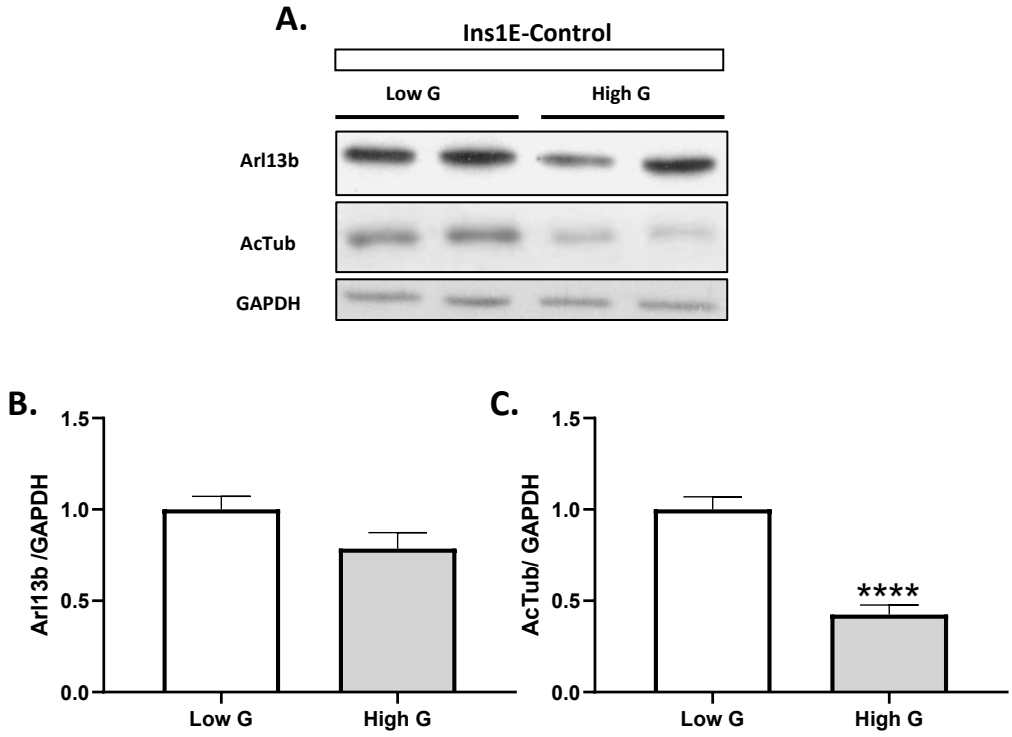

Figure 49: Protein levels of cilia and tubulin intensity in Control Ins1E cells under basal and secretory conditions. A: Representative WB panel of proteins assessed. **B:** Quantification of Arl13b by WB. **C:** Quantification of acetylated tubulin by WB. (N=3, in duplicates). ****p<0.0001 by Student´s t-test. Data are presented as means ± SEM.

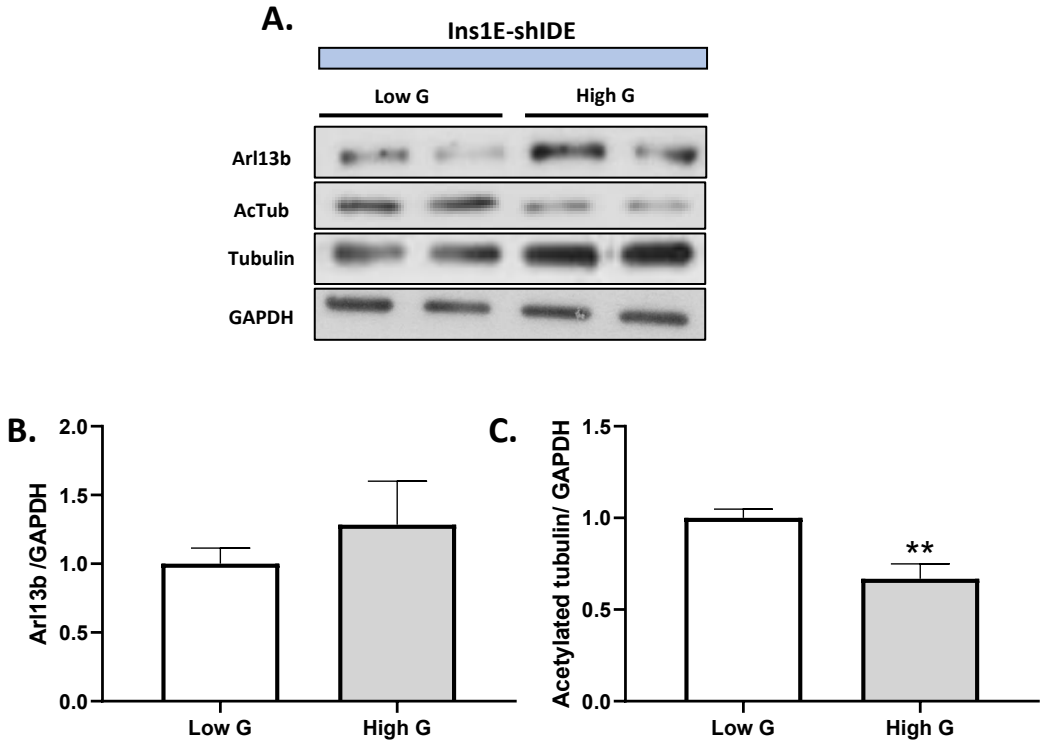

Figure 50: Protein levels of cilia and tubulin intensity in shIDE-Ins1E cells under basal and secretory conditions. A: Representative WB panel of proteins assessed. **B**: Quantification of Arl13b by WB. **C**: Quantification of acetylated tubulin by WB. (N=3, in duplicates). **p<0.01 by Student´s t-test. Data are presented as means ± SEM.

B.) Impact of glucose and IDE depletion on cilia marker levels in Min6-cells

Following our analysis of tubulin regulation, with the aim of confirming these results in a different model and to directly compare the effects of glucose on cilium regulation in the presence or absence of IDE, we performed the same experiment in parallel using Min6-Control and Min6-shIDE cells.

In Min6-Control cells, we observed a significant decrease in acetylated tubulin levels when cells were exposed to high-glucose conditions compared to low glucose. Additionally, acetylated tubulin levels were significantly reduced in IDE knockdown cells under both low- and high-glucose conditions compared to control cells. Interestingly, in Min6-shIDE cells, total tubulin levels did not exhibit glucose-dependent regulation **(Figure 51).**

These findings suggest that both glucose and IDE, regulate acetylated tubulin levels. Moreover, glucose may regulate acetylated tubulin through IDE.

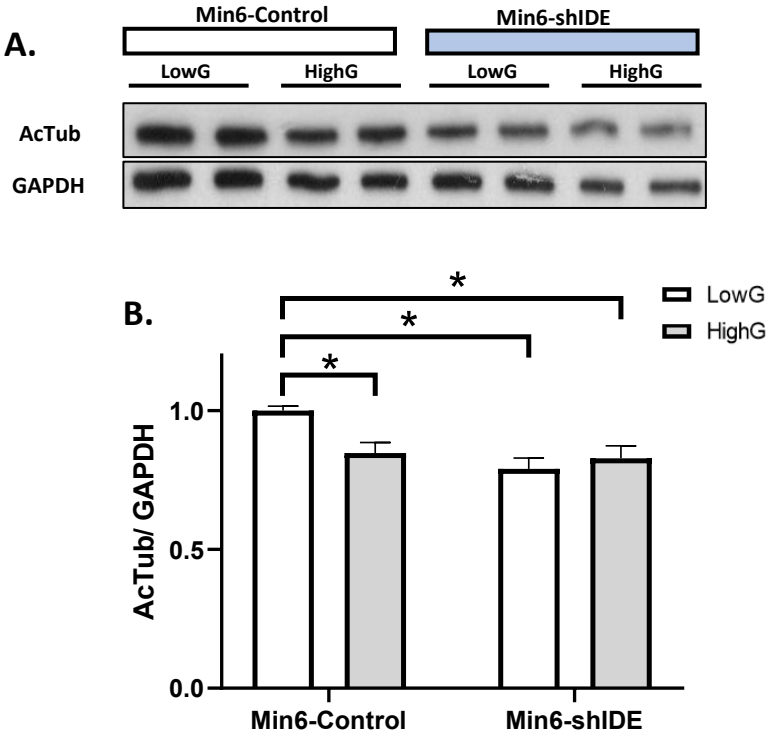

Figure 51: Protein levels of acetylated tubulin in Control and shIDE Min6 cells under basal (Low G) and secretory conditions (High G). A: Representative WB panel of acetylated tubulin**. B:** Quantification of acetylated tubulin by WB. (N=3, in duplicates). *p<0.05 by two-way ANOVA. Data are presented as means ± SEM.

C.) Impact of glucose and IDE in ciliogenesis

To further explore this mechanism, we quantified cilia number. We performed this by counting cilia stained by acetylated tubulin, using the same experimental conditions (Min6-Control and Min6-shIDE in high and low glucose). We also measured cilium length conditions **(Figure 52).** Cilia number were 50% decreased between shIDE and control group, as expected. But no significant differences were found in cilia number **(Figure 52 B)** or length **(Figure 52 C)** between low- and high-glucose conditions. Interestingly, there is a tendency to decrease cilia length in high glucose.

These results reveal that IDE plays a crucial role in regulating ciliogenesis in pancreatic β-cells.

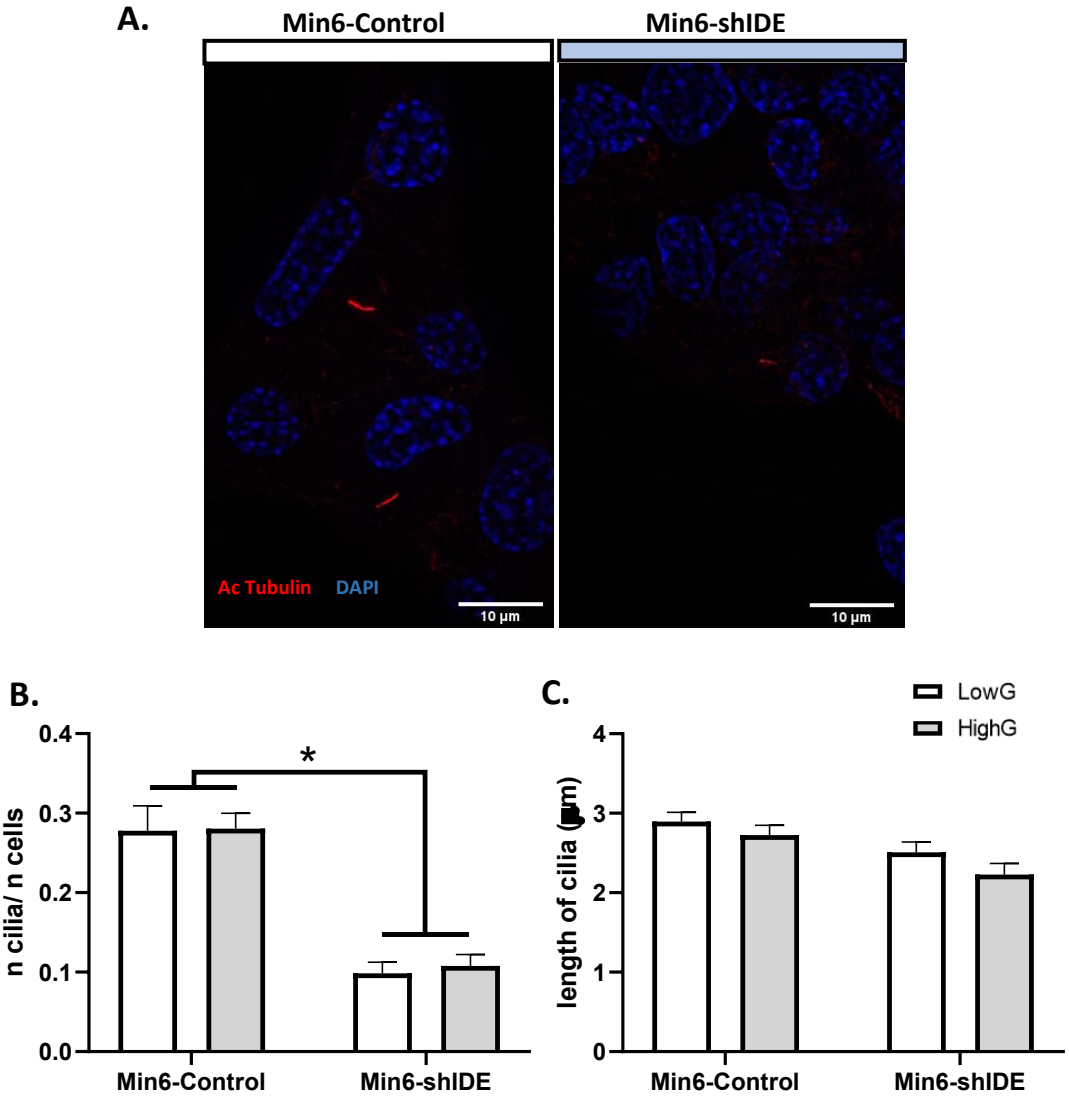

Figure 52: Cilia in Control and shIDE Min6 cells under basal (Low G) and secretory conditions (High G). A: Representative staining images of Acetylated tubulin. **B:** Quantification of average of number of cilia per cell. **C:** Quantification of cilia length. (N=3, 10 images per N). *p<0.05 by two-way ANOVA. Data are presented as means ± SEM.

2.4 Paracrine Regulation of β-cells IDE knockdown

2.4.1 Insulin and glucagon receptor protein levels in β-cells IDE-KD

The deletion of IDE in the liver led to decreased levels of insulin receptor (IR) protein (160). Recent unpublished results from our laboratory indicate that IDE depletion in α-cells leads to a significant reduction in both insulin and glucagon receptors, the main receptors involved in pancreatic islet paracrine signaling (264). Based on these findings, we investigated the effect of IDE knockdown on IR and glucagon receptor (GcgR) levels in pancreatic β-cells. Our results showed a significant reduction of approximately 70 and 60% in GcgR and IR protein levels in Min6-shIDE cells respectively **(Figure 53).**

These results suggest that IDE knockdown affects the expression of receptors involved in paracrine signaling.

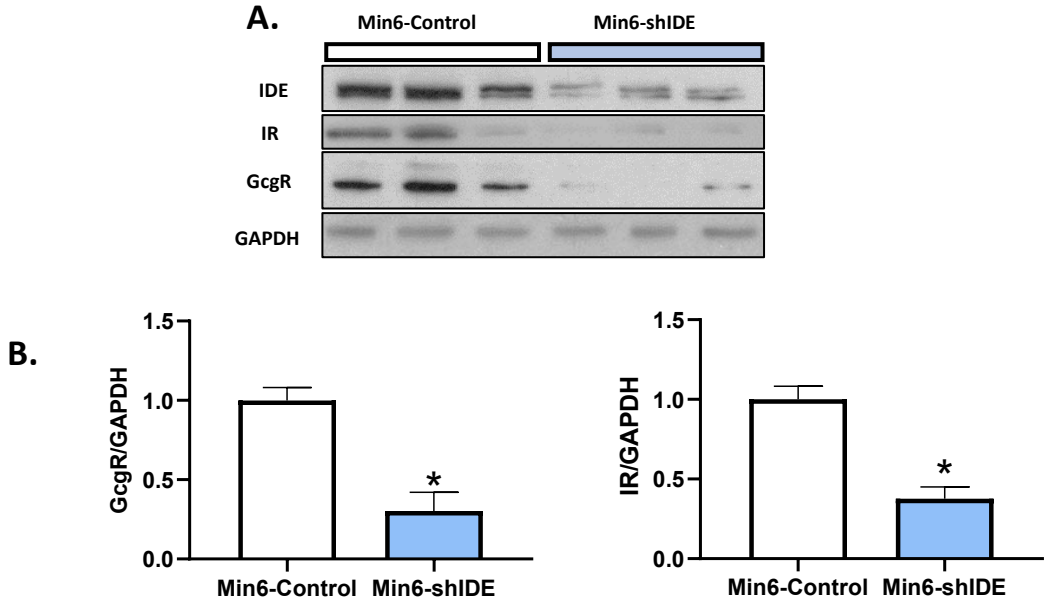

Figure 53: Protein and mRNA levels of insulin (IR) and glucagon receptor (GcgR) in Control and shIDE Min6 cells. A: Representative WB of IDE levels in control and shIDE Min6 cells. **B**: Quantification of IDE by WB. (N=3, in triplicates). *p<0.05 by Student´s t-test. Data are presented as means ± SEM**.**

2.4.2 Insulin and glucagon receptor levels in basal versus secretory conditions in β-cells.

In pancreatic α-cells, high glucose induces 30% decrease in IR protein levels and a 40% decrease in GcgR protein levels (264).

A.) Impact of glucose and IDE depletion on IR and GcgR levels in Ins1E-cells

To determine whether this glucose-dependent regulation of receptors also occurs in pancreatic β-cells, we quantified IR **(Figure 54 B)** and GcgR **(Figure 54 C)** protein levels under low-glucose (3 mM) and high-glucose (16 mM) conditions in Ins1E-Control cells. We observed that in both cases, glucose significantly decreased the levels of these receptors.

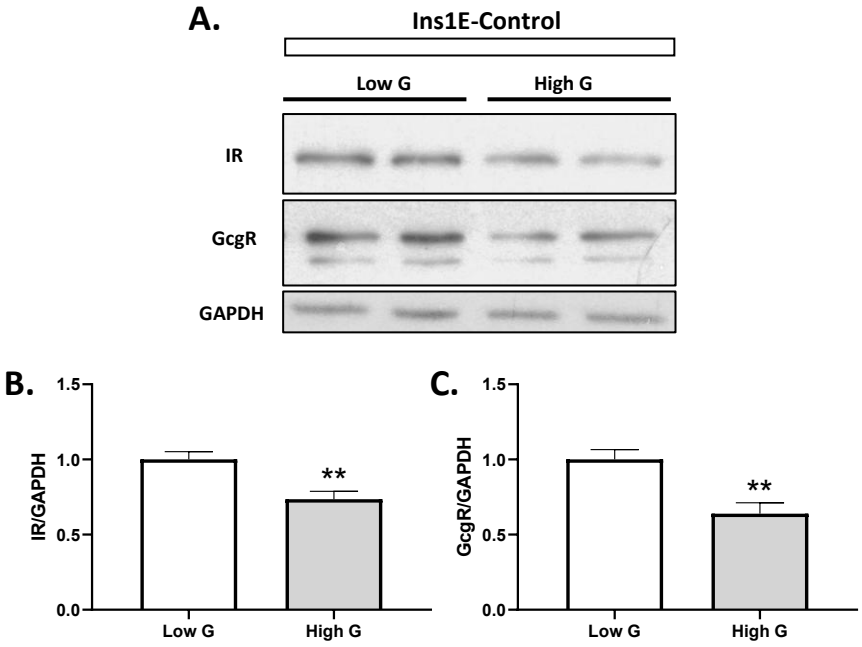

Figure 54: Protein levels of paracrine receptors in Ins1E-Control under basal (LowG) and secretory (HighG) conditions. A: Representative WB panel of Ins1E-Control proteins assessed. **B:** Quantification of IR by WB. **C:** Quantification of GcgR by WB. (N=3, in duplicates). **p<0.01 by Student´s t-test. Data are presented as means ± SEM

Previous findings suggest that IDE mediates glucose-dependent regulation of various proteins. Given this, we questioned whether IDE depletion would disrupt the glucose-induced regulation of receptor levels. Additionally, our previous results in IDE knockdown models (Min6-shIDE) already indicated that IDE deficiency alone reduces both IR and GcgR levels.

To investigate the effect of glucose on insulin and glucagon receptor regulation in IDE-deficient β-cells, we performed the same analysis in Ins1E-shIDE cells. In this case, the glucose-dependent regulation of insulin and glucagon receptor levels was completely lost **(Figure 55).**

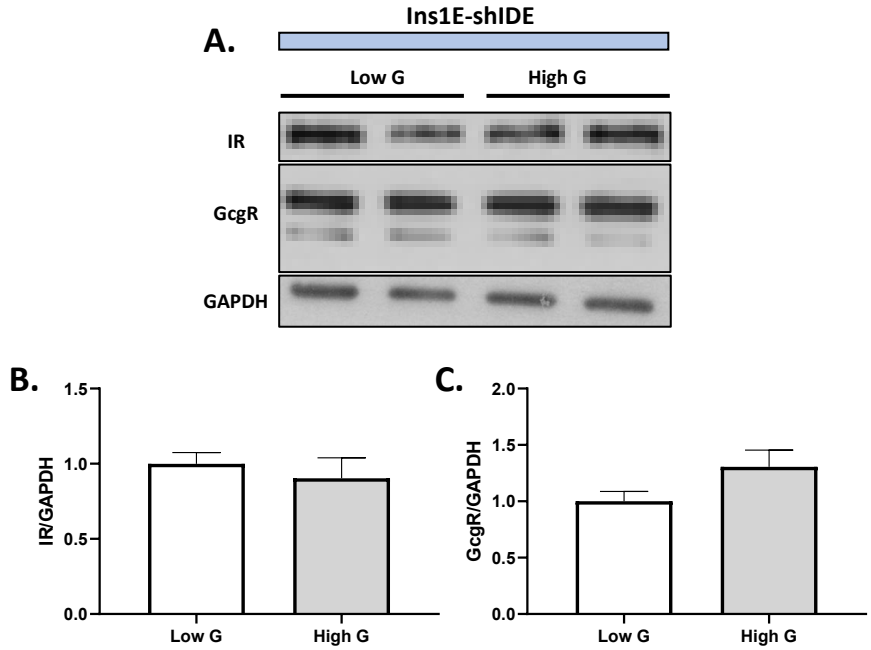

Figure 55: Protein levels of paracrine receptors in Ins1E-shIDE under basal (LowG) and secretory (HighG) conditions. A: Representative WB panel of Ins1E-shIDE proteins assessed. **B:** Quantification of IR by WB. **C:** Quantification of GcgR by WB. (N=3, in duplicates. Data are presented as means ± SEM.

B.) Impact of glucose and IDE depletion on IR and GcgR levels in Min6-cells

To further validate these findings, we conducted the same experiment in the Min6 cell model, analyzing receptor levels in parallel in both control and shIDE cells under low- and high-glucose conditions **(Figure 56).** The results were consistent with those observed in Ins1E cells: in control Min6 cells, high glucose reduced IR and GcgR levels (**Figure 56 C, D)**. However, in Min6-shIDE cells, receptor levels were already lower at baseline, and glucose was unable to regulate their expression **(Figure 56 C, D).**

Alll together, these results highlight that IDE is involved in the regulation of insulin and glucagon receptors; and their modulation in response to glucose levels.

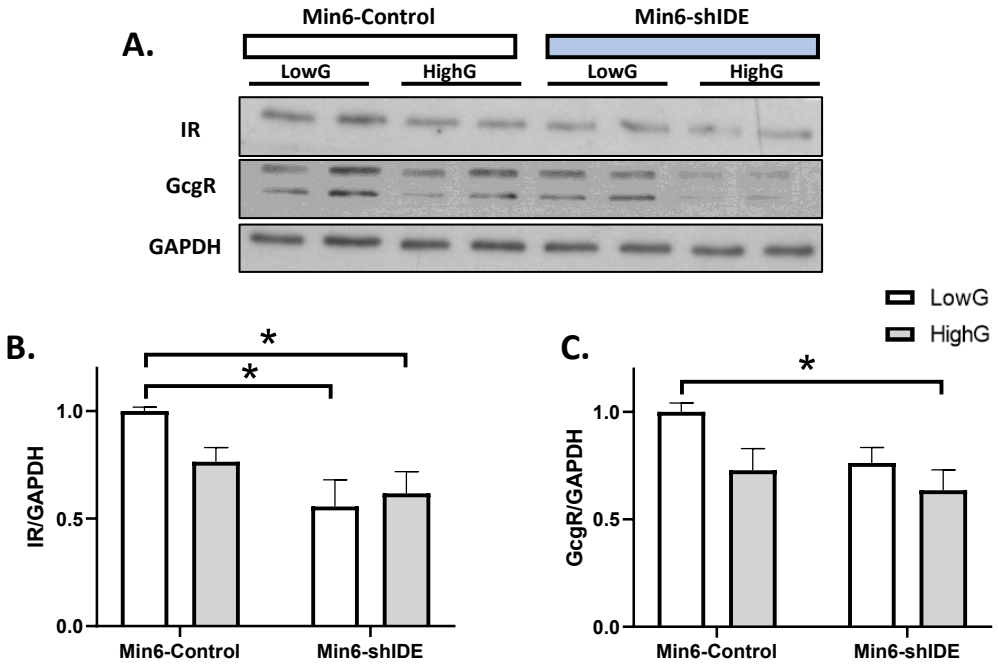

Figure 56: Protein levels of paracrine receptors in Control and shIDE Min6 cells under basal (LowG) and secretory (HighG) conditions. A: Representative WB panel of proteins assessed. **B:** Quantification of IR by WB. **C:** Quantification of GcgR by WB. (N=3, in duplicates). *p<0.05 by two-way ANOVA. Data are presented as means ± SEM.

2.4.3 Glucagon signaling after glucagon treatment in IDE-KD β-cells

Glucagon is a key hormone involved in glucose metabolism regulation. It binds to its G-protein-coupled receptor (GcgR) and is known to enhance insulin secretion in β-cells in synergy with high glucose levels (265). Our findings indicate that IDE plays a crucial role in regulating the GcgR. Specifically, when IDE is reduced, GcgR protein levels also decrease.

The reduction of IDE appears to induce a functional defect in glucagon signaling in β-cells. To investigate this further, we analyzed key target proteins of the glucagon signaling pathway in Min6-Control and Min6-shIDE cells under basal (unstimulated) conditions and after glucagon stimulation for 0, 10, and 30 min **(Figure 57):** pPKA/PKA, pCREB/CREB, pERK/ERK.

When we quantified phosphorylation of PKA substrates, no significant differences were observed in Min6-shIDE cells in response to glucagon stimulation at 10 and 30 min compared to control cells **(Figure 57 B).** However, there was a lack of response to glucagon in Min6-shIDE. This absence of response may be due to the basal activation

of PKA in Min6-shIDE cells, showing increased phosphorylation of PKA substrates at time ¨0¨ compared to their controls.

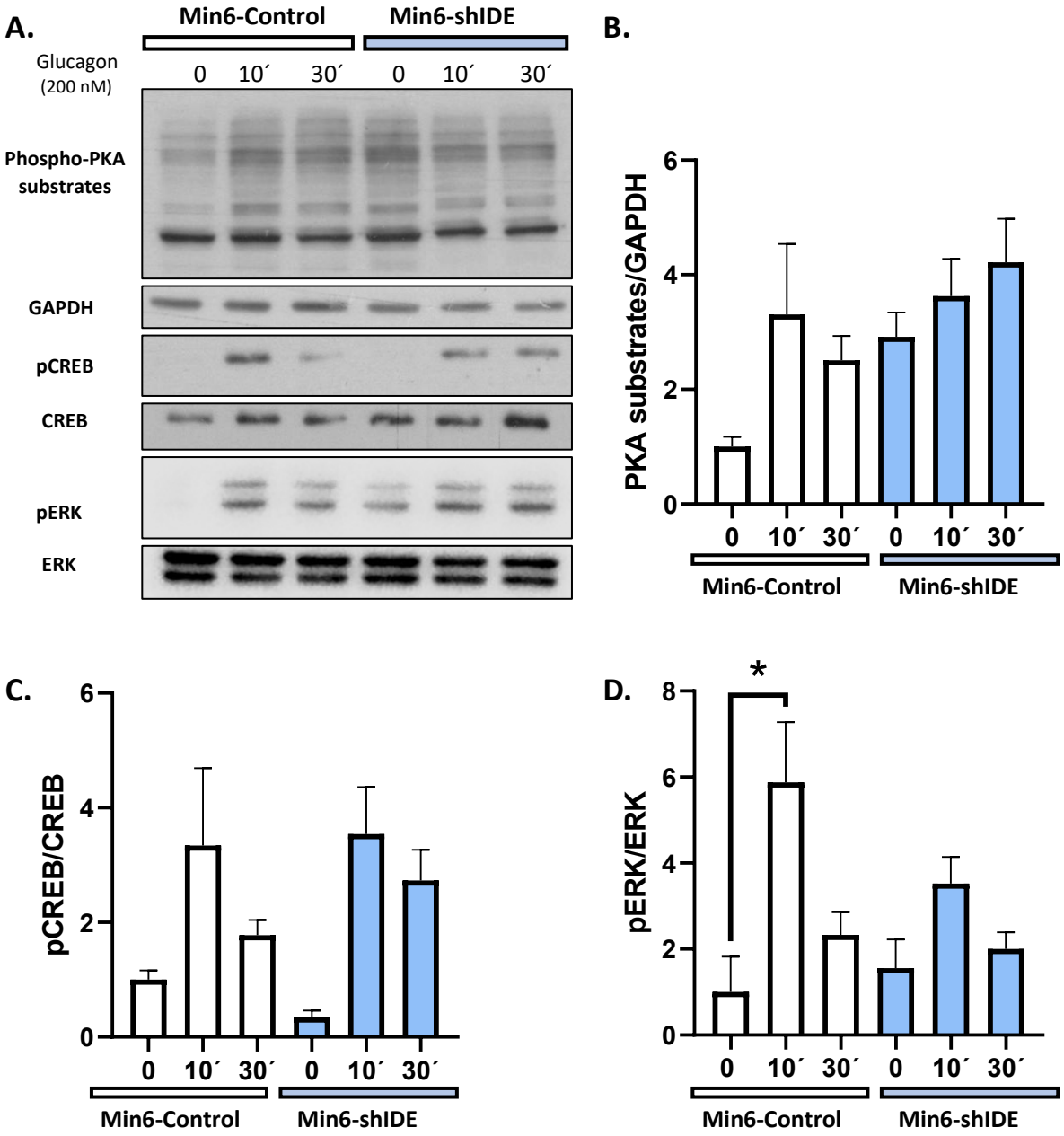

Figure 57: Glucagon signaling in Min6-Control and shIDE. A: Representative WB of glucagon signaling in Min6 cells at 10 and 30 minutes. **B:** Quantification of pPKA-substrates protein levels by WB after 200 nM glucagon exposure. **C**: Quantification of pCREB/CREB protein levels by WB after 200 nM glucagon exposure. **D:** Quantification of pERK/ERK protein levels by WB after 200 nM glucagon exposure. N=4. *p<0.05 by two-way Anova test. Data are represented as mean ± SEM.

In contrast, when we quantified pCREB levels **(Figure 57 C),** we found that pCREB phosphorylation was lower in Min6-shIDE cells compared to controls under unstimulated conditions. However, in both control and Min6-shIDE cells, pCREB appeared to be activated similarly in response to glucagon.

Downstream of this signaling we studied pERK/ERK levels **(Figure 57 D),** we observed a significant response in Min6-Control cells following glucagon treatment for 10 min. This response was lost in Min6-shIDE cells, where the trend remained but did not reach statistical significance.

Altogether, our results point to a dysregulation downstream of glucagon signaling in Min6 cells when IDE expression is decreased.

Summary of Findings Part 2:

- **Insulin secretion defects**: Reduced IDE in β-cells causes defects in glucose-stimulated insulin secretion.
- **Protein alterations**: IDE knockdown alters proteins related to the primary cilium, tubulin cytoskeleton, and insulin and glucagon receptors.
- **Tubulin Regulation by Glucose**: High glucose reduces tubulin levels and regulates its distribution in β-cells, making it more intense near the membrane. In the absence of IDE, this regulation is lost, leading to a much higher intensity of tubulin, particularly around the nucleus. This suggests glucose regulates microtubules via IDE.
- **Microtubule changes in IDE-KD**: In low glucose, microtubules are significantly longer and more curved in IDE knockdown cells compared to controls.
- **Primary cilium regulation by IDE**: IDE is required for β-cell ciliogenesis independently of glucose levels.
- **Regulation of insulin and glucagon receptors**: High glucose regulates insulin and glucagon receptor levels, but this regulation is lost in the absence of IDE.
- **Glucagon signaling impairment**: Basal pCREB levels are reduced, while basal PKA phosphorylation is elevated, both in basal conditions, without stimulation. These findings suggest that IDE is required for physiological glucagon signaling.

The reduction of IDE in β-cells impairs glucose-stimulated insulin secretion and glucagon receptor function, disrupting microtubule regulation, primary cilium dynamics, and intracellular signaling. These findings highlight the crucial role of IDE in maintaining proper beta cell function and the cellular response to glucose and glucagon.

PART 3: IFT88 KNOCKDOWN IN BETA CELLS:

Primary cilia functions as sensory organelles that detect changes in the local cellular environment. They express numerous receptors on their surface and mediate critical signaling pathways essential for proper cellular function. We have seen that IDE is regulating primary cilia, cytoskeleton, and insulin and glucagon receptors. To investigate the relationship between the cytoskeleton, insulin secretion, and ciliogenesis, independently of IDE, we generated a model of impaired ciliogenesis by targeting IFT88, a key component of ciliary assembly.

3.1 Generation and analysis of IFT88-KD in Min6 cells

To inhibit IFT88 expression, we used shRNA-IFT88, as described in the Material and Methods section. To confirm the efficiency of the knockdown, we assessed IFT88 protein levels **(Figure 58 A, B)** and observed a reduction of more than 50%, confirming successful inhibition. Next, we performed acetylated tubulin staining to label primary cilia **(Figure 58 C)** and quantified the number of cilia per cell **(Figure 58 D)** in Min6-IFT88-KD cells compared to controls. We observed an almost 50% reduction in the number of cilia, indicating that IFT88 knockdown significantly impairs ciliogenesis. However, when we measured cilia length **(Figure 58 E),** no significant differences were detected between Min6-IFT88-KD cells and their controls.

These results confirm that IFT88 knockdown effectively impairs ciliogenesis without affecting the overall length of the remaining cilia.

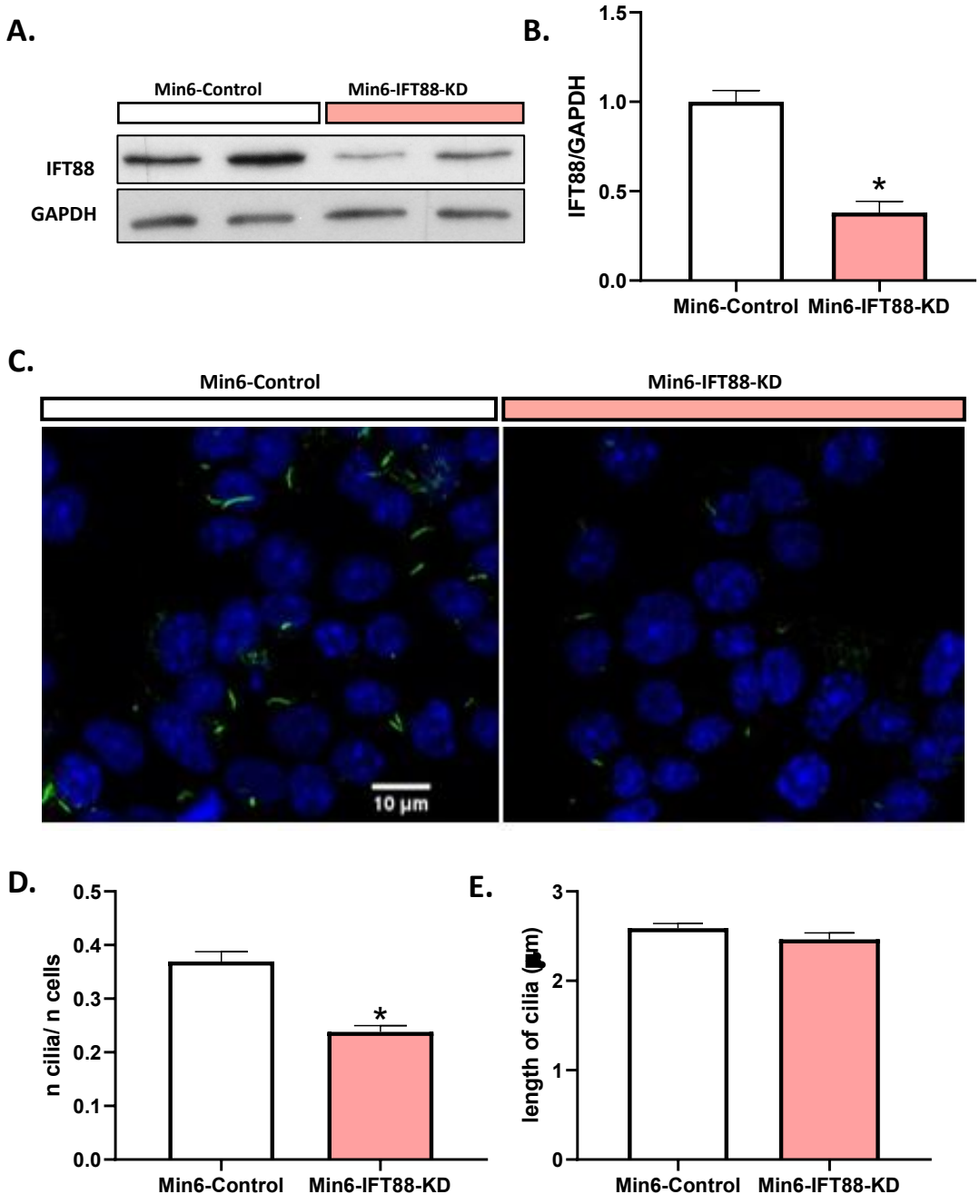

Figure 58: Generation of Min6-IFT88-KD. A: Representative WB of IFT88 levels in control and IFT88-KD Min6 cells. **B:** Quantification of IFT88 by WB. **C:** Representative immunostaining of acetylated tubulin showing cilia in Min6 and Min6-IFT88-KD cells. **D:** Quantification of the number of cilia per cell. **E**: Measurement of cilia length. *p<0.05 versus Control by Student´s t-test. Data are presented as means ± SEM.

3.2 β-cells IFT88-KD characterization

We next analyzed whether IDE levels were affected by ciliogenesis impairment. Quantification of IDE protein expression in Min6-IFT88-KD cells did not reveal significant differences compared to control cells **(Figure 59 A, B).**

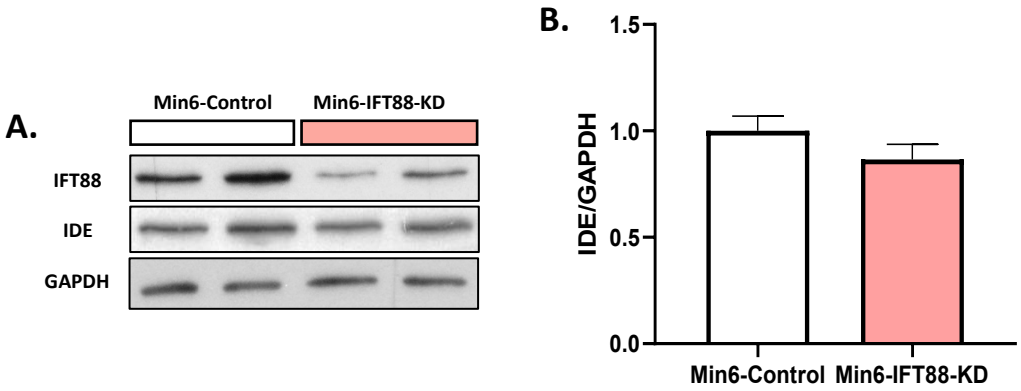

Figure 59: Protein levels of IDE in Control and Min6-IFT88-KD cells. A: Representative WB of IDE levels in control and Min6-IFT88-KD cells. **B:** Quantification of IDE by WB. Statistical analysis was performed using Student´s t-test. Data are presented as means ± SEM.

These results suggest that ciliogenesis impairment does not regulate IDE protein levels, indicating that IDE is upstream in the regulation of primary cilia in β-cells.

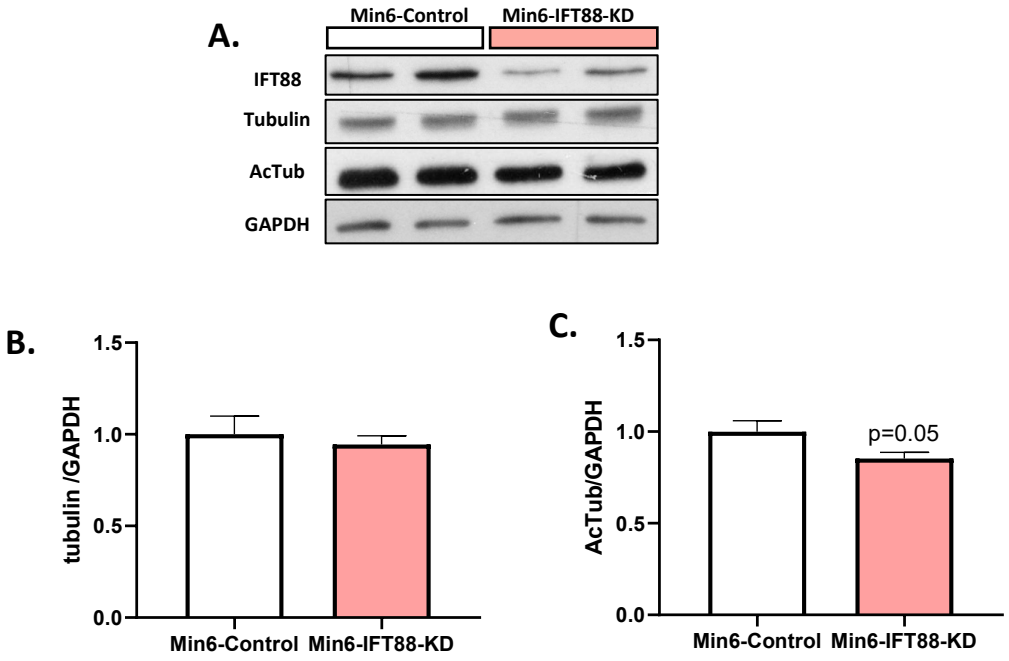

Figure 60: Protein levels of cytoskeleton in Control and Min6-IFT88-KD cells. A: Representative WB of tubulin and acetylated tubulin levels in control and IFT88-KD Min6 cells. **B:** Quantification of tubulin by WB. **C:** Quantification of acetylated tubulin by WB. (N=3, in triplicates). p=0,05 Student's t-test. Data are presented as means ± SEM.

To further investigate the relationship between primary cilia and the cytoskeleton, we analyzed tubulin levels in Min6-IFT88-KD cells compared to Min6-Control cells. Our

results show that total tubulin levels remain unchanged between both conditions **(Figure 60 A, B).** However, we observed a no-significant decrease in acetylated tubulin levels in Min6-IFT88-KD cells **(Figure 60 A, C).**

These findings suggest that primary cilia do not regulate the overall tubulin cytoskeleton. The decrease in tubulin acetylation may reflect the decrease of primary cilium number.

In Min6-IFT88-KD cells, we observed a 40% reduction in IR protein levels **(Figure 61 A, B)** and a 50% reduction in GcgR protein levels **(Figure 61 A, C).**

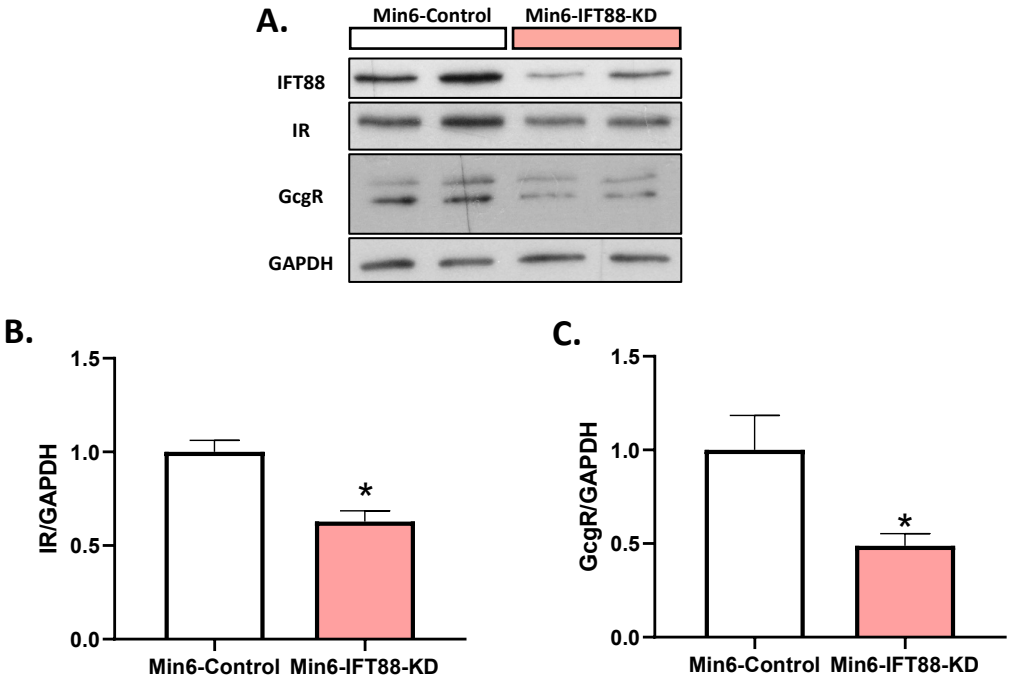

Figure 61: Protein levels of insulin (IR) and glucagon receptor (GcgR) in Control and Min6-IFT88-KD cells. A: Representative WB of insulin (IR) and glucagon receptor (GcgR) levels in control and IFT88-KD Min6 cells. **B**: Quantification of IR by WB. **C:** Quantification of GcgR by WB. (N=3, in triplicates). *p<0.05 by Student's t-test. Data are presented as means ± SEM.

Since a similar decrease in insulin and glucagon receptor levels were previously observed in IDE-deficient models, our results suggest that primary cilia act downstream of IDE to regulate the abundance of these receptors.

3.3 Glucagon signaling after glucagon treatment in IFT88-KD β-cells

Given that IFT88 knockdown reduces GcgR levels, we aimed to determine the biological and functional implications of this reduction. To this end, we analyzed key target proteins of the glucagon signaling pathway in Min6-Control and Min6-IFT88-KD cells under basal (unstimulated) conditions and after glucagon stimulation for 0, 10, and 30 min **(Figure 26).**

Our results showed no significant differences in Min6-IFT88-KD cells compared to controls, either under basal conditions or after glucagon stimulation at 10 and 30 min. Neither the pCREB levels **(Figure 62 A, B),** not pERK activation **(Figure 62 A, C)** exhibited any notable changes in response to glucagon stimulation.

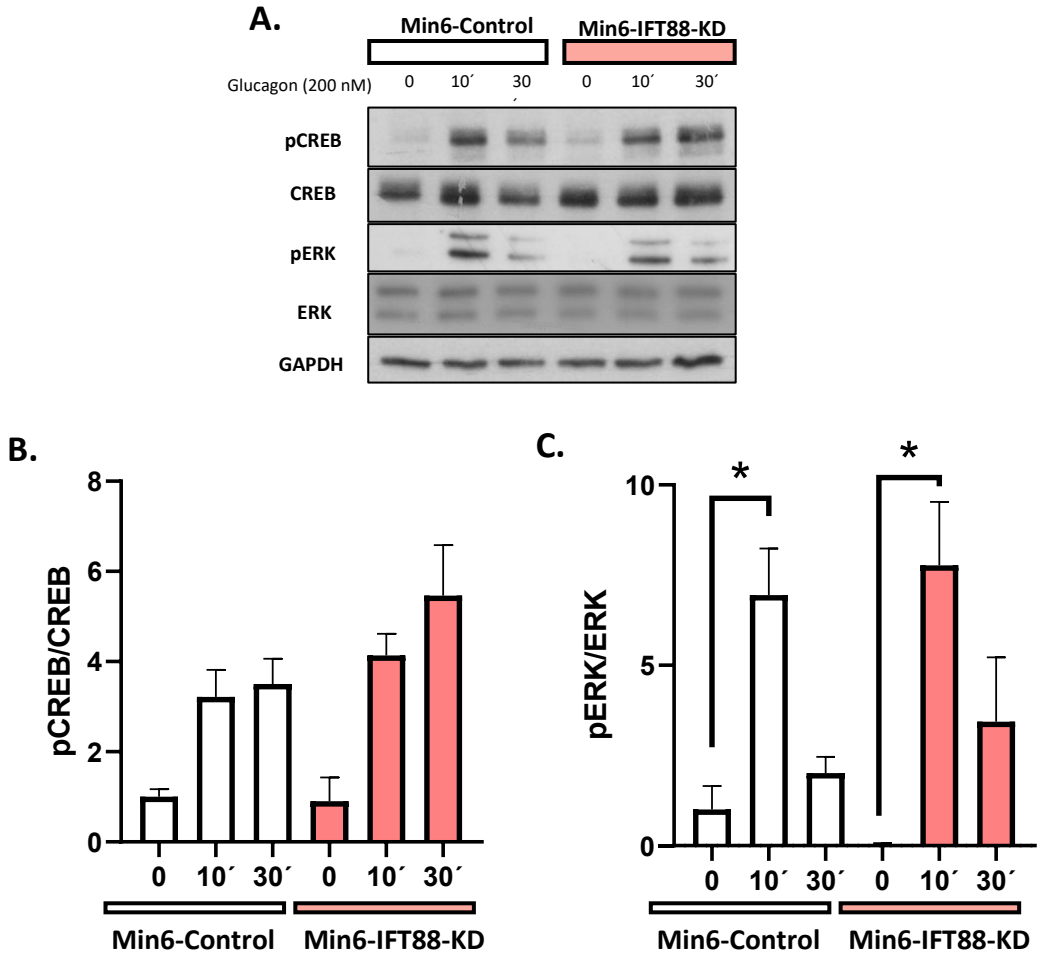

Figure 62: Glucagon signaling in Min6-Control and IFT88-KD. A: Representative WB of glucagon signaling in Min6 cells at 10 and 30 min of stimulation with 200 nM of glucagon. **B.** Quantification of pCREB/CREB protein levels by WB. **C:** pERK/ERK protein levels by WB after 200 nM glucagon exposure. N=3. *p<0.05 by two-way ANOVA. Data are represented as mean ± SEM.

These findings indicate that the absence of primary cilia do not play a direct role in glucagon signaling regulation in β-cells.

Summary of Findings Part 3

- **IFT88 deficiency**: IFT88 knockdown in β-cells impairs ciliogenesis and reduces the number of primary cilia.
- **Regulation of insulin and glucagon receptor levels:** Receptor levels (insulin and glucagon) are reduced in IFT88-KD β-cells.
- **Stable IDE expression:** IDE expression remains unaffected by ciliogenesis impairment.
- **Preserved glucagon signaling:** Glucagon signaling is unchanged despite reduced glucagon receptor levels.

Intact primary cilia is required for normal insulin and glucagon receptor levels. Although primary cilium impairment does not affect glucagon signaling. not impact glucagon signaling directly.

PART 4: COLOCALIZATION:

4.1 IDE and cilia

All previously shown results previously shown confirm that IDE regulates the primary cilium in both in vivo and in vitro. To determine whether this regulation occurs directly, we performed immunostaining for acetylated tubulin and IDE and analyzed IDE localization at cilia structure using confocal microscopy and STORM. Representative images from confocal microscopy **(Figure 63 A)** and STORM **(Figure 63 C)** clearly show that IDE is not present in the primary cilium. This observation is further supported by colocalization analysis using Pearson´s coefficient, which confirms the absence of IDE in the primary cilium of Min6-cells **(Figure 63 B).**

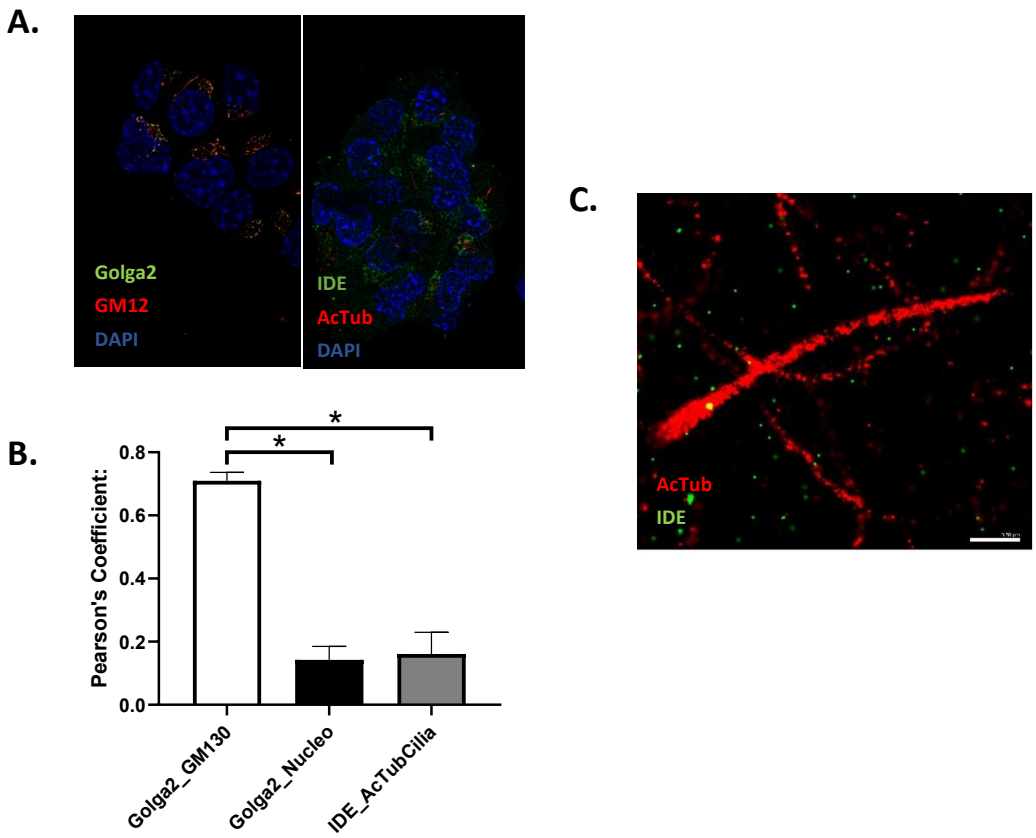

Figure 63: Colocalization of IDE and the Golgi in Min6 cells using the Pearsons' coefficient. A: Representative confocal microscopy image showing IDE localization and cilia stained by acetylated tubulin. **B**: Quantification of colocalization using GM130 and Golga2 as Golgi colocalization controls, and GM130 with the nucleus as a negative control. **C:** Representative STORM images confirming the colocalization observed in confocal microscopy. N=4. *p<0.05 by one-way ANOVA. Data are represented as mean ± SEM.

4.2 IDE and Golgi

Interestingly IDE staining in these cells, labeled a prominent cytoplasmic structure. To identify the organelle, we performed double staining for IDE and Golgi markers, (Golga2 and GM130) followed by colocalization analysis. The Manders' coefficient revealed that approximately 45% of IDE signal overlapped with the Golgi area, indicating partial colocalization between these two proteins and suggesting colocalization of IDE with the Golgi apparatus. **Figure 64 A** presents a representative confocal image, while **Figure 64 C** shows STORM microscopy images that provide higher resolution and further confirm these findings.

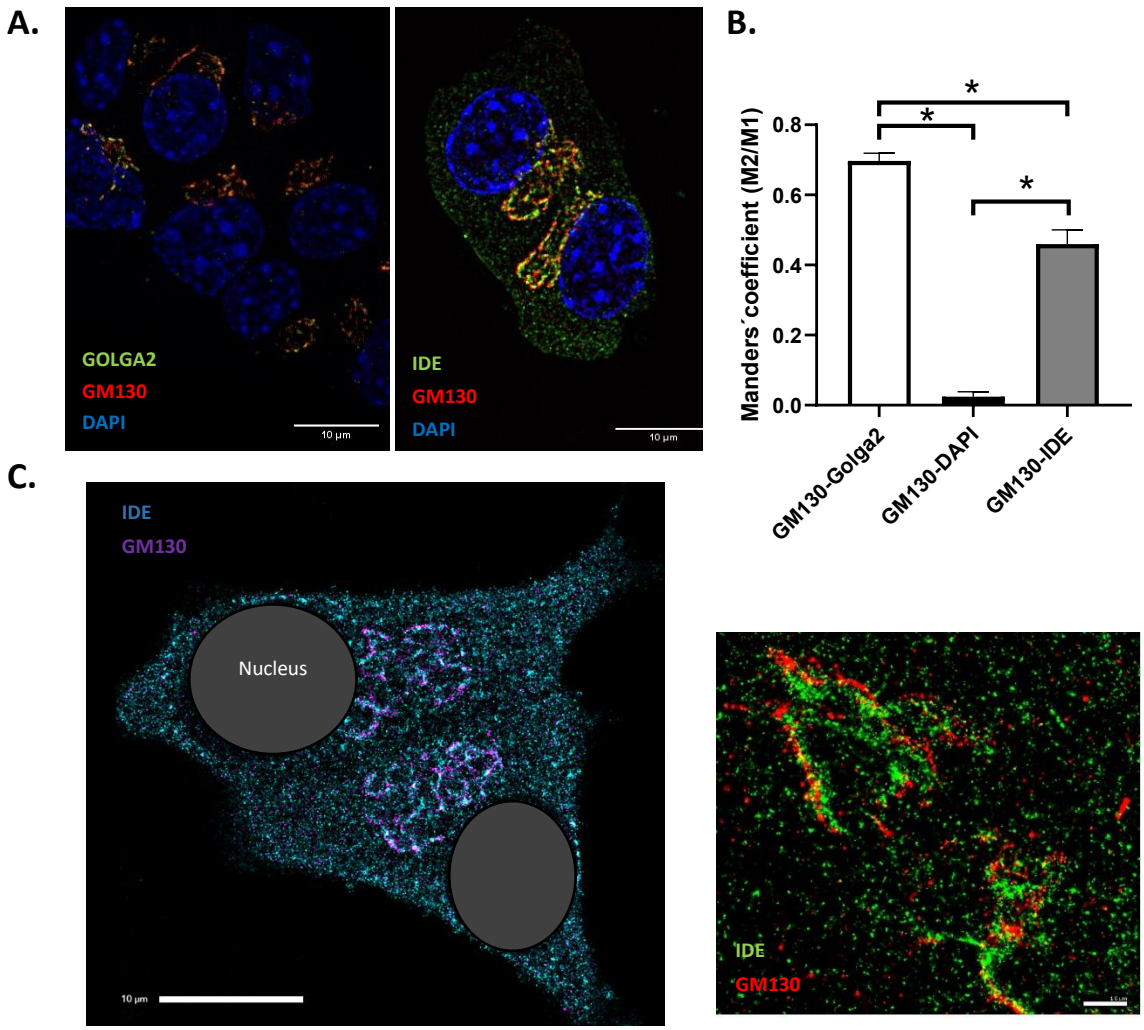

Figure 64. Colocalization of IDE and the Golgi in Min6 cells using the Manders' coefficient. A: Representative confocal microscopy image showing IDE localization in relation to the Golgi. **B:** Quantification of colocalization using GM130 and Golga2 as Golgi colocalization controls, and GM130 with the nucleus as a negative control. **C:** Representative STORM images confirming the colocalization observed in confocal microscopy. N=8. *p<0.05 by one-way ANOVA. Data are represented as mean ± SEM.

Summary of Findings Part 4

- **IDE localization:**
  - IDE regulates the primary cilium but is not present in it.
  - IDE partially colocalizes with the Golgi (45% overlap).

DISCUSSION

7. DISCUSSION

Several cellular processes have been implicated in β-cell failure in diabetes onset, including increased apoptosis (266), de-differentiation (267), trans-differentiation into other endocrine cell types (268), and loss of β-cell identity (269). Together, these phenomena contribute to the progressive decline of functional β-cell mass, ultimately impairing insulin secretion in response to glucose. Despite significant progress over the past decades, key questions remain open about the molecular and cellular mechanisms that drive β-cell dysfunction in T2D. A deeper understanding of these processes is essential to identify new strategies aimed at preserving or restoring β-cell function and improving therapeutic outcomes.

According to the World Health Organization, there are three fundamental pillars to reduce the burden of T2D: prevention, diagnosis, and treatment. In this context, the insulin-degrading enzyme (IDE) has emerged as a molecule of interest. Although traditionally known for its role in insulin clearance, recent studies suggest that IDE also exerts non-proteolytic functions that influence β-cell signaling, structure, and function, (168). Supporting its relevance to T2D, genetic polymorphisms in the *Ide* gene have been linked to impaired insulin metabolism and increased disease risk (152–156), and reduced IDE levels have been reported in β-cells from patients with T2D (162). Consistently, mouse models with β-cell-specific IDE deletion (B-IDE-KO) exhibit impaired insulin secretion and display molecular signatures of disrupted β-cell identity, further highlighting the importance of IDE in maintaining β-cell function and glucose homeostasis (168).

In this study, we investigated the role of IDE in β-cell physiology using both cellular and animal KD models, with a particular focus on its involvement in the regulation of the primary cilium, the cytoskeleton, and paracrine signaling-key elements in β-cell function. Our findings indicate that adequate IDE levels are essential for maintaining β-cell structural integrity and functional capacity, supporting a broader role for IDE in preserving islet cell homeostasis.

1. Role of IDE in β-cell function

Under physiological conditions, blood glucose levels rise following food intake. In response, pancreatic β-cells secrete insulin, which promotes glucose uptake into peripheral tissues. Pathophysiological conditions such as diabetes often arise from defects on insulin secretion (270).

To investigate the role of IDE in this context, we employed both cellular models of IDE inhibition in β-cells and a mouse model with partial β-cell-specific IDE deletion (B-IDE-HT). GSIS assays performed in both systems revealed a significant reduction in insulin secretion at high glucose concentrations, underscoring the importance of IDE in maintaining proper stimulus-secretion coupling in β-cells. These findings are in line with previous studies suggesting a link between IDE and insulin release. For example, (166) reported impaired insulin secretion in a global IDE knockout mouse model, while a complete β-cell-specific deletion of IDE (B-IDE-KO) resulted in constitutive insulin secretion, as described by (168) Together, these studies support a critical role for IDE in regulating β-cell function. It is worth noting, however, that while the B-IDE-KO model presents a complete absence of IDE in β-cells, both our B-IDE-HT mouse model and the cellular systems used in our study exhibit only partial IDE deficiency. These models resemble what our group has described in T2D, where IDE pancreatic levels are decreased in β-cells (162). This difference in the degree of IDE loss could underlie the distinct insulin secretion patterns observed, highlighting the possibility of a dose-dependent effect of IDE on β-cell physiology.

Calcium is a pivotal second messenger in β-cell function, acting as the final trigger for insulin granule exocytosis following glucose stimulation. This process relies on tightly regulated calcium fluxes between the cytosol, the extracellular space, and intracellular stores such as the ER (270). Dysregulation of calcium homeostasis has been widely documented in diabetic conditions and is considered a key contributor to β-cell dysfunction. To explore whether IDE deficiency affects calcium signaling, we analyzed intracellular calcium dynamics in isolated islets from B-IDE-HT mice. Notably, we observed abnormal calcium responses in both the cytosol (at 8 and 16 mM glucose) and the ER. These findings suggest that IDE deficiency disrupts calcium handling at multiple levels. The impaired calcium mobilization in response to glucose correlates with the reduced insulin secretion observed in IDE-deficient islets, indicating a failure of β-cells to properly coordinate calcium signaling and insulin exocytosis. Supporting this idea, recent studies have linked ER calcium dysregulation to impaired insulin secretion and the pathogenesis of T2D (270). For example, sorcin, a calcium-sensing protein that regulates ER luminal calcium, has been shown to be essential for normal GSIS. Its deficiency leads to ER calcium depletion and defective insulin secretion (271). Although IDE has not been directly linked to calcium regulation before, our findings suggest that it may influence this pathway. The impaired insulin secretion and disrupted calcium homeostasis observed in our model could result from downstream defects. However, this

mechanism was not explored in depth, and further studies are needed to assess the involvement of calcium channels and regulators in the context of IDE deficiency.

It is also important to investigate upstream events in the insulin secretion pathway, such as glucose uptake and ATP production. Deficiencies in glucose sensing, due to altered expression or trafficking of glucose transporters or reduced glucokinase activity, could compromise membrane depolarization and calcium influx. Reduced ATP production may also impair these events, thereby contributing to the observed phenotype (60,272–275). In this sense, Fernandez-Diaz et al showed, using the B-IDE-KO model, an upregulation of genes involved in glucose transport (*Glut1*) and calcium signaling; likely reflecting a compensatory response to complete IDE loss. Interestingly, in this model, Glut2 (Km ≈ 15-20 mM), the principal glucose transporter in murine β-cells, was found to be reduced at the plasma membrane despite unchanged transcript levels, suggesting potential post-translational or trafficking defects (168). In our model of partial IDE inhibition (B-IDE-HT), we did not evaluate the expression or localization of glucose transporters, so we cannot rule out that impaired glucose uptake may also contribute to the defective insulin secretion observed.

Together, our findings suggest that IDE plays a role in regulating insulin secretion in β-cells, through a mechanism that involves calcium transport. Its deficiency contributes to early alterations in β-cell function characteristic of T2D.

2. Role of IDE in glucose-mediated β-cell responses

2.1 IDE regulates glucose-induced microtubule remodeling

Microtubules exhibit dynamic instability driven by GTP hydrolysis on β-tubulin, allowing continuous cycles of polymerization and depolymerization essential for cytoskeletal remodeling and intracellular trafficking. In pancreatic β-cells, microtubules form a dense, non-radial network originating from the Golgi apparatus and extending throughout the cytoplasm (76,80,81). This architecture is crucial for guiding insulin granules toward the plasma membrane to support GSIS. High glucose levels promote cytoskeletal remodeling by inducing peripheral microtubule disassembly and stimulating nucleation at the Golgi (76). These processes are regulated by glucose-activated kinases, such as PKA, PKC, GSK3, and CDK5, which phosphorylate MAPs like Tau, thereby destabilizing microtubules (232). Although most studies support this model, recent experimental and computational work (276) has suggested that random, diffusion-like movement may also contribute to granule transport in β-cells.

Previous work by Steneberg et al. (166) and observations in α-cells (264) have suggested a role for IDE in cytoskeletal regulation. Based on this, we investigated whether IDE is also required for cytoskeletal remodeling in β-cells, particularly in the context of glucose stimulation. In both, Ins1E and Min6 wild type cells, high glucose exposure caused a mild, non-significant reduction, in total tubulin intensity and a redistribution toward the cell periphery, as shown by heatmap-based spatial analysis. In contrast, IDE-deficient cells (Ins1E-shIDE and Min6-shIDE) displayed increased tubulin intensity under high glucose, especially near the nucleus, suggesting a failure in the redistribution of microtubules to the cell periphery.

These results support the notion that high glucose induces microtubule reorganization, and that IDE is necessary for the proper redistribution of tubulin. This phenotype observed in absent of IDE, could aligns with observations by Kaverina and colleagues, who showed that microtubules are targeted to specific subcellular locations such as focal adhesions and the Golgi apparatus through tightly regulated capture and stabilization mechanisms (229,277). The tubulin mislocalization observed in Min6-shIDE cells, particularly under high glucose conditions, could therefore reflect a disruption of these targeting mechanisms, possibly mediated by impaired interactions with MAPs or defects in motor protein function.

It is important to note, however, that the antibodies used detect both free tubulin dimers and polymerized microtubules, so these changes reflect global tubulin distribution rather than specific alterations in microtubule structures.

To further explore how glucose and IDE influence microtubule architecture, we quantified microtubule length. In control cells, high glucose showed a tendency to reduce microtubule length, though the effect was not statistically significant. This trend aligns with previous studies showing that glucose destabilizes microtubules, promoting their peripheral disassembly. Simultaneously, glucose enhances microtubule nucleation at the Golgi, accelerating polymerization of new filaments (234). Given this dynamic balance, net microtubule length may remain unchanged despite active remodeling, possibly explaining the lack of significant differences observed in our data.

We next analyzed the spatial relationship between IDE and the microtubule network under low- and high-glucose conditions. When quantifying the tubulin signal overlapping with major cytoplasmic IDE structures, mostly localized near the Golgi, we found no significant differences. However, when we analyzed the proportion of IDE signal overlapping with tubulin-positive areas, we observed a consistent, though non-

significant, increase under high-glucose conditions. This suggests that **glucose may enhance the recruitment or association of IDE with the microtubule network**.

IDE-deficient cells displayed a distinct phenotype. Under low-glucose conditions, microtubules were significantly longer and more curved compared to controls. In these cells, colocalization between IDE and tubulin was reduced. These **findings suggest that IDE contributes to microtubule destabilization, a function that may be enhanced under high-glucose conditions**, where IDE increasingly localizes to microtubule-rich regions. In the partial absence of IDE, this destabilization process is impaired, resulting in abnormally long and possibly more stable microtubules, which maybe affecting insulin vesicle traffic towards the plasma membrane.

We hypothesize that IDE might act as a MAP (microtubule associated protein) or it maybe modulating MAP activity. For instance, IDE might directly affect microtubule stability or influence the phosphorylation state of MAPs such as Tau. It may also interact with regulatory kinases (e.g., PKA, GSK3), modulate GTP-tubulin pools, or affect nucleation rates at Golgi.

Consistently, we observed that IDE predominantly localizes to a perinuclear structure reminiscent of Golgi apparatus. This structure was still present in IDE-deficient cells, albeit smaller. This reduction may result from technical limitations (e.g., partial knockdown or non-specific antibody staining) or reflect selective depletion of the cytoplasmic pool while sparing Golgi-associated IDE. The proximity between IDE and the Golgi supports a role for IDE in microtubule remodeling at this site. Given Golgi's role as a microtubule-organizing center (MTOC) in β-cells (229), IDE may locally regulate microtubule nucleation and stability.

Altogether, these findings suggest that **IDE plays a previously unrecognized role in cytoskeletal remodeling in β-cells, potentially linking metabolic cues as glucose to structural reorganization during insulin secretion.**

2.2 IDE coordinates paracrine receptor regulation in response to glucose

Paracrine receptors, such as the IR and GcgR, integrate signals from neighboring islet cells and fine-tune β-cell function. Their correct expression, trafficking, and localization at the plasma membrane are essential for β-cell responsiveness and systemic glucose homeostasis. Both IR and GcgR are membrane proteins, their correct folding, processing, and transport to the cell surface require passage through the ER and Golgi and depend on an intact microtubule network (278). Moreover, cytoskeletal components have also been implicated in receptor recycling, as shown for the GcgR (279).

Interestingly, glucose itself modulates the levels of these receptors. In hepatocyte cell lines (HepG2 cells), high glucose increases *IR* gene expression, suggesting transcriptional regulation (280). Similarly, primary rat hepatocytes exposed to high glucose exhibit a two-fold increase in GcgR mRNA compared to low-glucose conditions (281). These findings indicate that glucose can upregulate receptor expression, at least in certain cell types. In contrast, our results show that acute glucose stimulation (30 min) in β-cell lines (Ins1E and Min6) leads to a reduction in total protein levels of both IR and GcgR. This discrepancy likely reflects differences in cell type and the duration of glucose exposure. While chronic glucose exposure may enhance receptor expression in hepatic cells, β-cells may undergo a rapid adaptation to acute stimulation, prioritizing insulin secretion over receptor synthesis or trafficking. In this context, transient receptor downregulation could represent a regulatory mechanism to fine-tune β-cell responses.

More importantly, partial loss of IDE resulted in reduced levels of both IR and GcgR, independently of glucose levels. Additionally, in IDE-deficient cells, these receptors no longer responded to glucose stimulation, indicating a loss of dynamic regulation. These findings suggest that **IDE is required for both basal receptor levels maintenance and their glucose-dependent regulation.**

Although our current analysis focused on total receptor protein levels, it remains to be determined whether the observed changes reflect altered trafficking, impaired recycling, or increased degradation. Given IDE's role in organizing the microtubule network, its absence could compromise receptor trafficking by disrupting vesicle transport or Golgi/ER function. In line with this, the partial colocalization of IDE with Golgi-associated structures, could suggest that its loss may indirectly impair protein processing and transport.

To further elucidate these mechanisms, future experiments should aim to distinguish free tubulin from polymerized microtubules, assess the phosphorylation status of MAPs such as Tau, and test for physical interactions between IDE and microtubules or microtubule-associated proteins using approaches such as co-immunoprecipitation or proximity ligation assays. It will also be important to determine whether IDE deficiency alters insulin granule dynamics or vesicle–microtubule interactions. In addition, investigating receptor localization in the absence of IDE would provide insights into the specific step at which receptor trafficking is disrupted. Together, these studies will help to clarify whether IDE works as a direct effector of microtubule remodeling, an upstream regulator of MAP activity, or a metabolic sensor that integrates structural and functional responses in pancreatic β-cells.

Based on findings from a recent study reporting that IDE acts as an allosteric modulator of the 20S proteasome and a potential competitor of the 19S regulatory particle (149), an additional hypothesis emerges that may help explain some of our observations. Under physiological conditions, IDE binding to the 20S proteasome may limit the assembly of the 26S proteasome, thereby restricting the degradation of ubiquitinated proteins. In contrast, in the absence of IDE, the 20S core would be more available to interact with the 19S regulatory particle, potentially enhancing 26S proteasome formation and overall proteolytic activity. This increased degradation capacity could lead to the accelerated turnover of proteins critical for β-cell function, including insulin and glucagon receptors and cytoskeletal components.

Beyond this post-traslational regulation, altered mRNA transcription, processing, or stability in IDE-deficient cells could contribute to the observed reduction in protein levels and mislocalization. If IDE directly or indirectly modulates RNA-binding proteins, signaling kinases, or chromatin regulators, it may serve as a key integrator of metabolic cues and gene expression programs in β-cells. In support of this, a recent study demonstrated that IDE modulaties mRNA processing pathways and potentially interacting with the CCR4–NOT complex, a key regulator of mRNA deadenylation and degradation (282). Future transcriptomic approaches, such as RNA sequencing or ribosome profiling, will be essential to determine whether IDE affects the transcription, stability, or translation efficiency of genes involved in cytoskeletal dynamics, vesicular trafficking, and receptor biology, ultimately impacting β-cell structure and function.

3. Role of IDE in ciliogenesis

Primary cilia are microtubule-based organelles essential for cellular signaling and metabolic regulation, whose proper structure and function, dependent on coordinated microtubule dynamics and protein trafficking, are crucial for insulin secretion in pancreatic β-cells. Disruption of these organelles leads to impaired glucose-stimulated insulin secretion, loss of β-cell identity, and defective glucose homeostasis (235,236). Consistently, evidence from ciliopathies, as well as from T2D patients and animal models, supports the link between ciliary dysfunction and β-cell failure (249), with pancreatic β-cells from individuals with type 2 diabetes exhibiting shorter primary cilia, highlighting a potential structural correlate of impaired β-cell function (250).

In our *in vivo* mouse models with partial (B-IDE-HT) or complete (B-IDE-KO) deletion of IDE, we observed a significant reduction in the number of primary cilia, indicating that cilium formation is sensitive to IDE dosage. Consistently, β-cell lines (Ins1E and Min6)

with chronic IDE knockdown displayed a marked reduction in both the number of primary cilia and the levels of ciliary markers such as acetylated tubulin (AcTub) and Arl13b. Taken together, these results suggest **that IDE positively regulates the formation and/or maintenance of primary cilia, and that sustained loss of IDE impairs this process.**

However, super-resolution microscopy experiments revealed that **IDE is not localized within the primary cilium**, suggesting that its regulation of ciliogenesis is not mediated by direct interaction with the ciliary structure. Instead, IDE appears to influence cilium formation through indirect mechanisms involving cytoskeletal dynamics and intracellular trafficking. It is also possible that IDE may be interacting with proteins required for ciliogenesis.

These observations are in line with our earlier findings, showing that IDE is required for remodeling the microtubule network. Given that the axoneme is built from stabilized microtubules, IDE deficiency may disrupt cilium biogenesis by impairing microtubule organization. In this context, excessively long or unstable microtubules, as observed in IDE-deficient cells, may fail to support the structural requirements for cilium formation.

In addition, primary cilium assembly depends not only on cytoskeletal integrity but also on vesicular transport through ER–Golgi–plasma membrane axis. Ciliary proteins must be correctly folded, processed, and delivered to the cilium basal body and growing axoneme (283). As shown in the previous section, IDE is distributed throughout cytoplasm but exhibits strong enrichment in perinuclear, Golgi-associated regions. This subcellular localization suggests that IDE may contribute to the regulation of ER and Golgi function, including protein maturation and folding, as well as the trafficking of cargo along the microtubule network. Just as we proposed for the trafficking of paracrine receptors, IDE could facilitate the delivery of ciliary components to their destination. Therefore, IDE deficiency may impair the maturation or transport of key ciliary proteins, ultimately leading to defective ciliogenesis and reduced cilium stability.

There are specific signaling pathways that regulate the formation of the primary cilium (283). When these pathways are disrupted, ciliogenesis can be impaired. IDE might influence some of these pathways, so it is possible that the loss of IDE indirectly affects cilium formation by interfering with these regulatory signals.

Notably, the mechanisms proposed in the previous chapter, ranging from impaired proteasome activity to widespread transcriptomic changes, may also contribute to the defects in ciliogenesis observed here.

Altogether, our findings support a model in which IDE plays a dual role in β-cells: regulating both microtubule architecture and protein trafficking, processes essential for membrane and organelle function, whose disruption may impair multiple interconnected pathways, ultimately leading to defective ciliogenesis.

3.1 IDE modulates the glucose-dependent regulation of cilia protein levels

The coordinated regulation of the primary cilium and the cell cycle has been extensively documented across various cell types. Primary cilia are typically present during the G0/G1 phase, where they contribute to cell polarity and differentiation, and are resorbed as cells prepare to enter the replicative S phase (284). In this context, studies using human retinal pigment epithelial cells (RPE-1) have shown that glucose deprivation promotes ciliogenesis by inhibiting the mTORC1 pathway (285). Conversely, high glucose activates mTORC1, which promotes cell growth and proliferation, conditions generally incompatible with ciliogenesis. In pancreatic β-cells, glucose is also known to stimulate proliferation, though this has mainly been observed after prolonged exposures of 24 h or more (286). However, direct evidence linking glucose concentrations to alterations in the number of primary cilia in β-cells has been limited. Nonetheless, some studies have suggested that ciliary function in pancreatic islets is glucose-dependent (287).

In our study, we observed that short-term (30 min) exposure to either low or high glucose concentrations did not significantly affect the number of primary cilia in pancreatic β-cells. This was true for both control and IDE-KD cells, which already display a reduced baseline number of cilia. It is worth noting that, under physiological conditions, β-cells are largely quiescent (G0 phase) and divide infrequently. While glucose can promote β-cell proliferation (286), the short duration of exposure in our experiments may be insufficient to initiate cilium resorption or cell cycle re-entry. Moreover, previous reports linking glucose levels to ciliogenesis typically involved different cell models and longer exposure periods, further supporting the idea that short-term glucose stimulation may not be enough to produce detectable changes in cilium number.

With respect to cilium length, we observed a tendency toward reduction after glucose stimulation, although the change was not statistically significant. Notably, recent work has highlighted the role of nutrient-sensing mechanisms, such as O-GlcNAcylation, in modulating ciliary length in neurons (288). O-GlcNAcylation is a glucose-sensitive post-translational modification that reflects intracellular glucose availability. In human cortical neurons derived from iPSCs, elevated O-GlcNAc levels were associated with shorter

cilia. These findings align with our observations, suggesting that glucose-induced O-GlcNAcylation could contribute to the subtle cilium shortening we observed in β-cells.

Interestingly, although the number of cilia remained unchanged in our experiments, we did observe glucose-dependent changes in ciliary protein markers in control cells. Specifically, levels of AcTub were significantly reduced under high glucose conditions, while Arl13b showed a decreasing trend that did not reach statistical significance. In IDE-KD cells, this regulation appeared to be disrupted: Arl13b levels showed a reversed, though non-significant, trend upon high glucose exposure, and AcTub followed the same direction as in control cells, but the effect was attenuated. It is worth noting that AcTub, while commonly used as a marker for stable microtubules and cilia, is itself a post-translational modification influenced by cellular context and metabolic status (235). Thus, its regulation may reflect early cytoskeletal changes rather than direct remodeling of the cilium. Our findings suggest that short-term glucose stimulation may begin to downregulate proteins associated with cilium structure and stability.

Taking together, these data suggest that IDE may play a role in modulating cilia-related protein expression in response to glucose, even without affecting cilium number during short-term glucose fluctuations. As previously observed with microtubule markers and paracrine signaling receptors, glucose appears to modulate the expression, stability, or trafficking of ciliary proteins in an IDE-dependent manner. In the absence of IDE, this regulation is either blunted or misdirected, reinforcing the hypothesis that **IDE participates in the metabolic coordination of intracellular trafficking or protein turnover**.

Although IDE protein levels do not appear to be directly regulated by glucose in β-cells, it is still possible that glucose modulates IDE activity through post-translational modifications. These modifications could alter IDE's function or its ability to interact with components of the cytoskeleton, potentially influencing how β-cells sense and respond to metabolic signals. Further research is needed to determine whether IDE is functionally linked to glucose-sensitive pathways, and whether such interactions play a role in regulating the structural or functional integrity of the cytoskeleton, paracrine receptors, and the primary cilium.

Future directions should aim to clarify the mechanisms by which IDE influences primary cilium regulation in pancreatic β-cells. Live-cell imaging of fluorescently tagged ciliary proteins could help determine whether their delivery to cilium is altered in IDE-deficient cells.

Additionally, since our current experiments involved only short-term glucose exposure (30 min), longer treatments (e.g., 4–24 h) could uncover delayed effects on cilium number or length, as previously observed in other cell types. In parallel, proteomic or Western blot analyses could be used to investigate whether IDE undergoes glucose-induced post-translational modifications as phosphorylation, acetylation or ubiquitination, that may regulate its activity or interactions with trafficking machinery.

To further explore whether defective intracellular transport contributes to the observed changes in ciliary protein levels, pharmacological inhibition of ER–Golgi trafficking (e.g., with Brefeldin A) could be employed. Finally, microtubule-targeting agents such as taxol or nocodazole could be used to assess whether changes in microtubule stability underlie the ciliary defects observed in IDE-deficient cells. Together, these approaches would provide valuable insights into how IDE integrates metabolic cues to regulate ciliary structure and function in β-cells.

4. Role of primary cilium in β-cell function

The primary cilium is increasingly recognized as a key signaling hub in β-cells, integrating environmental cues and contributing to insulin secretion and glucose homeostasis. It hosts specific GPCRs and signaling components, such as the somatostatin receptor 3 (SSTR3), which localizes to the cilium and mediates the suppressive effect of somatostatin on insulin secretion and calcium oscillations (250,289). However, whether other receptors critical for paracrine regulation, such as the IR or the GcgR, also localize to the β-cell cilium remains unclear.

Previous studies using β-cell-specific knockout of ciliogenesis genes, including *Ift88* and *Kif3a*, have shown that ciliary disruption in mice leads to impaired GSIS without affecting β-cell mass (249,290). These defects were attributed to alterations in calcium signaling and disrupted coupling between extracellular signals and intracellular responses. Accordingly, ciliary dysfunction has been proposed as a contributing factor to T2D susceptibility, highlighting the importance of ciliary integrity in metabolic regulation.

Importantly, ciliary inhibition using IFT88-knock-down in our hands caused a marked reduction in both IR and GcgR protein levels, replicating the phenotype seen in IDE-deficient cells. However, IDE expression itself remained unchanged in the absence of cilia, indicating that **IDE does not depend on ciliary function but may act upstream to regulate ciliogenesis**. This aligns with our previous data showing that IDE modulates cytoskeletal dynamics essential for ciliary assembly and maintenance.

The reduced expression of paracrine receptors in cilium-deficient cells suggests that ciliary signaling is necessary to maintain receptor homeostasis, even if IR and GcgR are not localized to the ciliary membrane. Although Gerdes et al (253) reported that insulin stimulation recruits IR to the β-cell cilium and that ciliary integrity is required for insulin signaling, this finding has not been widely replicated, and evidence for constitutive localization of IR or GcgR in the cilium remains limited.

One possible explanation, besides the possibility that these receptors localize directly to cilium and decrease in its absence, is that the primary cilium functions as a scaffold for multiple signaling pathways that regulate β-cell function. These pathways may influence receptor expression, trafficking, and stability. For example, the cilium hosts signaling routes such as the Hedgehog (Hh) pathway (235), which has been shown to modulate insulin gene expression, maintain β-cell identity, and protect against ER stress-induced apoptosis. Through these mechanisms, the absence of primary cilium could indirectly impair the maturation and trafficking of key proteins.

Together, our findings suggest that **primary cilia serve not only as structural organelles but also as essential regulators of β-cell receptor composition and insulin secretion**. The observed reduction in IR and GcgR expression following cilium disruption highlights a broader role for ciliary signaling in coordinating paracrine responsiveness and the intracellular trafficking machinery critical for β-cell function and glucose homeostasis.

We propose a model in which IDE and the primary cilium work in a coordinated but distinct manner to regulate β-cell function. IDE promotes cytoskeletal remodeling, which supports the assembly of the primary cilium. Meanwhile, cilium itself is essential for maintaining the expression of key paracrine receptors. These pathways likely converge on vesicle trafficking and signal integration, processes that are critical for fine-tuning β-cell responses to glucose and signals from the islet microenvironment.

Future work should aim to determine whether IR and GcgR localize to the cilium under basal conditions or specific stimuli, such as acute glucose exposure or insulin/glucagon stimulation. It will also be important to assess whether ciliary inhibition alters receptor trafficking routes, mRNA levels, or protein degradation pathways. Live-cell imaging of receptor dynamics in cilium-deficient cells, combined with rescue experiments using alternative knockdown methods (e.g., siRNA or CRISPR), would help to validate these findings. Finally, proteomic or transcriptomic analysis of cilium-deficient versus control β-cells may uncover novel regulatory axes linking ciliary signaling to receptor homeostasis and insulin secretion.

5. Role of IDE and cilia in glucagon action and β-Cell function

Glucagon, a key regulator of glucose homeostasis, exerts systemic effects primarily through hepatic gluconeogenesis and glycogenolysis but also plays an important paracrine role within the pancreatic islet. In β-cells, glucagon enhances insulin secretion and promotes gene transcription via activation of GPCRs, mainly the glucagon receptor (GcgR) and the GLP-1 receptor (GLP-1R). These receptors activate the cAMP/PKA and EPAC signaling pathways, resulting in increased calcium influx, insulin exocytosis, and CREB-mediated transcriptional programs that support β-cell function and survival. Additionally, the MAPK/ERK pathway, activated through PKA-dependent and β-arrestin-mediated mechanisms, further supports β-cell proliferation and insulin biosynthesis (95,95,265,265).

Given the multifaceted role of glucagon in β-cell biology, we investigated whether the downregulation of GcgR observed in IDE-deficient and cilia-deficient cells translated into impaired glucagon signaling and β-cell function.

Islets from B-IDE-HT and B-IDE-WT mice were stimulated with glucagon for 30 min under high-glucose conditions. Although insulin secretion in response to high glucose plus glucagon was significatively higher in control mice compared to B-IDE-HT, the B-IDE-HT mice still exhibited a glucagon-induced increase relative to high glucose alone. Whether there is an impairment in glucagon stimulation of B-IDE-HT insulin secretion require of further experimentation.

Interestingly, when examining the glucagon signaling cascade, we observed that in IDE knockdown cells, basal phosphorylation of PKA substrates was elevated and not further regulated by glucagon. In other words, in the absence of glucagon, PKA substrate phosphorylation was significantly increased, pointing to constitutive active PKA in IDE-KD cells. This constitutive activation might reflect a compensatory or dysregulated state: IDE loss disrupts insulin secretion and other cellular functions, prompting the cell to activate signaling pathways (such as glucagon signaling that promotes insulin secretion) to compensate for this dysregulation, possibly by improving calcium flux or insulin release. Alternatively, IDE deficiency may disrupt negative feedback loops regulating this signaling.

In contrast, pCREB levels were significantly reduced under basal conditions in Min6-shIDE cells despite the high basal phosphorylation of PKA substrates. This apparent disconnection could be explained by spatial differences in PKA activity or impaired nuclear translocation of active PKA/CREB. Upon glucagon stimulation, both control and IDE-deficient cells showed a similar increase in pCREB, indicating partial preservation

of this signaling axis under acute stimulation. It is possible that, in the absence of glucagon stimulation, PKA preferentially phosphorylates other substrates related to immediate cellular needs (such as calcium handling or insulin secretion) due to IDE deficiency, but upon glucagon stimulation, PKA can activate CREB, triggering transcription of genes involved in β-cell survival, proliferation, and insulin biosynthesis.

In wild type Min6 cells, glucagon induces robust ERK activation, but this response is significantly blunted in IDE knockdown cells (Min6-shIDE). ERK activation depends on a well-coordinated network of upstream signals, including PKA, EPAC, and β-arrestin scaffolds, that require proper spatial organization within the cell. IDE is known to regulate cytoskeletal dynamics and vesicle trafficking. Without IDE, this organization is disrupted, leading to mislocalization or faulty trafficking of receptors or signaling complexes, which likely explains the reduced ERK activation in response to glucagon.

To determine whether these phenotypes were specific to IDE deficiency or also influenced by structural changes such as loss of the primary cilium, we analyzed glucagon signaling in IFT88 knockdown cells. Despite reduced GcgR expression, these cells responded normally to glucagon stimulation, with intact pCREB activation, and ERK signaling. This indicates that cilia are not essential for glucagon signaling in β-cells, at least under the conditions tested. However, it is important to note that this was not a complete cilium knockout, so residual cilia might suffice to maintain this activity. Also, since glucagon can signal through the GLP-1 receptor, which was not quantified here, it is possible that GLP-1R levels remain unchanged in cilia-deficient cells or that glucagon signaling compensates through this receptor.

Interestingly, the preservation of glucagon responsiveness despite reduced GcgR expression suggests that additional, non-canonical signaling routes may compensate for impaired receptor availability. One plausible mechanism involves β-arrestin-dependent pathways, which can mediate receptor desensitization and internalization but also initiate alternative signaling cascades independently of G protein activation (291). These β-arrestin-mediated signals, such as activation of ERK and other kinases, might sustain downstream effects like pCREB activation despite diminished classical receptor signaling. Therefore, potentially other unidentified pathways could explain the maintenance of glucagon response in conditions of reduced receptor expression or altered ciliary structure.

Although both models (IDE-KD and IFT88-KD) show decreased glucagon receptor protein expression, the downstream signaling defects appear more pronounced in IDE

deficiency. This difference suggests that loss of IDE is primarily responsible for functional impairments in the glucagon pathway.

Together, our findings support a model in which **IDE plays a critical role in maintaining proper β-cell responsiveness to glucagon by preserving receptor levels and enabling effective signal transduction.** This role extends beyond protein receptor expression, likely involving spatial organization and trafficking of signaling components. While the primary cilium is important for other β-cell functions, it does not appear to directly modulate glucagon signaling, though its influence on receptor levels suggests a role in upstream processes such as receptor biogenesis or localization.

To deepen our understanding of how IDE regulates glucagon signaling, future research should explore its impact on Golgi organization and cytoskeletal dynamics, as these structures are key to receptor trafficking and spatial signaling integration. In parallel, dissecting the crosstalk between glucagon and GLP-1 receptor pathways in IDE- and cilia-deficient cells may uncover compensatory or synergistic mechanisms that shape β-cell responses to paracrine cues. Importantly, generating models with complete ablation of the primary cilium in β-cells will be essential to conclusively assess its role in glucagon receptor regulation and signaling fidelity.

In summary, our findings reveal a multifaceted and previously underappreciated role for IDE in pancreatic β-cell physiology, extending well beyond its classical function in insulin degradation. **We demonstrate that IDE is essential not only for maintaining glucose-stimulated insulin secretion and calcium dynamics, but also for orchestrating cytoskeletal remodeling and regulating ciliogenesis.** Specifically, we show that IDE modulates microtubule dynamics, cilia and paracrine receptor expression in a glucose-dependent manner, suggesting that it acts as a molecular hub linking metabolic stimuli to cytoskeletal reorganization and vesicular trafficking.

Moreover, although IDE is not localized within the primary cilium, its deficiency leads to a marked reduction in the number of primary cilia in β-cells. We further show that the primary cilium is essential not only for β-cell function, as previously known, but also for the regulation of key paracrine receptors.

Taken together, **these findings position both IDE and the primary cilium as central regulators of β-cell homeostasis**, influencing not only insulin secretion but also the structural and sensory components that support endocrine function. Our study opens new avenues for targeting IDE and ciliary pathways as promising therapeutic strategies to preserve islet function and delay β-cell failure in the context of T2D.

CONCLUSIONS

8. CONCLUSIONS

1. **IDE is essential for proper β-cell function**, its default leads to: impaired GSIS and disrupted calcium dynamics.
2. **IDE regulates the tubulin cytoskeleton in a glucose-dependent manner**, affecting microtubule organization, distribution, and response to metabolic stimuli.
3. **IDE is not localized in the primary cilium of pancreatic β-cells, although it is linking cytoskeletal regulation to the cilium dynamics.**
4. **Loss of IDE disrupts the regulation of insulin and glucagon receptors**, impairing paracrine signaling and β-cell responsiveness to glucagon.
5. Our findings highlight a central role for IDE in coordinating β-cell cytoarchitecture and function through the regulation of microtubules, primary cilia, and paracrine receptor dynamics. Thus, targeting IDE may represent a promising strategy to preserve β-cell function and prevent diabetes progression.

REFERENCES

9. REFERENCES

1. Röder PV, Wu B, Liu Y, Han W. Pancreatic regulation of glucose homeostasis. Exp Mol Med. 2016 Mar 11;48(3):e219.
2. Magliano DJ, Boyko EJ, IDF Diabetes Atlas 10th edition scientific committee. IDF DIABETES ATLAS [Internet]. 10th edn. Brussels: International Diabetes Federation; 2021 [cited 2025 June 26]. (IDF Diabetes Atlas). Available from: http://www.ncbi.nlm.nih.gov/books/NBK581934/
3. Duong DT, Waltner-Law ME, Sears R, Sealy L, Granner DK. Insulin inhibits hepatocellular glucose production by utilizing liver-enriched transcriptional inhibitory protein to disrupt the association of CREB-binding protein and RNA polymerase II with the phosphoenolpyruvate carboxykinase gene promoter. J Biol Chem. 2002 Aug 30;277(35):32234–42.
4. Nakae J, Kitamura T, Silver DL, Accili D. The forkhead transcription factor Foxo1 (Fkhr) confers insulin sensitivity onto glucose-6-phosphatase expression. J Clin Invest. 2001 Nov;108(9):1359–67.
5. McTernan PG, Harte AL, Anderson LA, Green A, Smith SA, Holder JC, et al. Insulin and rosiglitazone regulation of lipolysis and lipogenesis in human adipose tissue in vitro. Diabetes. 2002 May;51(5):1493–8.
6. Biolo G, Declan Fleming RY, Wolfe RR. Physiologic hyperinsulinemia stimulates protein synthesis and enhances transport of selected amino acids in human skeletal muscle. J Clin Invest. 1995 Feb;95(2):811–9.
7. Diabetes [Internet]. [cited 2025 June 26]. Available from: https://www.who.int/es/news-room/fact-sheets/detail/diabetes
8. Unger RH, Cherrington AD. Glucagonocentric restructuring of diabetes: a pathophysiologic and therapeutic makeover. J Clin Invest. 2012 Jan;122(1):4–12.
9. DiMeglio LA, Evans-Molina C, Oram RA. Type 1 diabetes. Lancet Lond Engl. 2018 June 16;391(10138):2449–62.
10. Li W, Huang E, Gao S. Type 1 Diabetes Mellitus and Cognitive Impairments: A Systematic Review. J Alzheimers Dis JAD. 2017;57(1):29–36.
11. Eizirik DL, Sammeth M, Bouckenooghe T, Bottu G, Sisino G, Igoillo-Esteve M, et al. The human pancreatic islet transcriptome: expression of candidate genes for type 1 diabetes and the impact of pro-inflammatory cytokines. PLoS Genet. 2012;8(3):e1002552.
12. Bluestone JA, Herold K, Eisenbarth G. Genetics, pathogenesis and clinical interventions in type 1 diabetes. Nature. 2010 Apr 29;464(7293):1293–300.
13. Ruze R, Liu T, Zou X, Song J, Chen Y, Xu R, et al. Obesity and type 2 diabetes mellitus: connections in epidemiology, pathogenesis, and treatments. Front Endocrinol. 2023;14:1161521.
14. Khan AH, Pessin JE. Insulin regulation of glucose uptake: a complex interplay of intracellular signalling pathways. Diabetologia. 2002 Nov;45(11):1475–83.
15. Petersen MC, Shulman GI. Mechanisms of Insulin Action and Insulin Resistance. Physiol Rev. 2018 Oct 1;98(4):2133–223.
16. da Silva Rosa SC, Nayak N, Caymo AM, Gordon JW. Mechanisms of muscle insulin resistance and the cross-talk with liver and adipose tissue. Physiol Rep. 2020 Oct;8(19):e14607.
17. Skyler JS, Bakris GL, Bonifacio E, Darsow T, Eckel RH, Groop L, et al. Differentiation of Diabetes by Pathophysiology, Natural History, and Prognosis. Diabetes. 2017 Feb;66(2):241–55.
18. Kahn SE, Cooper ME, Del Prato S. Pathophysiology and treatment of type 2 diabetes: perspectives on the past, present, and future. Lancet Lond Engl. 2014 Mar 22;383(9922):1068–83.
19. Unger RH, Grundy S. Hyperglycaemia as an inducer as well as a consequence of impaired islet cell function and insulin resistance: implications for the management of diabetes. Diabetologia. 1985 Mar;28(3):119–21.
20. Poitout V, Robertson RP. Glucolipotoxicity: fuel excess and beta-cell dysfunction. Endocr Rev. 2008 May;29(3):351–66.
21. Oyadomari S, Araki E, Mori M. Endoplasmic reticulum stress-mediated apoptosis in pancreatic beta-cells. Apoptosis Int J Program Cell Death. 2002 Aug;7(4):335–45.
22. Shoelson SE, Lee J, Goldfine AB. Inflammation and insulin resistance. J Clin Invest. 2006 July;116(7):1793–801.

23. Donath MY, Shoelson SE. Type 2 diabetes as an inflammatory disease. Nat Rev Immunol. 2011 Feb;11(2):98–107.
24. Leung PS. Physiology of the pancreas. Adv Exp Med Biol. 2010;690:13–27.
25. Dolenšek J, Rupnik MS, Stožer A. Structural similarities and differences between the human and the mouse pancreas. Islets. 2015;7(1):e1024405.
26. Leung PS, Ip SP. Pancreatic acinar cell: its role in acute pancreatitis. Int J Biochem Cell Biol. 2006;38(7):1024–30.
27. The Pancreas. [cited 2025 June 26]; Available from: https://onlinelibrary.wiley.com/doi/epub/10.1002/9781119876007
28. In't Veld P, Marichal M. Microscopic anatomy of the human islet of Langerhans. Adv Exp Med Biol. 2010;654:1–19.
29. Jolles S. Paul Langerhans. J Clin Pathol. 2002 Apr;55(4):243.
30. Goldstein MB, Davis EA. The three dimensional architecture of the islets of Langerhans. Acta Anat (Basel). 1968;71(2):161–71.
31. Campbell JE, Newgard CB. Mechanisms controlling pancreatic islet cell function in insulin secretion. Nat Rev Mol Cell Biol. 2021 Feb;22(2):142–58.
32. Betts JG, Young KA, Wise JA, Johnson E, Poe B, Kruse DH, et al. 17.9 The Endocrine Pancreas - Anatomy and Physiology | OpenStax [Internet]. OpenStax; 2013 [cited 2025 June 26]. Available from: https://openstax.org/books/anatomy-and-physiology-2e/pages/17-9-the-endocrine-pancreas
33. Gao R, Acreman S, Ma J, Abdulkader F, Wendt A, Zhang Q. α-cell electrophysiology and the regulation of glucagon secretion. J Endocrinol. 2023 Aug 1;258(2):e220295.
34. Brissova M, Fowler MJ, Nicholson WE, Chu A, Hirshberg B, Harlan DM, et al. Assessment of human pancreatic islet architecture and composition by laser scanning confocal microscopy. J Histochem Cytochem Off J Histochem Soc. 2005 Sept;53(9):1087–97.
35. Gao R, Yang T, Zhang Q. δ-Cells: The Neighborhood Watch in the Islet Community. Biology. 2021 Jan 21;10(2):74.
36. Katsuura G, Asakawa A, Inui A. Roles of pancreatic polypeptide in regulation of food intake. Peptides. 2002 Feb;23(2):323–9.
37. Khandekar N, Berning BA, Sainsbury A, Lin S. The role of pancreatic polypeptide in the regulation of energy homeostasis. Mol Cell Endocrinol. 2015 Dec 15;418 Pt 1:33–41.
38. Aragón F, Karaca M, Novials A, Maldonado R, Maechler P, Rubí B. Pancreatic polypeptide regulates glucagon release through PPYR1 receptors expressed in mouse and human alpha-cells. Biochim Biophys Acta. 2015 Feb;1850(2):343–51.
39. Cabrera O, Berman DM, Kenyon NS, Ricordi C, Berggren PO, Caicedo A. The unique cytoarchitecture of human pancreatic islets has implications for islet cell function. Proc Natl Acad Sci U S A. 2006 Feb 14;103(7):2334–9.
40. Benitez CM, Goodyer WR, Kim SK. Deconstructing pancreas developmental biology. Cold Spring Harb Perspect Biol. 2012 June 1;4(6):a012401.
41. Zaret KS, Grompe M. Generation and regeneration of cells of the liver and pancreas. Science. 2008 Dec 5;322(5907):1490–4.
42. Desgraz R, Herrera PL. Pancreatic neurogenin 3-expressing cells are unipotent islet precursors. Dev Camb Engl. 2009 Nov;136(21):3567–74.
43. Azzarelli R, Hurley C, Sznurkowska MK, Rulands S, Hardwick L, Gamper I, et al. Multi-site Neurogenin3 Phosphorylation Controls Pancreatic Endocrine Differentiation. Dev Cell. 2017 May 8;41(3):274-286.e5.
44. Arda HE, Benitez CM, Kim SK. Gene regulatory networks governing pancreas development. Dev Cell. 2013 Apr 15;25(1):5–13.
45. Veres A, Faust AL, Bushnell HL, Engquist EN, Kenty JHR, Harb G, et al. Charting cellular identity during human in vitro β-cell differentiation. Nature. 2019 May;569(7756):368–73.
46. Servitja JM, Ferrer J. Transcriptional networks controlling pancreatic development and beta cell function. Diabetologia. 2004 Apr;47(4):597–613.
47. Ganic E, Singh T, Luan C, Fadista J, Johansson JK, Cyphert HA, et al. MafA-Controlled Nicotinic Receptor Expression Is Essential for Insulin Secretion and Is Impaired in Patients with Type 2 Diabetes. Cell Rep. 2016 Mar 1;14(8):1991–2002.
48. Remedi MS, Emfinger C. Pancreatic β-cell identity in diabetes. Diabetes Obes Metab. 2016 Sept;18 Suppl 1(Suppl 1):110–6.
49. Weiss M, Steiner DF, Philipson LH. Insulin Biosynthesis, Secretion, Structure, and Structure-Activity Relationships. In: Feingold KR, Ahmed SF, Anawalt B, Blackman MR, Boyce A, Chrousos G, et al., editors. Endotext [Internet]. South Dartmouth (MA):

MDText.com, Inc.; 2000 [cited 2025 June 27]. Available from: http://www.ncbi.nlm.nih.gov/books/NBK279029/
50. Tokarz VL, MacDonald PE, Klip A. The cell biology of systemic insulin function. J Cell Biol. 2018 July 2;217(7):2273–89.
51. Ataie-Ashtiani S, Forbes B. A Review of the Biosynthesis and Structural Implications of Insulin Gene Mutations Linked to Human Disease. Cells. 2023 Mar 25;12(7):1008.
52. Sander M, Neubüser A, Kalamaras J, Ee HC, Martin GR, German MS. Genetic analysis reveals that PAX6 is required for normal transcription of pancreatic hormone genes and islet development. Genes Dev. 1997 July 1;11(13):1662–73.
53. Ahlgren U, Jonsson J, Edlund H. The morphogenesis of the pancreatic mesenchyme is uncoupled from that of the pancreatic epithelium in IPF1/PDX1-deficient mice. Dev Camb Engl. 1996 May;122(5):1409–16.
54. Zhang C, Moriguchi T, Kajihara M, Esaki R, Harada A, Shimohata H, et al. MafA is a key regulator of glucose-stimulated insulin secretion. Mol Cell Biol. 2005 June;25(12):4969–76.
55. Naya FJ, Huang HP, Qiu Y, Mutoh H, DeMayo FJ, Leiter AB, et al. Diabetes, defective pancreatic morphogenesis, and abnormal enteroendocrine differentiation in BETA2/neuroD-deficient mice. Genes Dev. 1997 Sept 15;11(18):2323–34.
56. Whelan J, Poon D, Weil PA, Stein R. Pancreatic beta-cell-type-specific expression of the rat insulin II gene is controlled by positive and negative cellular transcriptional elements. Mol Cell Biol. 1989 Aug;9(8):3253–9.
57. Leibiger IB, Leibiger B, Moede T, Berggren PO. Exocytosis of insulin promotes insulin gene transcription via the insulin receptor/PI-3 kinase/p70 s6 kinase and CaM kinase pathways. Mol Cell. 1998 May;1(6):933–8.
58. Chang SG, Choi KD, Jang SH, Shin HC. Role of disulfide bonds in the structure and activity of human insulin. Mol Cells. 2003 Dec 31;16(3):323–30.
59. Liu M, Weiss MA, Arunagiri A, Yong J, Rege N, Sun J, et al. Biosynthesis, structure, and folding of the insulin precursor protein. Diabetes Obes Metab. 2018 Sept;20 Suppl 2(Suppl 2):28–50.
60. Berger C, Zdzieblo D. Glucose transporters in pancreatic islets. Pflugers Arch. 2020 Sept;472(9):1249–72.
61. McCulloch LJ, van de Bunt M, Braun M, Frayn KN, Clark A, Gloyn AL. GLUT2 (SLC2A2) is not the principal glucose transporter in human pancreatic beta cells: implications for understanding genetic association signals at this locus. Mol Genet Metab. 2011 Dec;104(4):648–53.
62. Lachaal M, Spangler RA, Jung CY. High Km of GLUT-2 glucose transporter does not explain its role in insulin secretion. Am J Physiol. 1993 Dec;265(6 Pt 1):E914-919.
63. Ashcroft FM, Harrison DE, Ashcroft SJ. Glucose induces closure of single potassium channels in isolated rat pancreatic beta-cells. Nature. 1984 Dec 29;312(5993):446–8.
64. Cook DL, Hales CN. Intracellular ATP directly blocks K+ channels in pancreatic B-cells. Nature. 1984 Sept 20;311(5983):271–3.
65. Rorsman P, Braun M, Zhang Q. Regulation of calcium in pancreatic α- and β-cells in health and disease. Cell Calcium. 2012;51(3–4):300–8.
66. Satin LS, Cook DL. Voltage-gated Ca2+ current in pancreatic B-cells. Pflugers Arch. 1985 Aug;404(4):385–7.
67. Kalwat MA, Thurmond DC. Signaling mechanisms of glucose-induced F-actin remodeling in pancreatic islet β cells. Exp Mol Med. 2013 Aug 23;45(8):e37.
68. Ravier MA, Güldenagel M, Charollais A, Gjinovci A, Caille D, Söhl G, et al. Loss of connexin36 channels alters beta-cell coupling, islet synchronization of glucose-induced Ca2+ and insulin oscillations, and basal insulin release. Diabetes. 2005 June;54(6):1798–807.
69. Satin LS, Butler PC, Ha J, Sherman AS. Pulsatile insulin secretion, impaired glucose tolerance and type 2 diabetes. Mol Aspects Med. 2015 Apr;42:61–77.
70. Rorsman P, Renström E. Insulin granule dynamics in pancreatic beta cells. Diabetologia. 2003 Aug;46(8):1029–45.
71. Straub SG, Shanmugam G, Sharp GWG. Stimulation of insulin release by glucose is associated with an increase in the number of docked granules in the beta-cells of rat pancreatic islets. Diabetes. 2004 Dec;53(12):3179–83.
72. Daniel S, Noda M, Straub SG, Sharp GW. Identification of the docked granule pool responsible for the first phase of glucose-stimulated insulin secretion. Diabetes. 1999 Sept;48(9):1686–90.

73. Zhao A, Ohara-Imaizumi M, Brissova M, Benninger RKP, Xu Y, Hao Y, et al. Gαo represses insulin secretion by reducing vesicular docking in pancreatic beta-cells. Diabetes. 2010 Oct;59(10):2522–9.
74. Hao M, Li X, Rizzo MA, Rocheleau JV, Dawant BM, Piston DW. Regulation of two insulin granule populations within the reserve pool by distinct calcium sources. J Cell Sci. 2005 Dec 15;118(Pt 24):5873–84.
75. Heaslip AT, Nelson SR, Lombardo AT, Beck Previs S, Armstrong J, Warshaw DM. Cytoskeletal dependence of insulin granule movement dynamics in INS-1 beta-cells in response to glucose. PloS One. 2014;9(10):e109082.
76. Bracey KM, Ho KH, Yampolsky D, Gu G, Kaverina I, Holmes WR. Microtubules Regulate Localization and Availability of Insulin Granules in Pancreatic Beta Cells. Biophys J. 2020 Jan 7;118(1):193–206.
77. Malaisse WJ, Orci L. The role of the cytoskeleton in pancreatic B-cell function. Methods Achiev Exp Pathol. 1979;9:112–36.
78. Kalwat MA, Thurmond DC. Signaling mechanisms of glucose-induced F-actin remodeling in pancreatic islet β cells. Exp Mol Med. 2013 Aug 23;45(8):e37.
79. Fye MA, Kaverina I. Insulin secretion hot spots in pancreatic β cells as secreting adhesions. Front Cell Dev Biol. 2023;11:1211482.
80. Liu Z, Vong QP, Zheng Y. CLASPing microtubules at the trans-Golgi network. Dev Cell. 2007 June;12(6):839–40.
81. Trogden KP, Lee J, Bracey KM, Ho KH, McKinney H, Zhu X, et al. Microtubules regulate pancreatic β-cell heterogeneity via spatiotemporal control of insulin secretion hot spots. eLife. 2021 Nov 16;10:e59912.
82. Zhu X, Hu R, Brissova M, Stein RW, Powers AC, Gu G, et al. Microtubules Negatively Regulate Insulin Secretion in Pancreatic β Cells. Dev Cell. 2015 Sept 28;34(6):656–68.
83. Hoboth P, Müller A, Ivanova A, Mziaut H, Dehghany J, Sönmez A, et al. Aged insulin granules display reduced microtubule-dependent mobility and are disposed within actin-positive multigranular bodies. Proc Natl Acad Sci U S A. 2015 Feb 17;112(7):E667-676.
84. Tomas A, Yermen B, Min L, Pessin JE, Halban PA. Regulation of pancreatic beta-cell insulin secretion by actin cytoskeleton remodelling: role of gelsolin and cooperation with the MAPK signalling pathway. J Cell Sci. 2006 May 15;119(Pt 10):2156–67.
85. Wang Z, Thurmond DC. Mechanisms of biphasic insulin-granule exocytosis - roles of the cytoskeleton, small GTPases and SNARE proteins. J Cell Sci. 2009 Apr 1;122(Pt 7):893–903.
86. Thurmond DC, Gonelle-Gispert C, Furukawa M, Halban PA, Pessin JE. Glucose-stimulated insulin secretion is coupled to the interaction of actin with the t-SNARE (target membrane soluble N-ethylmaleimide-sensitive factor attachment protein receptor protein) complex. Mol Endocrinol Baltim Md. 2003 Apr;17(4):732–42.
87. Nagamatsu S, Nakamichi Y, Yamamura C, Matsushima S, Watanabe T, Ozawa S, et al. Decreased expression of t-SNARE, syntaxin 1, and SNAP-25 in pancreatic beta-cells is involved in impaired insulin secretion from diabetic GK rat islets: restoration of decreased t-SNARE proteins improves impaired insulin secretion. Diabetes. 1999 Dec;48(12):2367–73.
88. Gaisano HY. Recent new insights into the role of SNARE and associated proteins in insulin granule exocytosis. Diabetes Obes Metab. 2017 Sept;19 Suppl 1:115–23.
89. Gilon P, Henquin JC. Mechanisms and physiological significance of the cholinergic control of pancreatic beta-cell function. Endocr Rev. 2001 Oct;22(5):565–604.
90. Jones B, Bloom SR, Buenaventura T, Tomas A, Rutter GA. Control of insulin secretion by GLP-1. Peptides. 2018 Feb;100:75–84.
91. Holst JJ, Gasbjerg LS, Rosenkilde MM. The Role of Incretins on Insulin Function and Glucose Homeostasis. Endocrinology. 2021 July 1;162(7):bqab065.
92. Kolic J, Sun WG, Johnson JD, Guess N. Amino acid-stimulated insulin secretion: a path forward in type 2 diabetes. Amino Acids. 2023 Dec;55(12):1857–66.
93. Yang J, Dolinger M, Ritaccio G, Mazurkiewicz J, Conti D, Zhu X, et al. Leucine stimulates insulin secretion via down-regulation of surface expression of adrenergic α2A receptor through the mTOR (mammalian target of rapamycin) pathway: implication in new-onset diabetes in renal transplantation. J Biol Chem. 2012 July 13;287(29):24795–806.
94. Huising MO. Paracrine regulation of insulin secretion. Diabetologia. 2020 Oct;63(10):2057–63.
95. Moede T, Leibiger IB, Berggren PO. Alpha cell regulation of beta cell function. Diabetologia. 2020 Oct;63(10):2064–75.

96. Svendsen B, Larsen O, Gabe MBN, Christiansen CB, Rosenkilde MM, Drucker DJ, et al. Insulin Secretion Depends on Intra-islet Glucagon Signaling. Cell Rep. 2018 Oct 30;25(5):1127-1134.e2.
97. Almaça J, Molina J, Menegaz D, Pronin AN, Tamayo A, Slepak V, et al. Human Beta Cells Produce and Release Serotonin to Inhibit Glucagon Secretion from Alpha Cells. Cell Rep. 2016 Dec 20;17(12):3281–91.
98. Rorsman P, Berggren PO, Bokvist K, Ericson H, Möhler H, Ostenson CG, et al. Glucose-inhibition of glucagon secretion involves activation of GABAA-receptor chloride channels. Nature. 1989 Sept 21;341(6239):233–6.
99. van der Meulen T, Donaldson CJ, Cáceres E, Hunter AE, Cowing-Zitron C, Pound LD, et al. Urocortin3 mediates somatostatin-dependent negative feedback control of insulin secretion. Nat Med. 2015 July;21(7):769–76.
100. Capozzi ME, Svendsen B, Encisco SE, Lewandowski SL, Martin MD, Lin H, et al. β Cell tone is defined by proglucagon peptides through cAMP signaling. JCI Insight. 2019 Mar 7;4(5):e126742, 126742.
101. Rodriguez-Diaz R, Dando R, Jacques-Silva MC, Fachado A, Molina J, Abdulreda MH, et al. Alpha cells secrete acetylcholine as a non-neuronal paracrine signal priming beta cell function in humans. Nat Med. 2011 June 19;17(7):888–92.
102. Noguchi GM, Huising MO. Integrating the inputs that shape pancreatic islet hormone release. Nat Metab. 2019 Dec;1(12):1189–201.
103. Hartig SM, Cox AR. Paracrine signaling in islet function and survival. J Mol Med Berl Ger. 2020 Apr;98(4):451–67.
104. Hartig SM, Cox AR. Paracrine signaling in islet function and survival. J Mol Med Berl Ger. 2020 Apr;98(4):451–67.
105. Asadi F, Dhanvantari S. Pathways of Glucagon Secretion and Trafficking in the Pancreatic Alpha Cell: Novel Pathways, Proteins, and Targets for Hyperglucagonemia. Front Endocrinol. 2021;12:726368.
106. Kawai K, Yokota C, Ohashi S, Watanabe Y, Yamashita K. Evidence that glucagon stimulates insulin secretion through its own receptor in rats. Diabetologia. 1995 Mar;38(3):274–6.
107. Moens K, Flamez D, Van Schravendijk C, Ling Z, Pipeleers D, Schuit F. Dual glucagon recognition by pancreatic beta-cells via glucagon and glucagon-like peptide 1 receptors. Diabetes. 1998 Jan;47(1):66–72.
108. Holz GG. Epac: A new cAMP-binding protein in support of glucagon-like peptide-1 receptor-mediated signal transduction in the pancreatic beta-cell. Diabetes. 2004 Jan;53(1):5–13.
109. Doyle ME, Egan JM. Mechanisms of action of glucagon-like peptide 1 in the pancreas. Pharmacol Ther. 2007 Mar;113(3):546–93.
110. Kashima Y, Miki T, Shibasaki T, Ozaki N, Miyazaki M, Yano H, et al. Critical role of cAMP-GEFII--Rim2 complex in incretin-potentiated insulin secretion. J Biol Chem. 2001 Dec 7;276(49):46046–53.
111. Shibasaki T, Takahashi H, Miki T, Sunaga Y, Matsumura K, Yamanaka M, et al. Essential role of Epac2/Rap1 signaling in regulation of insulin granule dynamics by cAMP. Proc Natl Acad Sci U S A. 2007 Dec 4;104(49):19333–8.
112. Gonzalez GA, Montminy MR. Cyclic AMP stimulates somatostatin gene transcription by phosphorylation of CREB at serine 133. Cell. 1989 Nov 17;59(4):675–80.
113. Hay CW, Sinclair EM, Bermano G, Durward E, Tadayyon M, Docherty K. Glucagon-like peptide-1 stimulates human insulin promoter activity in part through cAMP-responsive elements that lie upstream and downstream of the transcription start site. J Endocrinol. 2005 Aug;186(2):353–65.
114. Jhala US, Canettieri G, Screaton RA, Kulkarni RN, Krajewski S, Reed J, et al. cAMP promotes pancreatic beta-cell survival via CREB-mediated induction of IRS2. Genes Dev. 2003 July 1;17(13):1575–80.
115. de Rooij J, Zwartkruis FJ, Verheijen MH, Cool RH, Nijman SM, Wittinghofer A, et al. Epac is a Rap1 guanine-nucleotide-exchange factor directly activated by cyclic AMP. Nature. 1998 Dec 3;396(6710):474–7.
116. Trümper J, Ross D, Jahr H, Brendel MD, Göke R, Hörsch D. The Rap-B-Raf signalling pathway is activated by glucose and glucagon-like peptide-1 in human islet cells. Diabetologia. 2005 Aug;48(8):1534–40.
117. Dalle S, Longuet C, Costes S, Broca C, Faruque O, Fontés G, et al. Glucagon promotes cAMP-response element-binding protein phosphorylation via activation of ERK1/2 in MIN6 cell line and isolated islets of Langerhans. J Biol Chem. 2004 May 7;279(19):20345–55.

118. Zaïmia N, Obeid J, Varrault A, Sabatier J, Broca C, Gilon P, et al. GLP-1 and GIP receptors signal through distinct β-arrestin 2-dependent pathways to regulate pancreatic β cell function. Cell Rep. 2023 Nov 28;42(11):113326.
119. González-Casimiro CM, Merino B, Casanueva-Álvarez E, Postigo-Casado T, Cámara-Torres P, Fernández-Díaz CM, et al. Modulation of Insulin Sensitivity by Insulin-Degrading Enzyme. Biomedicines. 2021 Jan 17;9(1):86.
120. Leissring MA, González-Casimiro CM, Merino B, Suire CN, Perdomo G. Targeting Insulin-Degrading Enzyme in Insulin Clearance. Int J Mol Sci. 2021 Feb 24;22(5):2235.
121. Affholter JA, Fried VA, Roth RA. Human insulin-degrading enzyme shares structural and functional homologies with E. coli protease III. Science. 1988 Dec 9;242(4884):1415–8.
122. Mirsky IA, Broh-Kahn RH. The inactivation of insulin by tissue extracts; the distribution and properties of insulin inactivating extracts. Arch Biochem. 1949 Jan;20(1):1–9.
123. Affholter JA, Hsieh CL, Francke U, Roth RA. Insulin-degrading enzyme: stable expression of the human complementary DNA, characterization of its protein product, and chromosomal mapping of the human and mouse genes. Mol Endocrinol Baltim Md. 1990 Aug;4(8):1125–35.
124. Song ES, Juliano MA, Juliano L, Hersh LB. Substrate activation of insulin-degrading enzyme (insulysin). A potential target for drug development. J Biol Chem. 2003 Dec 12;278(50):49789–94.
125. Song ES, Rodgers DW, Hersh LB. A monomeric variant of insulin degrading enzyme (IDE) loses its regulatory properties. PloS One. 2010 Mar 16;5(3):e9719.
126. Shen Y, Joachimiak A, Rosner MR, Tang WJ. Structures of human insulin-degrading enzyme reveal a new substrate recognition mechanism. Nature. 2006 Oct 19;443(7113):870–4.
127. Zhang Z, Liang WG, Bailey LJ, Tan YZ, Wei H, Wang A, et al. Ensemble cryoEM elucidates the mechanism of insulin capture and degradation by human insulin degrading enzyme. eLife. 2018 Mar 29;7:e33572.
128. Shen Y, Joachimiak A, Rosner MR, Tang WJ. Structures of human insulin-degrading enzyme reveal a new substrate recognition mechanism. Nature. 2006 Oct 19;443(7113):870–4.
129. Akiyama H, Shii K, Yokono K, Yonezawa K, Sato S, Watanabe K, et al. Cellular localization of insulin-degrading enzyme in rat liver using monoclonal antibodies specific for this enzyme. Biochem Biophys Res Commun. 1988 Sept 15;155(2):914–22.
130. Duckworth WC. Insulin degradation: mechanisms, products, and significance. Endocr Rev. 1988 Aug;9(3):319–45.
131. Seabright PJ, Smith GD. The characterization of endosomal insulin degradation intermediates and their sequence of production. Biochem J. 1996 Dec 15;320 (Pt 3)(Pt 3):947–56.
132. Song ES, Jang H, Guo HF, Juliano MA, Juliano L, Morris AJ, et al. Inositol phosphates and phosphoinositides activate insulin-degrading enzyme, while phosphoinositides also mediate binding to endosomes. Proc Natl Acad Sci U S A. 2017 Apr 4;114(14):E2826–35.
133. Authier F, Bergeron JJ, Ou WJ, Rachubinski RA, Posner BI, Walton PA. Degradation of the cleaved leader peptide of thiolase by a peroxisomal proteinase. Proc Natl Acad Sci U S A. 1995 Apr 25;92(9):3859–63.
134. Leissring MA, Farris W, Wu X, Christodoulou DC, Haigis MC, Guarente L, et al. Alternative translation initiation generates a novel isoform of insulin-degrading enzyme targeted to mitochondria. Biochem J. 2004 Nov 1;383(Pt. 3):439–46.
135. Duckworth WC. Insulin degradation by liver cell membranes. Endocrinology. 1979 June;104(6):1758–64.
136. Yokono K, Roth RA, Baba S. Identification of insulin-degrading enzyme on the surface of cultured human lymphocytes, rat hepatoma cells, and primary cultures of rat hepatocytes. Endocrinology. 1982 Oct;111(4):1102–8.
137. Sanderson RD, Bandari SK, Vlodavsky I. Proteases and glycosidases on the surface of exosomes: Newly discovered mechanisms for extracellular remodeling. Matrix Biol J Int Soc Matrix Biol. 2019 Jan;75–76:160–9.
138. Shen Y, Joachimiak A, Rosner MR, Tang WJ. Structures of human insulin-degrading enzyme reveal a new substrate recognition mechanism. Nature. 2006 Oct 19;443(7113):870–4.
139. Hulse RE, Ralat LA, Wei-Jen T. Structure, function, and regulation of insulin-degrading enzyme. Vitam Horm. 2009;80:635–48.

140. Ciaccio C, Tundo GR, Grasso G, Spoto G, Marasco D, Ruvo M, et al. Somatostatin: a novel substrate and a modulator of insulin-degrading enzyme activity. J Mol Biol. 2009 Feb 6;385(5):1556–67.
141. Bennett RG, Duckworth WC, Hamel FG. Degradation of amylin by insulin-degrading enzyme. J Biol Chem. 2000 Nov 24;275(47):36621–5.
142. Kurochkin IV, Goto S. Alzheimer's beta-amyloid peptide specifically interacts with and is degraded by insulin degrading enzyme. FEBS Lett. 1994 May 23;345(1):33–7.
143. Malito E, Hulse RE, Tang WJ. Amyloid beta-degrading cryptidases: insulin degrading enzyme, presequence peptidase, and neprilysin. Cell Mol Life Sci CMLS. 2008 Aug;65(16):2574–85.
144. Kupfer SR, Wilson EM, French FS. Androgen and glucocorticoid receptors interact with insulin degrading enzyme. J Biol Chem. 1994 Aug 12;269(32):20622–8.
145. Chou YH, Kuo WL, Rosner MR, Tang WJ, Goldman RD. Structural changes in intermediate filament networks alter the activity of insulin-degrading enzyme. FASEB J Off Publ Fed Am Soc Exp Biol. 2009 Nov;23(11):3734–42.
146. Ahuja N, Schwer B, Carobbio S, Waltregny D, North BJ, Castronovo V, et al. Regulation of insulin secretion by SIRT4, a mitochondrial ADP-ribosyltransferase. J Biol Chem. 2007 Nov 16;282(46):33583–92.
147. Sharma SK, Chorell E, Wittung-Stafshede P. Insulin-degrading enzyme is activated by the C-terminus of α-synuclein. Biochem Biophys Res Commun. 2015 Oct 16;466(2):192–5.
148. Li F, Yang J, Villar VAM, Asico LD, Ma X, Armando I, et al. Loss of renal SNX5 results in impaired IDE activity and insulin resistance in mice. Diabetologia. 2018 Mar;61(3):727–37.
149. Sbardella D, Tundo GR, Coletta A, Marcoux J, Koufogeorgou EI, Ciaccio C, et al. The insulin-degrading enzyme is an allosteric modulator of the 20S proteasome and a potential competitor of the 19S. Cell Mol Life Sci CMLS. 2018 Sept;75(18):3441–56.
150. Bennett RG, Fawcett J, Kruer MC, Duckworth WC, Hamel FG. Insulin inhibition of the proteasome is dependent on degradation of insulin by insulin-degrading enzyme. J Endocrinol. 2003 June;177(3):399–405.
151. Kuo WL, Montag AG, Rosner MR. Insulin-degrading enzyme is differentially expressed and developmentally regulated in various rat tissues. Endocrinology. 1993 Feb;132(2):604–11.
152. Karamohamed S, Demissie S, Volcjak J, Liu C, Heard-Costa N, Liu J, et al. Polymorphisms in the insulin-degrading enzyme gene are associated with type 2 diabetes in men from the NHLBI Framingham Heart Study. Diabetes. 2003 June;52(6):1562–7.
153. Groves CJ, Wiltshire S, Smedley D, Owen KR, Frayling TM, Walker M, et al. Association and haplotype analysis of the insulin-degrading enzyme (IDE) gene, a strong positional and biological candidate for type 2 diabetes susceptibility. Diabetes. 2003 May;52(5):1300–5.
154. Kwak SH, Cho YM, Moon MK, Kim JH, Park BL, Cheong HS, et al. Association of polymorphisms in the insulin-degrading enzyme gene with type 2 diabetes in the Korean population. Diabetes Res Clin Pract. 2008 Feb;79(2):284–90.
155. Rudovich N, Pivovarova O, Fisher E, Fischer-Rosinsky A, Spranger J, Möhlig M, et al. Polymorphisms within insulin-degrading enzyme (IDE) gene determine insulin metabolism and risk of type 2 diabetes. J Mol Med Berl Ger. 2009 Nov;87(11):1145–51.
156. Lu X, Huang Y, Liu Y, Wu X, Shi X. Variants in the insulin-degrading enzyme gene are associated with metabolic syndrome in Chinese elders. Metabolism. 2009 Oct;58(10):1465–9.
157. Sofer Y, Nash Y, Osher E, Fursht O, Goldsmith G, Nahary L, et al. Insulin-degrading enzyme higher in subjects with metabolic syndrome. Endocrine. 2021 Feb;71(2):357–64.
158. Pivovarova O, von Loeffelholz C, Ilkavets I, Sticht C, Zhuk S, Murahovschi V, et al. Modulation of insulin degrading enzyme activity and liver cell proliferation. Cell Cycle Georget Tex. 2015;14(14):2293–300.
159. Fosam A, Sikder S, Abel BS, Tella SH, Walter MF, Mari A, et al. Reduced Insulin Clearance and Insulin-Degrading Enzyme Activity Contribute to Hyperinsulinemia in African Americans. J Clin Endocrinol Metab. 2020 Apr 1;105(4):e1835-1846.
160. Villa-Pérez P, Merino B, Fernández-Díaz CM, Cidad P, Lobatón CD, Moreno A, et al. Liver-specific ablation of insulin-degrading enzyme causes hepatic insulin resistance and glucose intolerance, without affecting insulin clearance in mice. Metabolism. 2018 Nov;88:1–11.
161. Fawcett J, Sang H, Permana PA, Levy JL, Duckworth WC. Insulin metabolism in human adipocytes from subcutaneous and visceral depots. Biochem Biophys Res Commun. 2010 Nov 26;402(4):762–6.

162. Fernández-Díaz CM, Escobar-Curbelo L, López-Acosta JF, Lobatón CD, Moreno A, Sanz-Ortega J, et al. Insulin degrading enzyme is up-regulated in pancreatic β cells by insulin treatment. Histol Histopathol. 2018 Nov;33(11):1167–80.
163. Fakhrai-Rad H, Nikoshkov A, Kamel A, Fernström M, Zierath JR, Norgren S, et al. Insulin-degrading enzyme identified as a candidate diabetes susceptibility gene in GK rats. Hum Mol Genet. 2000 Sept 1;9(14):2149–58.
164. Farris W, Mansourian S, Chang Y, Lindsley L, Eckman EA, Frosch MP, et al. Insulin-degrading enzyme regulates the levels of insulin, amyloid beta-protein, and the beta-amyloid precursor protein intracellular domain in vivo. Proc Natl Acad Sci U S A. 2003 Apr 1;100(7):4162–7.
165. Abdul-Hay SO, Kang D, McBride M, Li L, Zhao J, Leissring MA. Deletion of insulin-degrading enzyme elicits antipodal, age-dependent effects on glucose and insulin tolerance. PloS One. 2011;6(6):e20818.
166. Steneberg P, Bernardo L, Edfalk S, Lundberg L, Backlund F, Ostenson CG, et al. The type 2 diabetes-associated gene ide is required for insulin secretion and suppression of α-synuclein levels in β-cells. Diabetes. 2013 June;62(6):2004–14.
167. Merino B, Fernández-Díaz CM, Parrado-Fernández C, González-Casimiro CM, Postigo-Casado T, Lobatón CD, et al. Hepatic insulin-degrading enzyme regulates glucose and insulin homeostasis in diet-induced obese mice. Metabolism. 2020 Dec;113:154352.
168. Fernández-Díaz CM, Merino B, López-Acosta JF, Cidad P, de la Fuente MA, Lobatón CD, et al. Pancreatic β-cell-specific deletion of insulin-degrading enzyme leads to dysregulated insulin secretion and β-cell functional immaturity. Am J Physiol Endocrinol Metab. 2019 Nov 1;317(5):E805–19.
169. Merino B, Casanueva-Álvarez E, Quesada I, González-Casimiro CM, Fernández-Díaz CM, Postigo-Casado T, et al. Correction to: Insulin-degrading enzyme ablation in mouse pancreatic alpha cells triggers cell proliferation, hyperplasia and glucagon secretion dysregulation. Diabetologia. 2024 Jan;67(1):218–9.
170. Leissring MA, Malito E, Hedouin S, Reinstatler L, Sahara T, Abdul-Hay SO, et al. Designed inhibitors of insulin-degrading enzyme regulate the catabolism and activity of insulin. PloS One. 2010 May 7;5(5):e10504.
171. Maianti JP, McFedries A, Foda ZH, Kleiner RE, Du XQ, Leissring MA, et al. Anti-diabetic activity of insulin-degrading enzyme inhibitors mediated by multiple hormones. Nature. 2014 July 3;511(7507):94–8.
172. Deprez-Poulain R, Hennuyer N, Bosc D, Liang WG, Enée E, Marechal X, et al. Catalytic site inhibition of insulin-degrading enzyme by a small molecule induces glucose intolerance in mice. Nat Commun. 2015 Sept 23;6:8250.
173. Durham TB, Toth JL, Klimkowski VJ, Cao JXC, Siesky AM, Alexander-Chacko J, et al. Dual Exosite-binding Inhibitors of Insulin-degrading Enzyme Challenge Its Role as the Primary Mediator of Insulin Clearance in Vivo. J Biol Chem. 2015 Aug 14;290(33):20044–59.
174. Cabrol C, Huzarska MA, Dinolfo C, Rodriguez MC, Reinstatler L, Ni J, et al. Small-molecule activators of insulin-degrading enzyme discovered through high-throughput compound screening. PloS One. 2009;4(4):e5274.
175. Charton J, Gauriot M, Totobenazara J, Hennuyer N, Dumont J, Bosc D, et al. Structure-activity relationships of imidazole-derived 2-[N-carbamoylmethyl-alkylamino]acetic acids, dual binders of human insulin-degrading enzyme. Eur J Med Chem. 2015 Jan 27;90:547–67.
176. Distefano A, Caruso G, Oliveri V, Bellia F, Sbardella D, Zingale GA, et al. Neuroprotective Effect of Carnosine Is Mediated by Insulin-Degrading Enzyme. ACS Chem Neurosci. 2022 May 18;13(10):1588–93.
177. Krasinski CA, Ivancic VA, Zheng Q, Spratt DE, Lazo ND. Resveratrol Sustains Insulin-Degrading Enzyme Activity toward Aβ42. ACS Omega. 2018 Oct 31;3(10):13275–82.
178. Weiss L, Bernstein S, Jones R, Amunugama R, Krizman D, Jebailey L, et al. Preimplantation factor (PIF) analog prevents type I diabetes mellitus (TIDM) development by preserving pancreatic function in NOD mice. Endocrine. 2011 Aug;40(1):41–54.
179. Sanz-González A, Cózar-Castellano I, Broca C, Sabatier J, Acosta GA, Royo M, et al. Pharmacological activation of insulin-degrading enzyme improves insulin secretion and glucose tolerance in diet-induced obese mice. Diabetes Obes Metab. 2023 Nov;25(11):3268–78.
180. Goodson HV, Jonasson EM. Microtubules and Microtubule-Associated Proteins. Cold Spring Harb Perspect Biol. 2018 June 1;10(6):a022608.

181. Hohmann T, Dehghani F. The Cytoskeleton-A Complex Interacting Meshwork. Cells. 2019 Apr 18;8(4):362.
182. McIntosh JR. Mitosis. Cold Spring Harb Perspect Biol. 2016 Sept 1;8(9):a023218.
183. Viswanadha R, Sale WS, Porter ME. Ciliary Motility: Regulation of Axonemal Dynein Motors. Cold Spring Harb Perspect Biol. 2017 Aug 1;9(8):a018325.
184. Barlan K, Gelfand VI. Microtubule-Based Transport and the Distribution, Tethering, and Organization of Organelles. Cold Spring Harb Perspect Biol. 2017 May 1;9(5):a025817.
185. Caudron N, Arnal I, Buhler E, Job D, Valiron O. Microtubule nucleation from stable tubulin oligomers. J Biol Chem. 2002 Dec 27;277(52):50973–9.
186. Tovey CA, Conduit PT. Microtubule nucleation by γ-tubulin complexes and beyond. Essays Biochem. 2018 Dec 7;62(6):765–80.
187. Mitchison T, Kirschner M. Dynamic instability of microtubule growth. Nature. 1984 Nov 15;312(5991):237–42.
188. Seetapun D, Castle BT, McIntyre AJ, Tran PT, Odde DJ. Estimating the microtubule GTP cap size in vivo. Curr Biol CB. 2012 Sept 25;22(18):1681–7.
189. Seetapun D, Castle BT, McIntyre AJ, Tran PT, Odde DJ. Estimating the microtubule GTP cap size in vivo. Curr Biol CB. 2012 Sept 25;22(18):1681–7.
190. Desai A, Mitchison TJ. Microtubule polymerization dynamics. Annu Rev Cell Dev Biol. 1997;13:83–117.
191. Dehmelt L, Halpain S. The MAP2/Tau family of microtubule-associated proteins. Genome Biol. 2005;6(1):204.
192. Bosc C, Andrieux A, Job D. STOP proteins. Biochemistry. 2003 Oct 28;42(42):12125–32.
193. Fourniol F, Perderiset M, Houdusse A, Moores C. Structural studies of the doublecortin family of MAPs. Methods Cell Biol. 2013;115:27–48.
194. L C. The oncoprotein 18/stathmin family of microtubule destabilizers. Curr Opin Cell Biol [Internet]. 2002 Feb [cited 2025 July 2];14(1). Available from: https://pubmed.ncbi.nlm.nih.gov/11792540/
195. Walczak CE, Gayek S, Ohi R. Microtubule-depolymerizing kinesins. Annu Rev Cell Dev Biol. 2013;29:417–41.
196. Sarbanes SL, Zehr EA, Roll-Mecak A. Microtubule-severing enzymes. Curr Biol CB. 2022 Oct 10;32(19):R992–7.
197. Sharp DJ, Ross JL. Microtubule-severing enzymes at the cutting edge. J Cell Sci. 2012 June 1;125(Pt 11):2561–9.
198. Walczak CE, Shaw SL. A MAP for bundling microtubules. Cell. 2010 Aug 6;142(3):364–7.
199. Suozzi KC, Wu X, Fuchs E. Spectraplakins: master orchestrators of cytoskeletal dynamics. J Cell Biol. 2012 May 14;197(4):465–75.
200. Bartolini F, Moseley JB, Schmoranzer J, Cassimeris L, Goode BL, Gundersen GG. The formin mDia2 stabilizes microtubules independently of its actin nucleation activity. J Cell Biol. 2008 May 5;181(3):523–36.
201. Akhmanova A, Hoogenraad CC. Microtubule minus-end-targeting proteins. Curr Biol CB. 2015 Feb 16;25(4):R162-171.
202. Alushin GM, Lander GC, Kellogg EH, Zhang R, Baker D, Nogales E. High-resolution microtubule structures reveal the structural transitions in αβ-tubulin upon GTP hydrolysis. Cell. 2014 May 22;157(5):1117–29.
203. Amos LA. What tubulin drugs tell us about microtubule structure and dynamics. Semin Cell Dev Biol. 2011 Dec;22(9):916–26.
204. Sebastian J, Rathinasamy K. Microtubules and Cell Division: Potential Pharmacological Targets in Cancer Therapy. Curr Drug Targets. 2023;24(11):889–918.
205. Janke C, Bulinski JC. Post-translational regulation of the microtubule cytoskeleton: mechanisms and functions. Nat Rev Mol Cell Biol. 2011 Nov 16;12(12):773–86.
206. Garnham CP, Roll-Mecak A. The chemical complexity of cellular microtubules: tubulin post-translational modification enzymes and their roles in tuning microtubule functions. Cytoskelet Hoboken NJ. 2012 July;69(7):442–63.
207. LeDizet M, Piperno G. Identification of an acetylation site of Chlamydomonas alpha-tubulin. Proc Natl Acad Sci U S A. 1987 Aug;84(16):5720–4.
208. Soppina V, Herbstman JF, Skiniotis G, Verhey KJ. Luminal localization of α-tubulin K40 acetylation by cryo-EM analysis of fab-labeled microtubules. PloS One. 2012;7(10):e48204.
209. Shida T, Cueva JG, Xu Z, Goodman MB, Nachury MV. The major alpha-tubulin K40 acetyltransferase alphaTAT1 promotes rapid ciliogenesis and efficient mechanosensation. Proc Natl Acad Sci U S A. 2010 Dec 14;107(50):21517–22.

210. Hubbert C, Guardiola A, Shao R, Kawaguchi Y, Ito A, Nixon A, et al. HDAC6 is a microtubule-associated deacetylase. Nature. 2002 May 23;417(6887):455–8.
211. Howes SC, Alushin GM, Shida T, Nachury MV, Nogales E. Effects of tubulin acetylation and tubulin acetyltransferase binding on microtubule structure. Mol Biol Cell. 2014 Jan;25(2):257–66.
212. Wloga D, Joachimiak E, Fabczak H. Tubulin Post-Translational Modifications and Microtubule Dynamics. Int J Mol Sci. 2017 Oct 21;18(10):2207.
213. Song Y, Kirkpatrick LL, Schilling AB, Helseth DL, Chabot N, Keillor JW, et al. Transglutaminase and polyamination of tubulin: posttranslational modification for stabilizing axonal microtubules. Neuron. 2013 Apr 10;78(1):109–23.
214. Hallak ME, Rodriguez JA, Barra HS, Caputto R. Release of tyrosine from tyrosinated tubulin. Some common factors that affect this process and the assembly of tubulin. FEBS Lett. 1977 Feb 1;73(2):147–50.
215. Szyk A, Deaconescu AM, Piszczek G, Roll-Mecak A. Tubulin tyrosine ligase structure reveals adaptation of an ancient fold to bind and modify tubulin. Nat Struct Mol Biol. 2011 Oct 23;18(11):1250–8.
216. Paturle-Lafanechère L, Eddé B, Denoulet P, Van Dorsselaer A, Mazarguil H, Le Caer JP, et al. Characterization of a major brain tubulin variant which cannot be tyrosinated. Biochemistry. 1991 Oct 29;30(43):10523–8.
217. Peris L, Wagenbach M, Lafanechère L, Brocard J, Moore AT, Kozielski F, et al. Motor-dependent microtubule disassembly driven by tubulin tyrosination. J Cell Biol. 2009 June 29;185(7):1159–66.
218. van Dijk J, Miro J, Strub JM, Lacroix B, van Dorsselaer A, Edde B, et al. Polyglutamylation is a post-translational modification with a broad range of substrates. J Biol Chem. 2008 Feb 15;283(7):3915–22.
219. Song Y, Brady ST. Post-translational modifications of tubulin: pathways to functional diversity of microtubules. Trends Cell Biol. 2015 Mar;25(3):125–36.
220. Wloga D, Webster DM, Rogowski K, Bré MH, Levilliers N, Jerka-Dziadosz M, et al. TTLL3 Is a tubulin glycine ligase that regulates the assembly of cilia. Dev Cell. 2009 June;16(6):867–76.
221. Wolff J, Zambito AM, Britto PJ, Knipling L. Autopalmitoylation of tubulin. Protein Sci Publ Protein Soc. 2000 July;9(7):1357–64.
222. Ren Y, Zhao J, Feng J. Parkin binds to alpha/beta tubulin and increases their ubiquitination and degradation. J Neurosci Off J Soc Neurosci. 2003 Apr 15;23(8):3316–24.
223. Rosas-Acosta G, Russell WK, Deyrieux A, Russell DH, Wilson VG. A universal strategy for proteomic studies of SUMO and other ubiquitin-like modifiers. Mol Cell Proteomics MCP. 2005 Jan;4(1):56–72.
224. Schjoldager KT, Narimatsu Y, Joshi HJ, Clausen H. Global view of human protein glycosylation pathways and functions. Nat Rev Mol Cell Biol. 2020 Dec;21(12):729–49.
225. Ji S, Kang JG, Park SY, Lee J, Oh YJ, Cho JW. O-GlcNAcylation of tubulin inhibits its polymerization. Amino Acids. 2011 Mar;40(3):809–18.
226. Jo S, Pritchard S, Wong A, Avula N, Essawy A, Hanover J, et al. Pancreatic β-cell hyper-O-GlcNAcylation leads to impaired glucose homeostasis in vivo. Front Endocrinol. 2022;13:1040014.
227. Miyazawa T, Nakagawa K, Shimasaki S, Nagai R. Lipid glycation and protein glycation in diabetes and atherosclerosis. Amino Acids. 2012 Apr;42(4):1163–70.
228. Bracey KM, Gu G, Kaverina I. Microtubules in Pancreatic β Cells: Convoluted Roadways Toward Precision. Front Cell Dev Biol. 2022;10:915206.
229. Zhu X, Kaverina I. Golgi as an MTOC: making microtubules for its own good. Histochem Cell Biol. 2013 Sept;140(3):361–7.
230. Ho KH, Yang X, Osipovich AB, Cabrera O, Hayashi ML, Magnuson MA, et al. Glucose Regulates Microtubule Disassembly and the Dose of Insulin Secretion via Tau Phosphorylation. Diabetes. 2020 Sept;69(9):1936–47.
231. Trogden KP, Lee J, Bracey KM, Ho KH, McKinney H, Zhu X, et al. Microtubules regulate pancreatic β-cell heterogeneity via spatiotemporal control of insulin secretion hot spots. eLife. 2021 Nov 16;10:e59912.
232. Müller A, Schmidt D, Xu CS, Pang S, D'Costa JV, Kretschmar S, et al. 3D FIB-SEM reconstruction of microtubule-organelle interaction in whole primary mouse β cells. J Cell Biol. 2021 Feb 1;220(2):e202010039.

233. Barbier P, Zejneli O, Martinho M, Lasorsa A, Belle V, Smet-Nocca C, et al. Role of Tau as a Microtubule-Associated Protein: Structural and Functional Aspects. Front Aging Neurosci. 2019;11:204.
234. Trogden KP, Zhu X, Lee JS, Wright CVE, Gu G, Kaverina I. Regulation of Glucose-Dependent Golgi-Derived Microtubules by cAMP/EPAC2 Promotes Secretory Vesicle Biogenesis in Pancreatic β Cells. Curr Biol CB. 2019 July 22;29(14):2339-2350.e5.
235. Pablos M, Casanueva-Álvarez E, González-Casimiro CM, Merino B, Perdomo G, Cózar-Castellano I. Primary Cilia in Pancreatic β- and α-Cells: Time to Revisit the Role of Insulin-Degrading Enzyme. Front Endocrinol. 2022;13:922825.
236. Moore ER. Primary Cilia: The New Face of Craniofacial Research. Biomolecules. 2022 Nov 22;12(12):1724.
237. Müller A, Klena N, Pang S, Garcia LEG, Topcheva O, Aurrecoechea Duran S, et al. Structure, interaction and nervous connectivity of beta cell primary cilia. Nat Commun. 2024 Oct 24;15(1):9168.
238. Berbari NF, O'Connor AK, Haycraft CJ, Yoder BK. The primary cilium as a complex signaling center. Curr Biol CB. 2009 July 14;19(13):R526-535.
239. Pedersen LB, Rosenbaum JL. Intraflagellar transport (IFT) role in ciliary assembly, resorption and signalling. Curr Top Dev Biol. 2008;85:23–61.
240. Cho JH, Hughes JW. Cilia Action in Islets: Lessons From Mouse Models. Front Endocrinol. 2022;13:922983.
241. Quarmby LM, Parker JDK. Cilia and the cell cycle? J Cell Biol. 2005 June 6;169(5):707–10.
242. Aughsteen AA. The ultrastructure of primary cilia in the endocrine and excretory duct cells of the pancreas of mice and rats. Eur J Morphol. 2001 Dec;39(5):277–83.
243. Badano JL, Mitsuma N, Beales PL, Katsanis N. The ciliopathies: an emerging class of human genetic disorders. Annu Rev Genomics Hum Genet. 2006;7:125–48.
244. Thomas MK, Rastalsky N, Lee JH, Habener JF. Hedgehog signaling regulation of insulin production by pancreatic beta-cells. Diabetes. 2000 Dec;49(12):2039–47.
245. Umeda H, Ozaki N, Mizutani N, Fukuyama T, Nagasaki H, Arima H, et al. Protective effect of hedgehog signaling on cytokine-induced cytotoxicity in pancreatic beta-cells. Exp Clin Endocrinol Diabetes Off J Ger Soc Endocrinol Ger Diabetes Assoc. 2010 Nov;118(10):692–8.
246. Yalcinkaya M, Kerksiek A, Gebert K, Annema W, Sibler R, Radosavljevic S, et al. HDL inhibits endoplasmic reticulum stress-induced apoptosis of pancreatic β-cells in vitro by activation of Smoothened. J Lipid Res. 2020 Apr;61(4):492–504.
247. Lodh S. Primary Cilium, An Unsung Hero in Maintaining Functional β-cell Population. Yale J Biol Med. 2019 Sept;92(3):471–80.
248. Ait-Lounis A, Baas D, Barras E, Benadiba C, Charollais A, Nlend Nlend R, et al. Novel function of the ciliogenic transcription factor RFX3 in development of the endocrine pancreas. Diabetes. 2007 Apr;56(4):950–9.
249. Hughes JW, Cho JH, Conway HE, DiGruccio MR, Ng XW, Roseman HF, et al. Primary cilia control glucose homeostasis via islet paracrine interactions. Proc Natl Acad Sci U S A. 2020 Apr 21;117(16):8912–23.
250. Nilsson CI, Dumral Ö, Sanchez G, Xie B, Müller A, Solimena M, et al. Somatostatin triggers local cAMP and Ca2+ signaling in primary cilia to modulate pancreatic β-cell function. EMBO J. 2025 Mar;44(6):1663–91.
251. Granot Z, Swisa A, Magenheim J, Stolovich-Rain M, Fujimoto W, Manduchi E, et al. LKB1 regulates pancreatic beta cell size, polarity, and function. Cell Metab. 2009 Oct;10(4):296–308.
252. Hearn T, Spalluto C, Phillips VJ, Renforth GL, Copin N, Hanley NA, et al. Subcellular localization of ALMS1 supports involvement of centrosome and basal body dysfunction in the pathogenesis of obesity, insulin resistance, and type 2 diabetes. Diabetes. 2005 May;54(5):1581–7.
253. Gerdes JM, Christou-Savina S, Xiong Y, Moede T, Moruzzi N, Karlsson-Edlund P, et al. Ciliary dysfunction impairs beta-cell insulin secretion and promotes development of type 2 diabetes in rodents. Nat Commun. 2014 Nov 6;5:5308.
254. Singh A, Haq N, Yang M, Luckey S, Mansouri S, Campbell-Thompson M, et al. Transcriptome-guided GLP-1 receptor therapy rescues metabolic and behavioral disruptions in a Bardet-Biedl syndrome mouse model. J Clin Invest. 2025 June 16;135(12):e184636.

255. Keller MP, Choi Y, Wang P, Davis DB, Rabaglia ME, Oler AT, et al. A gene expression network model of type 2 diabetes links cell cycle regulation in islets with diabetes susceptibility. Genome Res. 2008 May;18(5):706–16.
256. Kluth O, Stadion M, Gottmann P, Aga H, Jähnert M, Scherneck S, et al. Decreased Expression of Cilia Genes in Pancreatic Islets as a Risk Factor for Type 2 Diabetes in Mice and Humans. Cell Rep. 2019 Mar 12;26(11):3027-3036.e3.
257. Herrera PL, Orci L, Vassalli JD. Two transgenic approaches to define the cell lineages in endocrine pancreas development. Mol Cell Endocrinol. 1998 May 25;140(1–2):45–50.
258. Manual_pPurGreen-081124_WEB.pdf [Internet]. [cited 2025 July 2]. Available from: https://www.systembio.com/wp/wp-content/uploads/Manual_pPurGreen-081124_WEB.pdf
259. Livak KJ, Schmittgen TD. Analysis of relative gene expression data using real-time quantitative PCR and the 2(-Delta Delta C(T)) Method. Methods San Diego Calif. 2001 Dec;25(4):402–8.
260. Schindelin J, Arganda-Carreras I, Frise E, Kaynig V, Longair M, Pietzsch T, et al. Fiji: an open-source platform for biological-image analysis. Nat Methods. 2012 June 28;9(7):676–82.
261. Cordelieres FP, Bolte S. JACoP v2.0: improving the user experience with co-localization studies.
262. Bankhead P, Loughrey MB, Fernández JA, Dombrowski Y, McArt DG, Dunne PD, et al. QuPath: Open source software for digital pathology image analysis. Sci Rep. 2017 Dec 4;7(1):16878.
263. Apaolaza PS, Petropoulou PI, Rodriguez-Calvo T. Whole-Slide Image Analysis of Human Pancreas Samples to Elucidate the Immunopathogenesis of Type 1 Diabetes Using the QuPath Software. Front Mol Biosci. 2021 June 11;8:689799.
264. TESIS-2279-240320.pdf [Internet]. [cited 2025 July 3]. Available from: https://uvadoc.uva.es/bitstream/handle/10324/66862/TESIS-2279-240320.pdf?sequence=1
265. Holter MM, Saikia M, Cummings BP. Alpha-cell paracrine signaling in the regulation of beta-cell insulin secretion. Front Endocrinol. 2022;13:934775.
266. Jurgens CA, Toukatly MN, Fligner CL, Udayasankar J, Subramanian SL, Zraika S, et al. β-cell loss and β-cell apoptosis in human type 2 diabetes are related to islet amyloid deposition. Am J Pathol. 2011 June;178(6):2632–40.
267. Efrat S. Beta-Cell Dedifferentiation in Type 2 Diabetes: Concise Review. Stem Cells Dayt Ohio. 2019 Oct;37(10):1267–72.
268. Chera S, Baronnier D, Ghila L, Cigliola V, Jensen JN, Gu G, et al. Diabetes recovery by age-dependent conversion of pancreatic δ-cells into insulin producers. Nature. 2014 Oct 23;514(7523):503–7.
269. Patel S, Yan Z, Remedi MS. Intermittent fasting protects β-cell identity and function in a type-2 diabetes model. Metabolism. 2024 Apr;153:155813.
270. Klec C, Ziomek G, Pichler M, Malli R, Graier WF. Calcium Signaling in ß-cell Physiology and Pathology: A Revisit. Int J Mol Sci. 2019 Dec 4;20(24):6110.
271. Marmugi A, Parnis J, Chen X, Carmichael L, Hardy J, Mannan N, et al. Sorcin Links Pancreatic β-Cell Lipotoxicity to ER Ca2+ Stores. Diabetes. 2016 Apr;65(4):1009–21.
272. Thorens B. Glucose sensing and the pathogenesis of obesity and type 2 diabetes. Int J Obes 2005. 2008 Dec;32 Suppl 6:S62-71.
273. Matschinsky FM. Regulation of pancreatic beta-cell glucokinase: from basics to therapeutics. Diabetes. 2002 Dec;51 Suppl 3:S394-404.
274. Wiederkehr A, Wollheim CB. Mitochondrial signals drive insulin secretion in the pancreatic β-cell. Mol Cell Endocrinol. 2012 Apr 28;353(1–2):128–37.
275. Maechler P, Wollheim CB. Mitochondrial function in normal and diabetic β-cells. Nature. 2001 Dec;414(6865):807–12.
276. Tabei SMA, Burov S, Kim HY, Kuznetsov A, Huynh T, Jureller J, et al. Intracellular transport of insulin granules is a subordinated random walk. Proc Natl Acad Sci U S A. 2013 Mar 26;110(13):4911–6.
277. Kaverina I, Rottner K, Small JV. Targeting, capture, and stabilization of microtubules at early focal adhesions. J Cell Biol. 1998 July 13;142(1):181–90.
278. Apodaca G. Endocytic traffic in polarized epithelial cells: role of the actin and microtubule cytoskeleton. Traffic Cph Den. 2001 Mar;2(3):149–59.

279. Krilov L, Nguyen A, Miyazaki T, Unson CG, Bouscarel B. Glucagon receptor recycling: role of carboxyl terminus, beta-arrestins, and cytoskeleton. Am J Physiol Cell Physiol. 2008 Nov;295(5):C1230-1237.
280. Briata P, Gherzi R, Adezati L, Cordera R. Effect of two different glucose concentrations on insulin receptor mRNA levels in human hepatoma HepG2 cells. Biochem Biophys Res Commun. 1989 May 15;160(3):1415–20.
281. Abrahamsen N, Lundgren K, Nishimura E. Regulation of glucagon receptor mRNA in cultured primary rat hepatocytes by glucose and cAMP. J Biol Chem. 1995 June 30;270(26):15853–7.
282. Bertocci B, Yilmaz A, Waeckel-Énée E, Guerrera C, Roger K, Touré L, et al. Insulin-Degrading Enzyme Regulates mRNA Processing and May Interact with the CCR4-NOT Complex. Cells. 2025 May 28;14(11):792.
283. Wang L, Dynlacht BD. The regulation of cilium assembly and disassembly in development and disease. Dev Camb Engl. 2018 Sept 17;145(18):dev151407.
284. Plotnikova OV, Pugacheva EN, Golemis EA. Primary cilia and the cell cycle. Methods Cell Biol. 2009;94:137–60.
285. Takahashi K, Nagai T, Chiba S, Nakayama K, Mizuno K. Glucose deprivation induces primary cilium formation through mTORC1 inactivation. J Cell Sci. 2018 Jan 8;131(1):jcs208769.
286. Stamateris RE, Sharma RB, Kong Y, Ebrahimpour P, Panday D, Ranganath P, et al. Glucose Induces Mouse β-Cell Proliferation via IRS2, MTOR, and Cyclin D2 but Not the Insulin Receptor. Diabetes. 2016 Apr;65(4):981–95.
287. Melnyk O, Guo JK, Li ZA, Jo JH, Hughes JW, Linnemann AK. Intravital imaging reveals glucose-dependent cilia movement in pancreatic islets in vivo. Metabolism. 2025 Feb;163:156105.
288. Tian JL, Huang CW, Eslami F, Mannino MP, Mai RL, Hart GW. Regulation of Primary Cilium Length by O-GlcNAc during Neuronal Development in a Human Neuron Model. Cells. 2023 May 31;12(11):1520.
289. Adamson SE, Li ZA, Hughes JW. Beta cell primary cilia mediate somatostatin responsiveness via SSTR3. Islets. 2023 Dec 31;15(1):2252855.
290. Volta F, Scerbo MJ, Seelig A, Wagner R, O'Brien N, Gerst F, et al. Glucose homeostasis is regulated by pancreatic β-cell cilia via endosomal EphA-processing. Nat Commun. 2019 Dec 12;10(1):5686.
291. Chen K, Zhang C, Lin S, Yan X, Cai H, Yi C, et al. Tail engagement of arrestin at the glucagon receptor. Nature. 2023 Aug;620(7975):904–10.